Thesis for the degree of Doctor of Philosophy

Cell Surface Display of Peptides to Recover Metals from Electronic Waste

Supervisor: Prof. Soon-Ho Hong

The Graduate School

University of Ulsan

Department of Chemical Engineering and Bioengineering

Vidhya Selvamani

Dedicated to my Family and people who love nature

ACKNOWLEDGEMENTS

I would like to show deep gratitude to my mentor, ***Prof. Soon-Ho Hong*** *for his excellence guidance, deep concern and constant encouragement throughout this study, for giving me a chance to write this thesis. It has been my honor to work under his guidance. I would never forget about this.*

I am thankful to the ***University of Ulsan****, for supporting my projects during this study.*

I am grateful to all the ***committee members*** *for their suggestions, review and comments on the thesis.*

I do really appreciate all the Professors and staff members of ***Department of Chemical Engineering and Bioengineering*** *for their lectures and support during the course.*

I am thankful to the Office Manager ***Lim kyoung Jo and other office staffs*** *for providing me all the facilities and helping me in all the official works whenever I am in need.*

I thankful to my present and former colleagues named ***Kim Ngan, Sivachandiran, Linda*** *of our lab for giving me indispensable help and support and creating a wonderful working environment.*

I am thankful to my friends in korea ***Monisha, Anju, Vikranthkumar, and Vimal*** *for their support*

I am thankful to my ever loving parents ***N. Selvamani, and S. Latha*** *who created my genes, and for their endless love. I am also very much grateful to my brother* ***Hari Prashanth*** *for his love and support.*

I am very grateful to my uncle and aunt in India ***Dr. S. Maruthamuthu, and M. Nageshwari*** *for their timely advice and love.*

Last but not least, I want to acknowlege my best friend and my husband ***Dr. M. Muralikannan*** *for being the wind beneath my wings.*

Cell Surface Display of Peptides to Recover Metals from Electronic Waste

Thesis for degree of Doctor of Philosophy

By

Vidhya Selvamani

has been approved by

위원장	교수	유익근
Committee Chair	Prof.	Yoo, Ik-Keun
위원	교수	류근갑
Committee Member	Prof.	Ryu, Kuen-Garp
위원	교수	홍순호
Committee Member	Prof.	Hong, Soon-Ho
위원	교수	강성구
Committee Member	Prof.	Kang, Sung-Gu
위원	교수	엄경태
Committee Member	Prof.	Eom, Gyeong-Tae

Department of Chemical Engineering and Bioengineering

University of Ulsan

December 2018

Table of Contents

NOMENCLATURE

Abbreviations used throughout the thesis are according to the recommendations of the IUPAC-IUBMB commission of biochemical nomenclature and of the ACS Style Guide.

Furthermore, the following abbreviations were used:

TCS	Two-component system
Kb	Kilo base (1000 base pairs)
bp	base pair
kD	Kilo Dalton
IPTG	Isopropyl ß-D-1-Thiogalactopyranoside
PCR	polymerase chain reaction
LB	Luria-Bertani broth
GFP	green fluorescent protein
SDS-PAGE	sodium dodecyl sulfate polyacrylamide gel electrophoresis

LIST OF TABLES

LIST OF FIGURES

Abstract

In an attempt to develop a system towards bioremediation of electronic waste (EW). Electronic have become an integral part of everyday life. The persistent growth in consumption and reduced life time of electrical and electronic goods resulted in piling up of EW. It is considered to be a huge problem for the environment. According to European Union 20 raw materials for the manufacture of electronics are at greater risk of supply. However EW can be considered as a valuable source of precious metals. Recycling of EW can mitigate high prices and limit reliance on exhaustible natural sources for metals. This study is focused recovery of lithium; cobalt and indium which are considered to be essential components for the manufacture of electronics. The technique employed in this study is microbial cell surface display (CSD) of metal binding peptides (MBP). CSD allows the expression of proteins, peptides and enzymes on the microbial surface with the aid of anchoring motif. In this study MBP for lithium, cobalt and indium are displayed on the surface of *E. coli*. Lithium and cobalt are rare and valuable elements used for its application in lithium-ion batteries (LIBs). Due to increased application of LIBs in portable electronic devices and vehicles, accumulation of spent batteries is huge. It is essential to recycle the spent LIBs.

In order to support a sustainable society based on renewable energy, it is necessary to explore appropriate recovery methods of lithium from various sources. Here we demonstrate a strategy for lithium extraction from battery polluted water using the whole-cell bio sorbent displayed lithium binding peptide (LBP). Three different lithium binding pentapeptides (GPGNP (LBP1), GPGDP (LBP2), and GPGAP (LBP3)) were displayed on the surface of *E. coli* as a fusion protein by cell surface display (CSD). The efficiency of the three different LBPs was evaluated in various environmental conditions such as Luria-Bertani (LB) medium,

artificially polluted wastewater (AWW) and lithium battery polluted wastewater (LBWW). Also, the lithium binding efficiency of the bio-sorbents was enhanced by developing dimeric, trimeric and tetrameric constructs. Among which trimeric construct of LBP_2 showed maximum lithium adsorption and the reason for the reduced performance by the tetrameric construct was determined by membrane topological study. The metal-peptide affinity resulted in the development of bio-friendly lithium nanoparticles on the surface of *E. coli* as visualized by Scanning Electron Microscopy (SEM) and Transmission Electron Microscopy (TEM). The application of surface displayed LBP system to the real wastewater was conducted by employing the LBWW for plant irrigation after lithium removal. **The method developed in this study describes a new path for green synthesis of metal nanoparticles and at the same time bioremediation of wastewater based on the design of synthetic peptides and their expression on the microbial surface.**

A recombinant *E. coli* was developed by cell surface engineering of cobalt binding peptide (CP1&CP2). The peptides were displayed with the aid of YiaT as an anchoring motif. The structure of the recombinant peptide (YiaTCP2 &YiaTCP3) was modelled. The difference in binding potential towards cobalt was evaluated. Further the ability of CP2 & CP3 to adsorb and recover cobalt was evaluated in three different environments including Luria-Bertani(LB), artificially polluted wastewater (AWW) and battery polluted wastewater (BWW). CP3 was observed to recover higher percentage of cobalt (1907.766 μmol/g drycell weight) when compared to CP2. Further the physio-chemical properties of recombinant cells after cobalt adsorption was characterized by fourier transform infrared spectroscopy (FT-IR), UV-Vis spectroscopy. The recombinant cells were exposed to cobalt at various pH (3, 5, 7, 9 and 11). The bound cobalt was observed to be a nano sized particles and visualized by

scanning emission microscopy (SEM) and transmission emission microscopy (TEM). The presence of cobalt on the cell surface was mapped by energy-dispersive X-ray spectroscopy (EDX). Further the recombinant strains bound with cobalt is used for photocatalytic reduction of methylene blue. The percentage of reduction was found to be 59.52%.

In Cell surface display the anchoring protein is vital for the efficient display of peptide on the microbial surface. In this study, a novel anchoring motif was developed with an outer membrane protein YaiO. Its topological study revealed the presence of 7 loops for the display. The loop 7 was truncated at 237^{th} amino acid residue to expose the peptides in the extracellular region. The efficiency of YaiO as an anchoring protein was evaluated by displaying indium binding peptides (IBP 1 & 2) SLAPDSTWFALF, TNSSSQEWAIP respectively. The ability of the displayed peptide to recover indium was analyzed. In addition, the recombinant *E. coli* were elongated by cisplatin treatment to increase the indium bio-adsorption. The cells with adsorbed indium were visualized by SEM and TEM techniques. The indium particles present on the bacterial surface was mapped by EDS analysis. Further Raman spectroscopy reveals that the indium is found as cubic In_2O_3.

Overview of Dissertation

The Dissertation on developing recombinant strains by synthetic biotechnology strategies for bioremediation of metals from the electronic waste like lithium (Li), Cobalt (Co), and Indium (In). This dissertation is structured as follows:

Chapter 1 covers the introduction of basic knowledge related to this work and objective significance of this work.

Chapter 2 describes **Lithium recovery as nanoparticles from lithium polluted water by cell surface displayed whole-cell bio-sorbent.**

Three Lithium binding peptides (LBP1, 2 & 3) were displayed on the surface of *E. coli* to recover lithium as nanoparticles from lithium polluted waste water. Further the lithium binding efficiency was enhanced by constructing dimeric, trimeric and tetrameric LBP repeats. The change in lithium recovering efficiency by these constructs was analysed by topological studies.

Chapter 3 describes **Cell surface display of cobalt binding peptide as whole-cell biocatalyst for photocatalytic reduction of methylene blue.** Recombinant *E. coli* was constructed to recover cobalt by cell surface display strategy. Two cobalt binding peptides (CP2 & 3) were displayed on the cell surface. The ability of this to recover cobalt was evaluated in three different environments LB, artificial wastewater (AWW), battery polluted wastewater (BWW). Further the photocatalytic reduction of the cell surface bound cobalt particles was studied.

Chapter 4 describes **Cell surface display of indium binding peptide with novel anchoring protein (yaiO**. The anchoring protein plays vital role in efficient display of carrier protein.

Considering this a novel anchoring protein was developed for cell surface display. An outer membrane protein YaiO was developed as an anchoring motif. Its loop structure was studied by topological studies. Further the loop seven was truncated to realize cell surface display of indium binding peptides (IP1 and IP2). The ability of this system to recover indium was evaluated.

Chapter — 1

Introduction

Chapter-1

1.1 Electronic waste (EW)

Electrical and electronic waste (EW) is generated when an electronic product is discarded after the end of its life. Nowadays, electronic and electrical equipment are vital part of everyday life. Common types of EW include the following;

- Infocomm technology (ICT) equipment, such as desktop, laptop and tablet computer, mobile phones, computer and mobile phone batteries, printer, peripherals and accessories such as keyboards, modems, monitors, computer mice, docking stations, hard disk drives, battery charges, etc.
- Home appliances, such as TVs, refrigerators, air conditioners, washing machines, rice cookers, microwave and toaster ovens, electric kettles, food processors and blenders, electric fans, DVD/video/music players, radios, hi-fis, vacuum cleaners, etc. Other types of e-waste include lamps and lighting devices, batteries, electronic toys, sports and leisure equipment, etc.

Recycling the EWW is necessary, it will reduce environmental pollution. Further the waste is rich in precious metals and valuable organic substance, it can be considered as a secondary raw material.

1.2 Impact of EWW towards environment

Roughly 40 million metric tons of EW are produced globally each year, and about 13% of that weight is recycled mostly in developing countries [1]. Informal recycling markets (developing countries) handle anywhere from 50% to 80% of this EW, often shredding, burning and dismantling the products in backyards. Emissions from these recycling practices are damaging human health and the environment [2]. Improper disposal of EW affects the soil, air and water components of the environment. Improper disposal of EW not only has

effect on the environment, it indirectly and ultimately poses stern dangers to humans and livestock (Fig. 1).

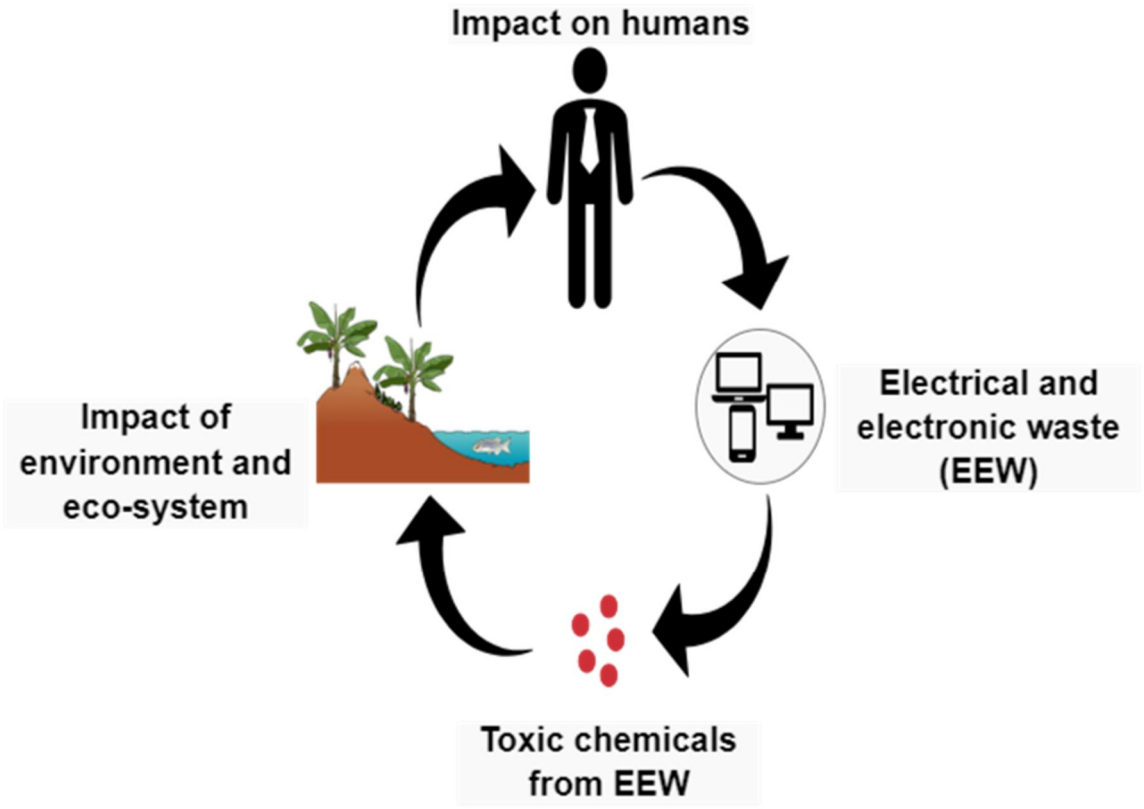

Figure 1.1. Improper disposal of electronic devices and its impacts on environment

1.2.1 Effects on soil

EW accounts for only 2% of the trash in landfills however; it is cause for 70% of the toxic heavy metals [3]. Soil is contaminated by EW in following ways;

- Through direct contact with contaminants from EW or byproducts of recycling and disposal.
- Indirectly through irrigation from contaminated water.

Thus it enters the "soil-crop-food pathway," one of the most significant routes for heavy metals exposure to humans. These chemicals are not biodegradable it persist in the environment for long periods of time, further increasing the risk of exposure. The danger is due to improper disposal on the environment ultimately having impacts on human beings. EW is suspected to cause following health effects which includes; birth defect (irreversible), brain, heart, liver, kidney and skeletal system damage[4]. EW is mostly made up of metal and plastic components, but also contains significant amounts of heavy metals and substances of concern (e.g., in printed circuit boards, batteries). EW is one of the fastest growing waste streams [5, 6]. The growing usage and shorter life time of the electronic devices has contributed in continuous increase in EW. An increasing amount of waste requires more land area for disposal further contributing in increased hazardous chemicals in the environment[7]. The increasing use of portable electronic devices is one of the primary reasons for increased disposal of portable batteries [6]. Lithium-ion batteries are the most commonly used type in portable electronic devices.

1.2.2 Effects on water

The electronics containing metals such as lead, barium, mercury, lithium (found in mobile phone and computer batteries), etc., are improperly disposed, these metals leach through soil and reach groundwater channels which eventually run to the surface as streams or small ponds of water. The toxic chemical and metals present in water causes death of plants and animals. Upon consuming the contaminated waters humans and animals may get exposed to toxic effects of metals. Toxins such as lead, mercury and cadmium (found in printed circuit boards and other electronics) impact the nervous and reproductive system[3]. Some of the heavy metals present in EW were considered to be carcinogenic.

Bioaccumulation of heavy metals within organisms like fish lead to contamination up the food chain, all the way to humans and are the primary route of exposure for many people to heavy metals.

1.2.3 Effect on air

Air can be contaminated by EW primarily when it is transported to countries where recycling processes are poorly regulated. In these countries the EW is often dismantled and shredded, releasing dust or large particulates into the immediate environment where the respiratory health of workers without proper respiratory protection is damaged chronically. Informal recycling of EW not only affects health of workers sometimes it can migrate to thousand miles away from the recycle site. As EW can be considered as valuable secondary raw materials it is burnt to extract lower cost products this causes release of dioxins into environment. Dioxins are linked with several forms of cancer, as it is fat soluble and hydrophobic, they accumulated and remain in body for a lifetime. Burning also releases fine particles leads chronic damage to respiratory health also increases the risk of wide range of chronic diseases including cancer. Precious metals of higher costs such as gold, silver etc., are extracted using acids, desoldreing and other chemical techniques further releasing toxic fumes. Open burning can result in release of hydrocarbons into the air [3].

1.3. Lithium-ion battery (LIB)

Batteries are considered to contain various toxic chemicals and metals. Primarily lithium-ion batteries are the most common battery type used in portable electronic devices and their use is expect to double from 2014 to 2020. According to environmental protection agency, Americans alone buy approximately three billion dry-cell batteries each year to power common household devices, including radios, toys phones and computers. Since 1990s,

lithium ion batteries (LIBs) have been widely used in portable electronic devices and electric vehicles [8-10] . Rechargeable lithium based batteries have displaced nickel-cadmium and nickel metal hydride batteries to become the dominant energy supply components in portable consumer electronic products. The advantages include superior energy density and slow discharge in idle mode[11], it lead to adoption of lithium batteries in electric vehicles, military, and aerospace applications[12]. The intention towards replacing cars that run on petrol and diesel with electric cars could leave us with big battery waste problem. The composition of battery varies with its size, application and cathode material. The relative shorter life span of rechargeable lithium ion batteries in portable electronic devices is leading the substantial increase in hazardous EW and is one of the fastest growing waste streams in U.S[13, 14]. Spent LIBs are a new kind of waste that is different from other kinds of solid waste. The purpose of recycling spent LIBs is to reduce or eliminate potential environment impacts; on the one hand, the purpose of recycling spent LIBs is to reduce or eliminate potential environment impacts. Further recycling also yields valuable metals, thus promotes the sustainable development of the LIB industry and industrial upgrading[15].

A LIB is usually contains a cathode, an anode, electrolyte, a separator and so on [16-19].The cathode materials of LIBs are mainly lithium intercalation oxides, such as $LiNiO_2$, $LiMnO_4$, $LiCoO_2$, $LiFePO_4$, $LiNi_xCo_yMn_{1-x-y}O_2$ and so on [20-22]. A typical Li-ion battery is composed of toxic metals and organic chemicals such as lithium, cobalt, nickel, copper, lead and electrolytes respectively (Fig. 2).

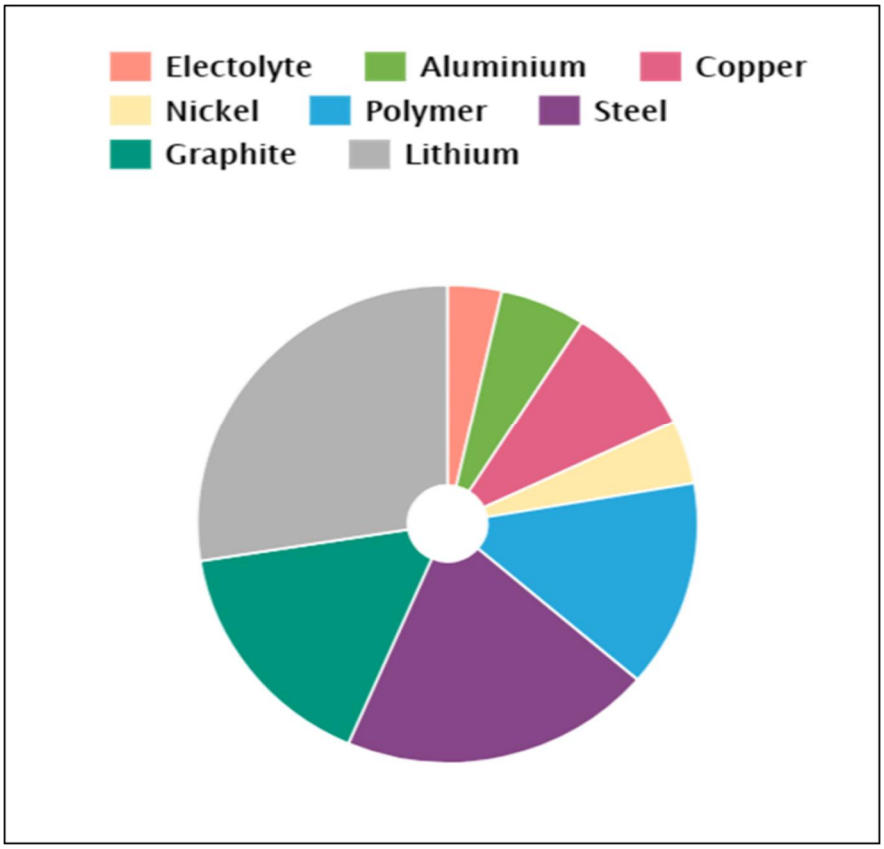

Figure 1.2. Composition of a typical Lithium ion battery

The compositions of the batteries were used to estimate the value for one ton of waste batteries (Table 1.1) [23-25]. LIBS have been considered to be greener and cleaner energy storage devices than other batteries because of their higher voltage, high energy density, low self-discharge efficiency, and lower harmfulness to the environment. However, it is still a threat to the environment and to human health due to the presence of few hazardous materials [15]. Human The lack of uniform regulatory policy on the disposal of Lithium batteries may contribute to environmental pollution and adverse human health impacts due to potentially toxic materials[12]. Human and environmental exposure to these toxic chemicals are regulated during the manufacture of lithium batteries through

occupational health and safety laws however there is inconsistent policy about the fate of discarded lithium batteries in EW that is distributed internationally [13, 26, 27].

A study reported that the battery contained high levels of aluminium (51800 to 341000 mg/Kg), cobalt (58000 to 278000 mg/Kg)), copper (54100 to 152000 mg/Kg) and lithium (9800 to 37200 mg/Kg). In article they also estimated the highest level measured in lithium batteries and regulatory threshold for hazardous waste (Fig. 3). These metals accounted for 97.32% of total metals of lithium batteries. From the economic point of view it will profitable to recover lithium and cobalt from the cathode material as it contributes the major part of LIB.

Table 1.1. Estimated value of major metals present lithium based batteries

Material	Price ($AUD/ton)	$AUD available/ton batteries
Nickel	18684.00	803.40
Aluminium	2464	135.55
Copper	8168	735.10
Steel	567	114.60
Lithium cobalt oxide	36370	10001.75

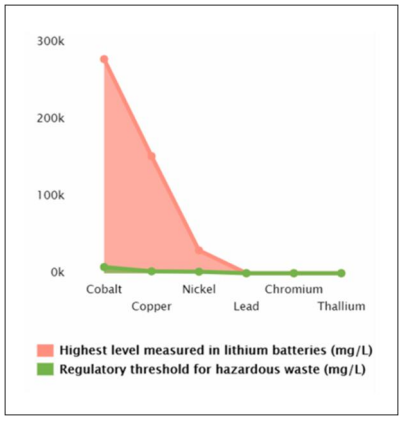

Figure 1.3 A comparison between hazardous metals present in lithium batteries vs regulatory threshold of respective metals in hazardous waste.

1.4. Metals recovered in this study

1.4.1. Lithium

Lithium is the lightest metal and has the ability to convert chemical energy into electrical energy (1). It is used in a variety of industries which includes construction, pharmaceuticals, ceramics, glass, automotive and battery industry. Lithium-ion batteries (LIBs) are extensively used as a power source in mobile phones, personal computers, video-cameras, electric vehicles and other modern-life appliances [28]. Due to superior electrochemical properties of lithium, it is considered as an attractive alternative to other metals for batteries [29, 30]. Higher concentration of lithium might have inhibited plant growth [31].

1.4.2. Cobalt

Cobalt (Co) is a naturally found element, a heavy metal, with versatile application. It is essential for animal metabolism as it is an important component of vitamin B_{12}. It is naturally found in the earth's crust combined form. Since ancient times cobalt is used in jewelry and paints for its distinct blue colour. In recent times it is effectively incorporated in making alloys, batteries, and electroplating. Around 40% of the world's cobalt is used for rechargeable batteries. Cobalt is used in the manufacture of super alloys, lithium ion batteries, oxidation catalysts, and as pigments in paints [32]. The allowable limits of cobalt in the irrigation water and cattle wastewater are 0.05 and 1.0 ppm, correspondingly. However, higher concentration of cobalt has deep ill-effects resulting in contact dermatitis, paralysis, lung irritation, bone defects, [33] low blood pressure, paralysis, diarrhea, lung irritation and bone defects [34].

1.4.3. Indium

Indium is as a soft ductile, manleable, lustrous metallic metal. Industrial emissions of indium are already larger than natural emissions. All indium compounds should be regarded as highly toxic. Indium compounds damage the heart, Kidney and liver and may be teratogenic. On its own indium ore is not available in earth's crust, it is extracted as a by-product of sulphide ore processing. Indium is extensively used in the manufacture of electronics especially in Liquid crystal display (LCD). Indium tin oxide coatings employed as a conductive film on the surface of LCD screens. It is used in flat screen TV's, mobile phones, computer, laptop's etc. These electronic scraps could be considered as an alternative secondary source for indium.

1.5. Metal recovery from spent EW

The methods available for the recovery of metals present in EW are pyro metallurgy, hydrometallurgy, and bio metallurgy[15] (Table 1.2).

Table 1.2. The advantages and disadvantages of the each process

Process	Advantages	Disadvantages	Environmental hazards
Pyro metallurgy	Great capacity, simple operation	High temperature, high energy consumption, low metal recovery rate	Waste gas, dust
Hydrometallurgy	Low energy consumption, high metal recovery rate, high product purity	Long recovery process, high chemical reagents consumption	Wastewater
Bio metallurgy	Low energy consumption, mild operating conditions, high metal recovery rate	Long reaction period, bacteria are difficult to cultivate	Wastewater

1.5.1 Microbial approach towards metal recovery

Alternatively microbes towards recovery of metals present in the EW can be considered cost effective and eco-friendly [35-38]. Bioleaching is another process in which microbes (bacteria, fungi) to transform solid compounds resulting in soluble and extractable elements[39]. This approach can be employed to recover metals from industrial residues[40]. From the industrial point of view this as a very promising technology for sustainable development[41]. Lower cost and higher efficiency at low metal concentrations make biotechnological processes very attractive in comparison to physicochemical methods for heavy metal removal [36]. The microbial processes for bioremediation of toxic metals and radionuclides from waste streams employ living cells, nonliving biomass, or biopolymers as biosorbents [36, 37, 42]. A wide variety of fungi, algae, and bacteria have been used as biosorbents for heavy metal remediation [36, 37, 42].

1.5.2 Cell surface engineering of microorganisms towards metal adsorption

A variety of approaches were carried out to display MBP on the microbial surface. One of the successful approaches is to employ outer membrane proteins as anchoring proteins for the display of MBP.

Microbial cell surface display of heterologous proteins on the bacterial surfaces has been an area of interest in synthetic biology, after the first report of this novel technology got published in 1986 by Freud et al. The surface display of heterologous proteins is usually made possible by translational fusion of target protein to one of the naturally occurring anchoring motif. The gram negative bacteria, which hold an inner cell membrane and an outer membrane, with a peptidoglycans cell wall in between. Therefore in order to conduct cell surface display, the proteins should cross both the cytoplasmic and the outer membrane before the display on the cell surface. This work was done by the protein called anchoring

motifs. The various anchoring motifs are OmpA, OmpC, LamB, OprF, PhoE, OmpS, OmpX, InP etc [43]. Many of these surface display applications were studied for various applications as a whole cell catalyst for environmental sensing and adsorption [43-54]. It is one of the efficient ways to engineer the whole cell as biocatalyst towards bioremediation. CSD allows peptide and protein display on the microbial surface as a fusion protein [46]. The advantage of developing whole cell biocatalyst makes the prepared simply culturing the cells, further reduces time, cost and purification [55]. The extracellular localization of the peptide eases the toxicity associated with heterologous peptide [55].

1.5.3 Metal binding peptides

Biomining of metals is a well-known biotechnological approach for processing ores in the mining industry [56]. Bacteria and higher organisms have developed resistance mechanisms to toxic metals to make them harmless. It respond to heavy metal stress using different defense systems, such as exclusion, compartmentalization, making complexes and the synthesis of binding proteins such as metallothioneins (MTs) or phytochelatins (PCs) [57]. Novel metal binding peptides (MBP) might offer a higher metal binding capacity, specificity and selectivity for the target metal ion. These peptides with unique binding properties can either be designed de novo or selected by screening peptide libraries[57].

Metal binding by the biomolecules like proteins and peptides can be considered as fortuitous. However, the affinities of metal ion towards biomolecules depend on the metal ions, as well as on the reactivity of the provided ligands. The principles governing the selectivity of biomolecules for metal ions are described as HSAB (hard and soft acids and bases) principle and Irwing-Williams series of stability constants for divalent ions. Anchoring of specific amino acid sequences to biosorbents material could contribute to the selectivity

for specific metal ions[58]. A stronger biosorbents could be identified by HSAB principles. The metal accumulation by bacterial can be increased by enriching bacterial surface with these ligands than those naturally present on the microbial surfaces[58, 59]. Surface exposure these metal binding peptides (MBP) can significantly enhance the metal recovery by the peptides [35, 38]. Several MBP's have been studied and displayed with the aim of increasing metal accumulation by the *E. coli*[60].

1.7. Research objective

The advent growth in electronic industry led to increase in demand for the metals used in manufacture of electronic. Additionally this paved the way to introduce of toxic metals into environment. It is high time to develop a cost effective metal recovery system to overcome the growing demand and depletion of natural resources. In this study, CSD of specific metal binding peptides were employed to recover metals. Further the application of recovered metals was studied;

- Lithium (Li) – Lithium recovery as nanoparticles from lithium polluted water by cell surface displayed whole-cell biosorbents.
- Cobalt (Co) – Cell surface display of cobalt binding peptide as whole-cell biocatalyst for photocatalytic reduction of methylene blue.
- Indium (In) – Cell surface display of indium binding peptide with novel anchoring protein (YaiO)

References

1. Abboud Y, Eddahbi A, Bouari A, Aitenneite H, Brouzi K, Mouslim J (2013) Microwave-assisted approach for rapid and green phytosynthesis of silver nanoparticles using aqueous onion (Allium cepa) extract and their antibacterial activity. *J Nanostruct Chem* 3.

2. Abedini A, Daud AR, Hamid MAA, Othman NK, Saion E (2013) A review on radiation-induced nucleation and growth of colloidal metallic nanoparticles. *Nanoscale Res Lett* 8.

3. (e-waste) IoW.

4. Abbaszadegan A, Ghahramani Y, Gholami A, Hemmateenejad B, Dorostkar S, Nabavizadeh M, Sharghi H (2015) The effect of charge at the surface of silver nanoparticles on antimicrobial activity against gram-positive and gram-negative bacteria: a preliminary study. J Nanomat.

5. (2013) StEP Initiative"E-waste world map reveals national volumes, international flows,".

6. Boyden A, Soo VK, Doolan M (2016) The Environmental Impacts of Recycling Portable Lithium-Ion Batteries. *Procedia CIRP* 48, 188-193.

7. Tammemagi HY (1999) The Waste Crisis: Landfills, Incinerators, and the Search for a Sustainable Future. 1 edition.

8. Li J, Wang G, Xu Z (2016) Environmentally-friendly oxygen-free roasting/wet magnetic separation technology for in situ recycling cobalt, lithium carbonate and graphite from spent LiCoO2/graphite lithium batteries. *Journal of Hazardous Materials* 302, 97-104.

9. Wang M-M, Zhang C-C, Zhang F-S (2016) An environmental benign process for cobalt and lithium recovery from spent lithium-ion batteries by mechanochemical approach. *Waste Management* 51, 239-244.

10. Guo Y, Li F, Zhu H, Li G, Huang J, He W (2016) Leaching lithium from the anode electrode materials of spent lithium-ion batteries by hydrochloric acid (HCl). *Waste Management* 51, 227-233.

11. BCC Research. Lithium Batteries: Markets and Materials; BCC ResearchLLC: Wellesley M (October 2009).

12. Kang DHP, Chen M, Ogunseitan OA (2013) Potential Environmental and Human Health Impacts of Rechargeable Lithium Batteries in Electronic Waste. *Environmental Science & Technology* 47, 5495-5503.

13. Ogunseitan OA, Schoenung JM, Saphores J-DM, Shapiro AA (2009) The Electronics Revolution: From E-Wonderland to E-Wasteland. *Science* 326, 670-671.

14. (September 2005) U.S. Environmental Protection Agency. Introduction to Hazardous Waste Identification (40 CFR Parts 261) EPA530-K-05-012; US EPA: Washington, DC

15. Zheng X, Zhu Z, Lin X, Zhang Y, He Y, Cao H, Sun Z (2018) A Mini-Review on Metal Recycling from Spent Lithium Ion Batteries. *Engineering* 4, 361-370.

16. Xu J, Thomas HR, Francis RW, Lum KR, Wang J, Liang B (2008) A review of processes and technologies for the recycling of lithium-ion secondary batteries. *Journal of Power Sources* 177, 512-527.

17. Ordoñez J, Gago EJ, Girard A (2016) Processes and technologies for the recycling and recovery of spent lithium-ion batteries. *Renewable and Sustainable Energy Reviews* 60, 195-205.

18. Takacova Z, Havlik T, Kukurugya F, Orac D (2016) Cobalt and lithium recovery from active mass of spent Li-ion batteries: Theoretical and experimental approach. *Hydrometallurgy* 163, 9-17.

19. Yang L, Xi G, Xi Y (2015) Recovery of Co, Mn, Ni, and Li from spent lithium ion batteries for the preparation of LiNixCoyMnzO2 cathode materials. *Ceramics International* 41, 11498-11503.

20. Yang Y, Huang G, Xu S, He Y, Liu X (2016) Thermal treatment process for the recovery of valuable metals from spent lithium-ion batteries. *Hydrometallurgy* 165, 390-396.

21. Wang J, Sun X (2015) Olivine LiFePO4: the remaining challenges for future energy storage. *Energy & Environmental Science* 8, 1110-1138.

22. Nam K-M, Kim H-J, Kang D-H, Kim Y-S, Song S-W (2015) Ammonia-free coprecipitation synthesis of a Ni–Co–Mn hydroxide precursor for high-performance battery cathode materials. *Green Chemistry* 17, 1127-1135.

23. (2014) London Metal Exchange: Pricing & data,.

24. Fox-Davies (Sep-2013.) The Lithium Market.

25. Keat CL, Aziz A, Eid AM, Elmarzugi NA (2015) Biosynthesis of nanoparticles and silver nanoparticles. *Bioresources and Bioprocessing* 2, 47.

26. Pant D, Singh A, Van Bogaert G, Irving Olsen S, Singh Nigam P, Diels L, Vanbroekhoven K (2012) Bioelectrochemical systems (BES) for sustainable energy production and product recovery from organic wastes and industrial wastewaters. *RSC Advances* 2, 1248-1263.

27. Schoenung JM, Ogunseitan OA, Saphores JDM, Shapiro AA (2004) Adopting Lead-Free Electronics: Policy Differences and Knowledge Gaps. *Journal of Industrial Ecology* 8, 59-85.

28. Nan J, Han D, Zuo X (2005) Recovery of metal values from spent lithium-ion batteries with chemical deposition and solvent extraction. *Journal of Power Sources* 152, 278-284.

29. Fergus JW (2010) Recent developments in cathode materials for lithium ion batteries. *Journal of Power Sources* 195, 939-954.

30. Zu C-X, Li H (2011) Thermodynamic analysis on energy densities of batteries. *Energy & Environmental Science* 4, 2614-2624.

31. Shahzad B, Tanveer M, Hassan W, Shah AN, Anjum SA, Cheema SA, Ali I (2016) Lithium toxicity in plants: Reasons, mechanisms and remediation possibilities – A review. *Plant Physiology and Biochemistry* 107, 104-115.

32. Vilvanathan S, Shanthakumar S (2015) Biosorption of Co(II) ions from aqueous solution using Chrysanthemum indicum: Kinetics, equilibrium and thermodynamics. *Process Safety and Environmental Protection* 96, 98-110.

33. Harreither W, Sygmund C, Augustin M, Narciso M, Rabinovich ML, Gorton L, Haltrich D, Ludwig R (2011) Catalytic Properties and Classification of Cellobiose Dehydrogenases from Ascomycetes. *Applied and environmental microbiology* 77, 1804-1815.

34. Oguz E, Ersoy M (2014) Biosorption of cobalt(II) with sunflower biomass from aqueous solutions in a fixed bed column and neural networks modelling. *Ecotoxicology and Environmental Safety* 99, 54-60.

35. Diels L, S. Van Roy, M. Mergeay, W. Doyen, S. Taghavi, and R. Leysen. (1993) Immobilization of bacteria in composite membranes and development

of tubular membrane reactors for heavy metal recuperation. *In R. Peterson (ed.), Effective membrane processes: new perspectives. KluwerAcademic Publishers, Dordrecht, The Netherlands.*

, p. 275–293.

36. Gadd GM (1992) Microbial control of heavy metal pollution, . *InJ. C. Fry, G. M. Gadd, R. A. Herbert, C. W. Jones, and I. A. Watson-Craik(ed.), Microbial control of pollution. Cambridge University Press, Cambridge,United Kingdom.*, p. 59–87.

37. Macaskie LE, and A. C. R. Dean. (1990.) Metal sequestering biochemicals, In B. Volesky (ed.), Biosorption of heavy metals. CRC Press,Boca Raton, Flap. 200–248. .

38. Macaskie LE, A. C. R. Dean, A. K. Cheetham, R. J. B. Jakeman, and A. J., . S (1987) Cadmium accumulation by Citrobacter sp.: the chemicalnature of the accumulated metal precipitate and its location on the bacterialcells. . *J. Gen. Microbiol.* 133:539–544.

39. Krebs W, Brombacher C, Bosshard PP, Bachofen R, Brandl H (1997) Microbial recovery of metals from solids. *FEMS Microbiology Reviews* 20, 605-617.

40. Torma AE (1988) Leaching of metals. In: Biotechnology, . *Verlag Chemie, Weinheim.* Vol. 6b, pp. 367–399. .

41. OECD ((1994)) Biotechnology for a Clean Environment: Prevention, Detection, Remediation. Organisation for Economic Cooperation and Development, Paris.

42. Volesky B, and Z. S. Holan (1995) Biosorption of heavy metals. *Biotechnol.Prog.* 11:235–250.

43. Wernérus H, Ståhl S (2004) Biotechnological applications for surface-engineered bacteria. *Biotechnology and Applied Biochemistry* 40, 209-228.

44. Cruz N, Le Borgne S, Hernández-Chávez G, Gosset G, Valle F, Bolivar F (2000) Engineering the Escherichia coli outer membrane protein OmpC for metal bioadsorption. *Biotechnology Letters* 22, 623-629.

45. Ferri S, Nakamura M, Ito A, Nakajima M, Abe K, Kojima K, Sode K (2015) Efficient surface-display of autotransporter proteins in cyanobacteria. *Algal Research* 12, 337-340.

46. Lee SY, Choi JH, Xu Z (2003) Microbial cell-surface display. *Trends in Biotechnology* 21, 45-52.

47. Li P-S, Tao H-C (2015) Cell surface engineering of microorganisms towards adsorption of heavy metals. *Critical Reviews in Microbiology* 41, 140-149.

48. Liu Y, Zhang R, Lian Z, Wang S, Wright AT (2014) Yeast cell surface display for lipase whole cell catalyst and its applications. *Journal of Molecular Catalysis B: Enzymatic* 106, 17-25.

49. Ramos J-L, Marqués S, van Dillewijn P, Espinosa-Urgel M, Segura A, Duque E, Krell T, Ramos-González M-I, Bursakov S, Roca A, Solano J, Fernádez M, Niqui JL, Pizarro-Tobias P, Wittich R-M (2015) Laboratory research aimed at closing the gaps in microbial bioremediation. *Trends in Biotechnology* 29, 641-647.

50. Tsai D-Y, Tsai Y-J, Yen C-H, Ouyang C-Y, Yeh Y-C (2015) Bacterial surface display of metal binding peptides as whole-cell biocatalysts for 4-nitroaniline reduction. *RSC Advances* 5, 87998-88001.

51. van Bloois E, Winter RT, Kolmar H, Fraaije MW (2011) Decorating microbes: surface display of proteins on Escherichia coli. *Trends in Biotechnology* 29, 79-86.

52. Wu CH, Mulchandani A, Chen W (2008) Versatile microbial surface-display for environmental remediation and biofuels production. *Trends in Microbiology* 16, 181-188.

53. Xu Z, Lee SY (1999) Display of Polyhistidine Peptides on the Escherichia coli Cell Surface by Using Outer Membrane Protein C as an Anchoring Motif. *Applied and Environmental Microbiology* 65, 5142-5147.

54. Yim S, An S, Han M-J, Choi J, Jeong K (2013) Isolation of a Potential Anchoring Motif Based on Proteome Analysis of Escherichia coli and Its Use for Cell Surface Display. *Appl Biochem Biotechnol* 170, 787-804.

55. Wendel S, Fischer EC, Martínez V, Seppälä S, Nørholm MHH (2016) A nanobody:GFP bacterial platform that enables functional enzyme display and easy quantification of display capacity. *Microbial Cell Factories* 15, 71.

56. Schippers A. HS, Vasters J., Drobe M., Sand W., Willscher S. In: (2013) Biomining: Metal Recovery from Ores with Microorganisms. *Geobiotechnology I. Advances in Biochemical Engineering/Biotechnology, Springer, Berlin, Heidelberg* 141.

57. Mejáre M, Bülow L (2001) Metal-binding proteins and peptides in bioremediation and phytoremediation of heavy metals. *Trends in Biotechnology* 19, 67-73.

58. Huber AL, Holbein BE, Kidby D (1990) Metal uptake by synthetic and biosynthetic chemicals. *Biosorption of heavy metals*, 249-292.

59. Macaskie LE, Dean AC (1990) Metal-sequestering biochemicals. *Biosorption of heavy metals*, 199-248.

60. Kotrba P, Dolečková L, de Lorenzo V, Ruml T (1999) Enhanced Bioaccumulation of Heavy Metal Ions by Bacterial Cells Due to Surface Display of Short Metal Binding Peptides. *Applied and Environmental Microbiology* 65, 1092-1098.

CHAPTER – 2

Lithium recovery as nanoparticles from lithium polluted water by cell surface displayed whole-cell bio-sorbents

Chapter-2

2.1 Abstract

In order to support a sustainable society based on renewable energy, it is necessary to explore appropriate recovery methods of lithium from various sources. Here we demonstrate a strategy for lithium extraction from battery polluted water using the whole-cell bio sorbent displayed lithium binding peptide (LBP). Three different lithium binding pentapeptides (GPGNP (LBP1), GPGDP (LBP2), and GPGAP (LBP3)) were displayed on the surface of *E. coli* as a fusion protein by cell surface display (CSD). The efficiency of the three different LBPs was evaluated in various environmental conditions such as Luria-Bertani (LB) medium, artificially polluted wastewater (AWW) and lithium battery polluted wastewater (LBWW). Also, the lithium binding efficiency of the bio-sorbents was enhanced by developing dimeric, trimeric and tetrameric constructs. Among which trimeric construct of LBP_2 showed maximum lithium adsorption and the reason for the reduced performance by the tetrameric construct was determined by membrane topological study. The metal-peptide affinity resulted in the development of bio-friendly lithium nanoparticles on the surface of *E. coli* as visualized by Scanning Electron Microscopy (SEM) and Transmission Electron Microscopy (TEM). The application of surface displayed LBP system to the real wastewater was conducted by employing the LBWW for plant irrigation after lithium removal. The method developed in this study describes a new path for green synthesis of metal nanoparticles and at the same time bioremediation of wastewater based on the design of synthetic peptides and their expression on the microbial surface.

2.2 Introduction

Lithium is recognized as “the 21st-century oil” due to its wide application in different

areas, especially in energy technology[1]. It is used in a variety of industries which includes construction, pharmaceuticals, ceramics, glass, automotive and battery industry. The global energy mix is expected to move from traditional carbon-based fuel towards a cleaner electricity-based and therefore the significance of lithium; a major substance in the battery is emphasized. Lithium-ion batteries (LIBs) are extensively used as a power source in mobile phones, personal computers, video cameras, electric vehicles, and other modern-life appliances[2-4]. In 2017, the worldwide production of lithium excluding U.S. production amounted to 43 thousand metric tons [5], which is seven times higher than that in 1995.

The market has grasped this circumstance, with the value of lithium increasing sharply year after year. The average price of lithium has increased by threefold since 2014 and expected to increase further [6]. Like petroleum in the 20^{th} century, lithium is not distributed evenly around the world and around 85% of the world's reserves are controlled by few countries known as the "lithium triangle" including Chile, Bolivia and Argentina [7]. Analysts at Morningstar predicted 100,000 tonnes a shortfall in lithium supply by 2025. In order to support the growing demands on lithium, it is necessary to explore appropriate recovery methods for various sources besides processing brine and spodumene.

Most electronic devices contain a variety of valuable metals and they can be used to establish a sustainable society based on recycling. According to the European Union (EU) around 24 kg of electrical and electronic waste is generated every year per citizen, this also includes a lithium discharge from high-tech industries [8]. Additionally, around 1,289 tons and 297 tons of LIB and lithium primary batteries respectively were collected by EU in the year 2010, which is only about 5% of lithium battery in the market. EU also has strict regulation towards the collection, recycling, and disposal of lithium batteries. Thus recycling

lithium can be employed to prevent environmental pollution[2]. Spent lithium batteries can be considered as a secondary raw material for lithium as it contains valuable materials [9]. A survey reported that the exhausted lithium batteries could exceed 25 billion units and 500 thousand tonnes by 2020 [10]. Thus the demand for recycling the spent LIB's is necessary for environmental protection as well as economic returns.

To recover valuable substances including lithium from effluent containing electronic wastes in a green manner, a method of selectively recovering them without further contamination is required. Many efforts have been made aiming at finding ways for lithium recovery such as chemical precipitation[11], electrochemical[12], and hydrothermal method[13]. But, these methods require heat or electricity as a driving force and harsh conditions due to the use of corrosive acids.

In this study, we tried biosorbents designed for selective recovery of lithium and bioremediation. Biomolecules such as peptides and nucleic acids have high affinity to specific metals and these sorbents could be designed and prepared elaborately by biotechnological tools. Several works have been reported regarding the preparation of designed peptides or proteins for metal recovery[14, 15]. A bio-based process is generally perceived as an environmentally benign approach, involving mild operating conditions and minimized energy input. However, direct use of the peptides or proteins is not suitable to recycle metals from wastes. The biomolecule itself is so expensive caused by purifying costs and also, it is difficult to achieve a high loading of the peptides in the process due to their small size. Cell surface display (CSD) of metal binding peptides (MBP) is a promising strategy to address these problems in terms of high cost and low operability and it is one of the efficient ways to engineer the whole cell as a bioagent towards bioremediation. CSD

allows peptide and protein display on the microbial surface as a fusion protein [16]. The advantage of developing whole cell biosorbents allows simple preparation, thus reducing time and cost for purification[17]. In addition to this, the extracellular localization of the peptide eases the toxicity associated with heterologous peptide[17]. CSD has been successfully employed in various platforms like bacteria, yeast, and phage[16]. Bacterial CSD has received more attention because of its simplicity and applicability towards industries. One of the efficient applications of bacterial CSD is to develop biosorbents for the recovery and removal of harmful chemicals and metals[18-23]. Engaging biotechnological method favours metal recovery even at lower concentrations[24].

Recently, we designed synthetic peptides having sequences of GPGXP (Glycine-Proline-Glycine- Asparagine or Aspartate or Alanine -Proline) [25] for extracting lithium from seawater based on the reports on the complexation of cyclic peptides and lithium ion[26]. In this study, we prepared whole-cell biosorbents by displaying these lithium binding peptides on the surface of recombinant *Escherichia coli* and applied them to lithium battery polluted wastewater (LBWW) for metal recovery and bioremediation. First, the CSD of the GPGXP (LBP1-3) on the *E. coli* was done by engaging OmpC as an anchoring motif. The presence of lithium binding peptide (LBP) was visualized by fusing GFP with the OmpC-LBP construct. Also, the ability of LBP on the surface of the microbes to selectively adsorb lithium ions was investigated using various environments including Luria-Bertani (LB) medium containing lithium ions, artificial polluted (AWW) wastewater composed of various metals and the real lithium battery polluted wastewater (LBWW). To enhance the performance of the whole-cell biosorbents, dimeric, trimeric and tetrameric constructs of OmpC-LBP were constructed and evaluated. Lithium binding properties of the fusion protein were interpreted by topological

studies. Also, physical and chemical properties of the recovered lithium particles were analyzed by field emission scanning emission spectroscopy (FE-SEM), transmission electron microscopy (TEM), Fourier-transform infrared spectroscopy (FT-IR), UV-Vis spectroscopy and Raman spectroscopy. To our knowledge, this study is a first report to demonstrate the novelty of the LBP displayed sorbents towards the green recovery of lithium from wastewater as nanoparticles. Finally, the real world application of this system was evaluated by employing LBWW after lithium removal for the growing *Brassica nigra*. These results describe the multifaceted application of LBP towards recovery, particle biosynthesis and bioremediation of lithium polluted water.

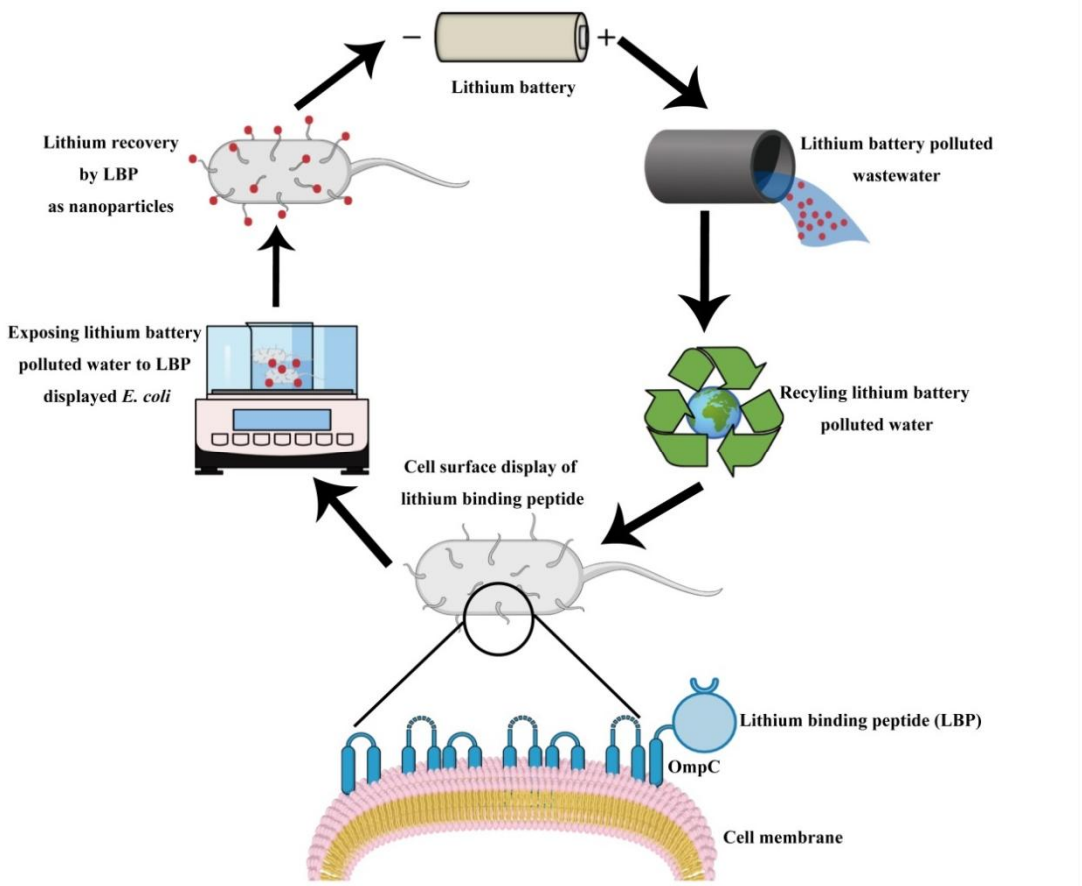

Fig. 2.1 Schematic representation of lithium binding peptide displayed on the surface of recombinant E. coli. The recombinant *E. coli* was engineered to selectively recover lithium present in lithium polluted waste water (LPWW). The recycled water was used for irrigation. Further the recovered lithium could be used for the battery manufacture.

In the present study, selective recovery of lithium was performed by CSD of LBP_1 (GPGDP) was displayed on *E.coli* surface. This was realized by integrating the peptide at the 8^{th} loop of OmpC. The efficiency of the recombinant peptide (OmpC-LBP_1) to recover lithium was evaluated in artificial wastewater (AWW) the recovered lithium was quantitatively measured by atomic absorption spectroscopy (AAS). Further, the ability of the engineered *E. coli* to be reused was determined. Lithium recovery was enhanced by developing constructs containing dimeric, trimeric and tetrameric LBP1 displayed *E. coli*.

2.3 Materials and methods

2.3.1 Construction of OmpC-LBP (1-3) x (1-4) expression plasmids

Primarily pET21a plasmid was used in this study for cloning and expression of OmpC-LBP(1-3) x (1-4). The fusion protein OmpC-LBP was cloned into the plasmid using *NdeI* and *BamHI* restriction enzymes. The fusion protein was constructed by integrating LBP1-3 at 8^{th} loop (993 bp) of truncated OmpC. The genes were amplified by polymerase chain reaction (PCR) with an MJ Mini Personal Thermal Cycler (Bio-Rad Laboratories, Hercules, CA, USA) using the Expand High Fidelity PCR system (Roche Molecular Biochemicals, Mannheim, Germany). The nucleotide sequences of the LBP peptides used in this study are listed in Table 1. Further dimeric (OmpC-LBP (1-3)x2), trimeric (OmpC-LBP(1-3)x3), and tetrameric (OmpC-LBP(1-3)x4) of the fusion peptide were also constructed. The recombinant plasmids were transformed into *E. coli* BL21 and cultivated in LB (Luria-Bertani) media for protein expression studies. Further, the *gfp* was cloned downstream of *ompC-LBP* using *BamHI* and *HindIII* restriction enzymes.

Table 2.1. Primers used in this work

Name	Sequence (5' to 3')
OmpC_F	**CATATG**AGGAGAAATATAATGAAAGTTAAAGTACTGTCCCTCCTGGTC
LBP1x1_R	**GGATCC**GGGTTGCCCGGGCCCATGTTTTTGTTGAAGTAGTAGGTAGCACCAACATCAACATA
LBP1x2R	**GGATCC**CGGGTTGCCCGGGCCCGCTTTCGCCGCCGCTTCCGCCGGGTTGCCCGGGCCCATGTTTTTGTTGAA
LBP1x3_OL_F	AAAACATGGGCCCGGGCAACCCGGCGGAAGCGGCGGCGAAAGCGGGCCCGGGCAACCCGGCGGAAGCGGCGGCGAAAGCG
LBP1x3_OL_R	CCGCTTCCGCCGGGTTGCCCGGGCCCGCTTTCGCCGCCGCTTCCGCCGGGTTGCCCGGGCCCGCTTTCGCCGCCGCTTCCGC
LBP1x3_R	**GGATCC**TTATTACGGGTTGCCCGGGCCCGCTTTC
LBP1x4_R	**GGATCC**GGATCCTTATTACGGGTTGCCCGGGCCCGCTTTCGCCGCCGCTTCCGCCGGGT
LBP2x1_R	**GGATCC**CGGATCGCCCGGGCCCATGTTTTTGTTGAAGTAGTAGGTAGCACCAACATCAACA
LBP2x2R	**GGATCC**GCCCGGGCCCGCTTTCGCCGCCGCTTCCGCCGGATCGCCCGGGCCCATGTTTTTGTTGAAGTA
LBP2x3_OL_F	GGCCCGGGCGCGCCGGCGGAAGCGGCGGCGAAAGCGGGCCCGGGCGCGCCGGCGGAA
LBP2x3_OL_R	CGGGCCCGCTTTCGCCGCCGCTTCCGCCGGCGCGCCCGGGCCCGCTTTCGCCGC
LBP2x3_R	**GGATCC**TTATTACGGATCGCCCGGGCCCGC
LBP2x4_R	**GGATCC**GGATCCTTATTACGGATCGCCCGGGCCCGCTTTCGCCGCCGCTTCCGCCGATCGCCCGGGCC
LBP3x1_R	**GGATCC**TTATTACGGCGCGCCCGGGCCCATGTTTTTGTTGAAGTAGTA
LBP3x2R	**GGATCC**TTATTAGGCGCGCCCGGGCCCGCTTTCGCCGCCGCTTCCGCCGGCGCGCCCGGGCC
LBP3x3_OL_F	GGCCCGGGCGCGCCGGCGGAAGCGGCGGCGAAAGCGGGCCCGGGCGCGCCGGCGGAA
LBP3x3_OL_R	CGGGCCCGCTTTCGCCGCCGCTTCCGCCGGCGCGCCCGGGCCCGCTTTCGCCGC
LBP3x3_R	**GGATCC**TTATTACGGCGCGCCCGGGCCCGC
LBP3x4_R	**GGATCC**TTATTAGGCGCGCCCGGGCCCGCTTTCGCCGCCGCTTCCGCCGGCGCGCCCGGGCC
GFP_F	**GGATCC**CATATGCAGTCTAAAGGAGAAGAACTTTTCACTGGAGTTGTCCCAATTCTT
GFP_R	**AAGCTT**TTACTCGATTATTAATGGTGATGGTGATGGTGTTTGTATAGTT

2.3.2 Recombinant *E. coli* growth conditions

The recombinant *E. coli* displaying the LBP (1-3) x (1-4) were cultured overnight in LB medium at 37 ^{o}C, and the cultures were then diluted 100-fold in the same. After reaching an optical density at 600 nm (OD600) reached 0.5, IPTG was added to the culture broth at different concentrations of 0 to 1 mM and further incubated at 30^{o}C for 5 h. The recombinant strains were harvested by centrifuging at 13,000 rpm for 10 minutes and incubated with B-7M urea buffer at room temperature for 30 minutes with agitation. The cells were centrifuged at 8,000 rpm to remove cell debris. The outer membrane fractions from the cell pellet were separated by adding 10 mM Tris-HCl (pH 7.5) and the suspended cells were kept in 4 ^{o}C overnight. The lifted the membrane fractions were analyzed by 12% (w/v) sodium dodecyl sulfate-polyacrylamide gel electrophoresis (SDS-PAGE)[27] and stained with Coomassie brilliant blue R-250 (Bio-Rad Laboratories, Hercules, CA, USA).

2.3.3. Fluorescence microscopy analysis of OmpC-LBP display

The display of the fusion protein (OmpC-LBP) was analyzed by a fluorescence microscope. The recombinant *E. coli* harboring OmpC-LBP-GFP was cultured and expressed by the addition of IPTG. The cells were centrifuged and washed with phosphate buffer saline (PBS) and immobilized with a thin layer of 1% agarose in PBS medium[28]. Fluorescence microscopy images were obtained using a reflected fluorescence microscope with a cooled, charge-coupled device camera (Photometric cool snap of Arizona, USA) using a 100X oil immersion objective (Olympus, Uplanfi, Japan). MetaMorph image analysis software was used to record the emission intensity

with the respective filters optimized for EGFP imaging (Molecular Devices, USA) [29].

2.3.4 Lithium recovery studies

The recombinant protein expressed cells were harvested by centrifugation and washed twice with 0.85% (w/v) of NaCl. The cells were incubated with varying concentration lithium chloride solution (0-20 mM). The specificity of the displayed peptide towards lithium was also evaluated. To realize this AWW containing lithium chloride (LiCl), copper chloride ($CuCl_2$), cobalt chloride ($CoCl_2$), chromium chloride ($CrCl_3$) 1000 ppm each was prepared. The real world application of this lithium recovery system was evaluated with LBWW. It was prepared by incubating lithium battery overnight in water (20g Li-coin cells). The adsorption experiment was performed at 25 ^oC for 30 minutes with agitation. After performing adsorption the cells were centrifuged and washed twice with 0.85% (w/v) of NaCl to remove the unbound lithium. The adsorbed lithium was eluted by incubating the cells with 1 mM EDTA for 30 minutes in ice. The eluted lithium was quantitatively measured using atomic absorption spectrophotometry (AA-7000, Shimadzu, Kyoto, Japan).

2.3.5 Molecular modeling and topological study

The possible sites of lithium binding by LBP were evaluated. Homologous model of OmpC-LBP1-3 was constructed using modeler [30, 31]. A search for potential structural templates was carried out using the Blastp tool against the protein databank (PDB) with default parameters[32]. The OmpC-LBP1-3 was aligned with the template sequence obtained from PDB using the align2D tool of Modeler. Based on the sequence alignment protein structure, homology models were constructed with the

default parameters. Further, the difference in lithium recovery by OmpC-LBP x (1-4) was determined by a topological study using betware predictor in bologna biocomputing group.

2.3.6 FE-SEM and TEM analysis

The properties of the lithium recovered by OmpC-LBP displayed *E. coli* was analyzed using Scanning emission microscopy (SEM) and Transmission emission microscopy (TEM). After lithium recovery, the recombinant strains were visualized by FE-SEM (JEOL JSM-6500F) and TEM. After washing the cells were fixed by incubating at 4^{o}C in 2.5% glutaraldehyde for 14 h. The fixed cells were washed with PBS and then the cells were mounted on ultra-flat silicon wafers and dried to visualize it on a field emission scanning emission microscopy (FE-SEM). Further, lithium recovered by the recombinant *E. coli* was visualized by TEM. The bacterial samples for the analysis were prepared using the drop-casting method. Sterile copper grids were coated with 20 µl of lithium adsorbed recombinant *E. coli* dissolved in PBS. After 3 minutes the majority of the liquid on the grid was removed by touching the edges using filter paper. Further, the grids were washed and air dried. The samples were visualized by TEM.

2.3.7 Bioremediation of LBWW using the OmpC-LBP system

An experiment was performed to observe the effect of lithium polluted water on the plant growth. Three different pots (a, b and c) were planted with mustard seeds (*Brassica nigra*). Each pot was watered regularly with water, LBWW, and LBWW after lithium recovery respectively. The growth of the plants in the pots a, b, and c was monitored regularly. Further, the stomatal quality of the leaves was observed using a

microscope. Leaves from the pot a, b, and c were gathered and coated with xylene on the lower epidermis. After drying the lower epidermis was peeled and stained with trypan blue (Sigma, USA) to visualize the stomata. Reflected microscope with a cooled, charge-coupled device camera (Photometric cool snap cf Arizona, USA) using a 100×objective (Olympus, Uplanfi, Japan). MetaMorph image analysis software was used to record the emission intensity with the respective filters optimized for EGFP imaging (Molecular Devices, USA)

2.3.8 Physiochemical characterization recovered lithium

The properties of the lithium recovered by OmpC-LBP displayed *E. coli* was analyzed using Fourier transform infrared spectroscopy (FT-IR), UV-Vis spectroscopy, and Raman spectroscopy.

2.3.9 FT-IR analysis

FT-IR (Nicolet iS5, Thermoscientific, Omnic spectra) analysis was carried out to determine the changes in functional groups after lithium recovery. Recombinant *E. coli* after lithium recovery were harvested and washed. The cells were lyophilized by EYELA FDU-2200 freeze dryer. The dried bacteria biomass was mixed and ground with 150 mg of KBr in a mortar. Translucent disks were prepared by pressing with a pressure bench press. The cell pellets were immediately analyzed with a spectrophotometer in the range of 4000-400 cm^{-1} with the resolution of 4 cm^{-1}. The influence of atmospheric water and CO_2 were subtracted from every measurement.

2.3.10 UV-Vis spectroscopy

Based on the Raman spectroscopic results, UV-Vis spectroscopic analysis was performed using Specord 210 plus and WinAspect plus software. Lithium adsorption

by OmpC-LBP displayed cells were performed in varying pH conditions (3, 5, 7, 9 and 12). The spectrum was recorded from 190nm to 1000nm.

2.3.11 Raman spectroscopy

The properties of lithium adsorbed by recombinant *E. coli* harboring OmpC-LBP was evaluated by Raman spectroscopy (Thermo- scientific, DXR Raman microscope 532nm full range). After adsorption, the cells were washed and lyophilized using EYELA FDU-2200 freeze dryer. Wild-type *E. coli* was included in the study as a control.

2.4. Results and discussion

2.4.1 Construction of CSD system with OmpC-LBP(1-3) x (1-4)

The surface display of the LBP (1-3) was executed as a fusion protein with outer membrane protein OmpC [20, 33, 34]. The fusion protein was cloned into the pET21a vector resulting in plasmids pET21LBP (1-3) respectively (Table 2.2 and fig. 2.2). The expression of the recombinant protein was induced by the addition of isopropyl β-D-1-thiogalactopyranoside (IPTG) regulated by the T7 promoter. Further dimeric, trimeric and tetrameric constructs of the recombinant strains were constructed by increasing the LBP repeat separated by a linker.

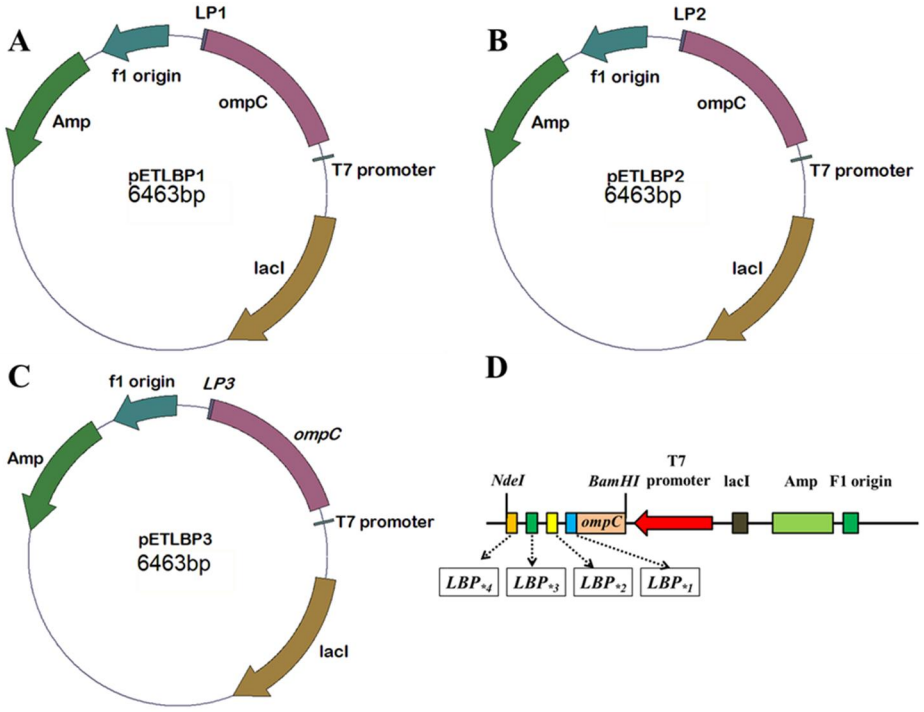

Fig. 2.2 Construction of recombinant plasmids. (A) OmpC-LBP1 (pETLBP1), (B) OmpC-LBP2 (pETLBP2) and (C) OmpC-LBP3 (pETLBP3) regulated by T7 promoter. The LBP repeats were increased to construct monomeric (OmpC-LBP (1-3) x 1), dimeric (OmpC-LBP (1-3) x 2), trimeric (OmpC-LBP (1-3) x 3) and tetrameric (OmpC-LBP (1-3) x 4) recombinant peptide constructs (D) respectively.

Table 2.2 List of bacterial strains and plasmids used in this study

Strain/Plasmid	Relevant genotype/ property	Source
BL21 (DE3)	*F– ompT gal dcm lon hsdS$_B$*(r_B^- m_B^-) *λ*(*DE3* [*lacI lacUV5-T7 gene 1 ind1 sam7 nin5*])	Novagen
TOP10	*F- mcrA Δ*(*mrr-hsdRMS-mcrBC*) *φ80lacZΔM15 ΔlacX74 nupG recA1 araD139 Δ*(*ara-leu*)*7697 galE15 galK16 rpsL*(*Str^R*) *endA1 λ-*	Stratagene
Plasmids		
pET-21a	ApR	NEB[a]
pETLBP1 x 1	pET-21a containing *ompC-LBP*1x1	This work
pETLBP1 x 2	pET-21a containing *ompC-LBP*1x2	This work
pETLBP1 x 3	pET-21a containing *ompC-LBP*1x3	This work
pETLBP1 x 4	pET-21a containing *ompC-LBP*1x4	This work
pETLBP2 x 1	pET-21a containing *ompC- LBP*2x1	This work
pETLBP2 x 2	pET-21a containing *ompC- LBP*2x2	This work
pETLBP2 x 3	pET-21a containing *ompC- LBP*2x3	This work
pETLBP2 x 4	pET-21a containing *ompC- LBP*2x4	This work
pETLBP3 x 1	pET-21a containing *ompC-LBP3*	This work
pETLBP3 x 2	pET-21a containing *ompC-LBP3*x2	This work
pETLBP3 x 3	pET-21a containing *ompC-LBP3*x3	This work
pETLBP3 x 4	pET-21a containing *ompC-LBP3*x4	This work
pETLBPGFP1	pET-21a containing *ompC*-gfp	This work

[a]New England Biolabs, Beverly, MA, U.S.A.

2.4.2 SDS-PAGE analysis

The expression of heterologous protein in *E. coli* results in metabolic liability, this leads to reduced protein expression, cell growth, and instability of recombinant plasmid[35]. It is essential to study and optimize the expression of the heterologous protein. The recombinant plasmids contain a T7 promoter and are induced by the addition of IPTG. The

concentration of IPTG (0.0-1.0 mM) was varied to optimize the expression of the OmpC-LBP1-3 peptide. The expression of the recombinant peptide (LBP (1-3) x (1-4)) was analyzed by SDS PAGE (Fig. 2.3). Optimum protein expression was observed with 0.5 mM of IPTG.

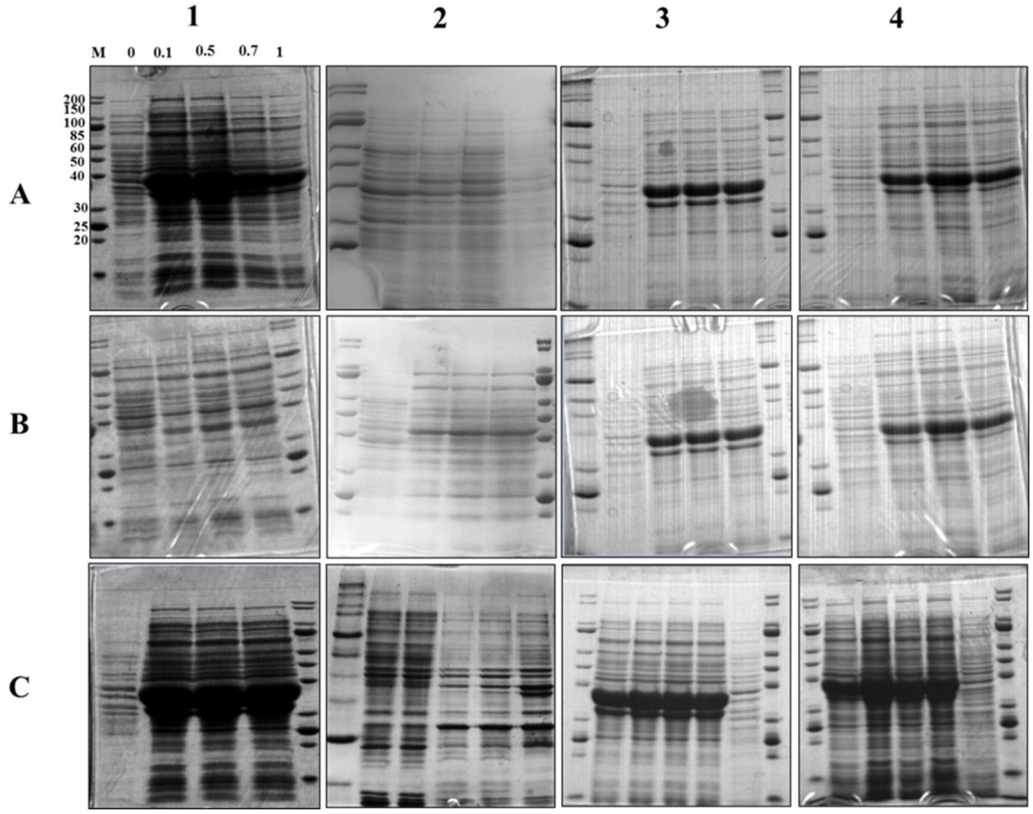

Fig. 2.3 Recombinant protein expression analysis (OmpC-LBP$_{2*(1-4)}$), SDS-PAGE analysis of all four peptides was performed. The effect of IPTG (0, 0.1, 0.5, and 1 mM) on recombinant peptide expression was determined. A$_{(1-4)}$ OmpC-LBP 1 x (1-4), B$_{(1-4)}$ OmpC-LBP 2 x (1-4), and C$_{(1-4)}$ OmpC-LBP 3 x (1-4). (OmpC-LBP x (1-4) 37, 38, 40.6 and 41.9 KDa respectively). M. Molecular weight marker in KDa.

2.4.3 Validation of LBP display by fluorescence microscopy

The ability to localize the OmpC-LBP on *E. coli* cell surface was validated by fluorescence microscopy with the help of GFP (Fig. 2.4). A *gfp* was cloned downstream of the OmpC-LBP resulting in pETLBPG1. The cell harboring the recombinant plasmid with

GFP was expressed by the addition of IPTG. Wild-type *E. coli* was included as a control. *E. coli* containing petLBPG1 plasmid was induced with 0.5 mM IPTG. After expression, the cells were harvested by centrifugation and washed. The cells were diluted with PBS and 10 µl of cells were mounted on a glass slide. The recombinant cells were observed under a fluorescence microscope. The cells display OmpC-LBP-GFP appeared as fluorescent halos, is an indication of cell surface localization of the recombinant protein (OmpC-LBP-GFP)[36].

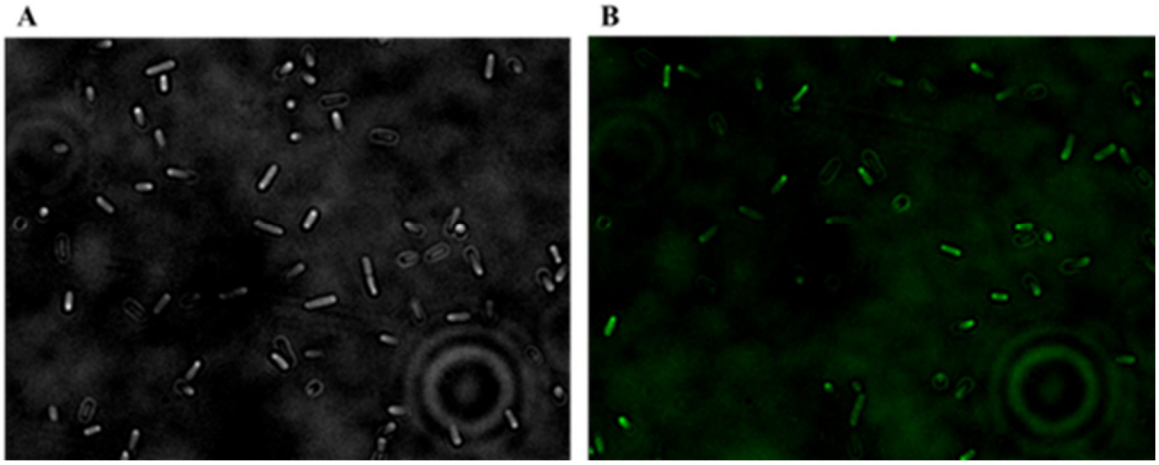

Fig. 2.4 Cell surface localization of OmpC-LBP by fluorescence microscope. (A) Wild-type *E. coli* and (B) Recombinant *E. coli* with OmpC-LBP-GFP.

2.4.4 Lithium recovery study in various environments

After the expression of recombinant peptide, OmpC-LBP (1-3) x (1-4), the cells were harvested by centrifugation. The cells were washed with NaCl and used for lithium recovery studies. It is essential to optimize the conditions like temperature, time of exposure of lithium for optimal recovery (Fig. 2.5). The cells were employed to recover lithium from LiCl solution of varying concentrations (0-20 mM) (Fig. 2.6 A). Further, the specificity of the peptides was analyzed with AWW (Fig. 2.6 B). The application of the current system to real

wastewater was evaluated by exposing the recombinant cells to LBWW (Fig. 2.6 C). Among the three peptides, LBP2 showed maximum lithium recovery in all three environments.

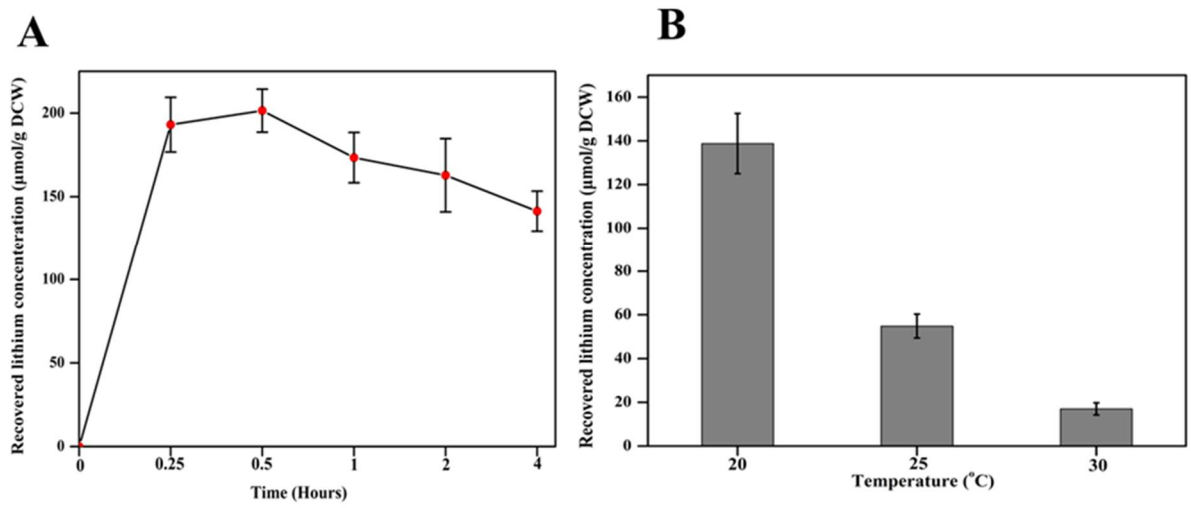

Fig. 2.5 Optimization of lithium recovery conditions by recombinant *E. coli.* (A) Effect of time on lithium recovery and (B) Effect temperature on lithium recovery.

Lithium recovery by monomeric LBP2 displayed *E. coli* was 267.33 µmol/g DCW. Though the adsorption amounts of lithium by the peptide continued to increase with an increase in lithium concentration a decline in the rate of recovery was observed hence, the experiment was limited to 20 mM. Also increasing the number on the peptide repeats[22] increased lithium recovery. However, lithium recovery declined with the tetrameric LBP displayed *E. coli*. The trimeric construct of LBP2 (OmpC-LBP2x3) containing recombinant *E. coli* showed maximum adsorption of lithium (3240.187 µmol/g DCW). Insignificant lithium recovery was observed with control strain without LBP. A study examined lithium recovery with 70 microorganisms (20 bacteria, 18 actinomycetes, 18 fungi and 14 yeasts). Among which 2 strains were *E. coli* and it accumulated 2.9 and 16.0 µmol/g DCW of lithium respectively [37]. Thus the increased lithium recovery by our system is mainly due to the LBP display on the surface of *E. coli*.

LBP prepared in this study showed the high specificity for lithium over other metals. In the experiment with AWW, the specificity of the sorbents was in the order of Li > Cu > Co > Cr. Similarly, with specific study of the peptides with AWW, the trimeric construct LBP2 x 3 showed maximum recovery. The observed results prove that the valuable metals could be selectively recovered using the peptide design and the surface display on the recombinant bacteria. Further, the recovery of lithium present in LBWW was performed with the recombinant strains. Analogous to previous studies the trimeric construct of LBP2x3 exhibited maximum lithium recovery. The concentration of lithium present in the LBWW was 1855.51 µmol/g DCW. This system managed to recover about 50.13% (925.42 µmol/g DCW) of lithium from LBWW in 30 minutes. Hartono et al., recovered 62.83% of lithium by mixed bacterial strains isolated from Mount merapi soil samples only after 15days of anaerobic incubation **[38].** In the present study, *E. coli* displayed with a specific peptides LBP (1-3) managed to recover a higher concentration of lithium. Considering the increasing demand for lithium It is essential to develop an efficient system to recover lithium from spent batteries [39] otherwise it would end up in environment.

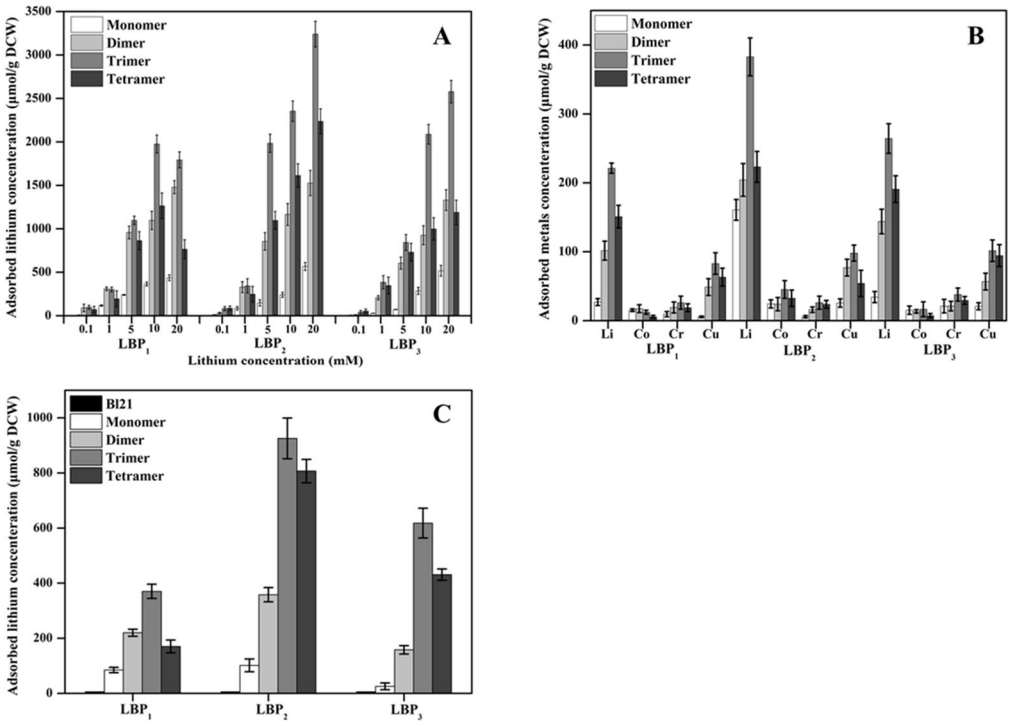

Fig.2.6 Lithium bio-adsorption studies with lithium binding peptide displayed *E. coli* in A, LB medium, B, AWW and C, LBWW. All the experiments were independently performed in triplicates and the standard deviation was determined.

2.4.5 Molecular modeling and topological study of LBP

The lithium binding properties of recombinant protein OmpC-LBP (1-3) was determined by constructing a homologous model using modeler (Fig. 2.7 A-C). The crystal structure coordinates of the peptide LBP3 (GPGAP) was obtained from a previous report [40]. The structures of LBP1 and LBP2 were generated by using the mutagenesis wizard in PyMOL software. The peptides were found to have cyclic conformation. The free form of the peptides has two intramolecular H-bonds between Glycine (1), Alanine (4) and Glycine (1), Glycine (3) respectively. These two bonds are responsible for the peptide stability. The carbonyl oxygens of the proline (2), glycine (3), and proline (5) in the peptide were responsible for the binding of lithium

[41]. The red spheres depict the preferred sites for lithium binding. A study reported by Anderson et al., 1997 showed the order of lithium-ion affinities towards the twenty common amino acids [42]. Among all glycine is the amino acid to show a third higher affinity towards lithium[42]. Thus the presence of two glycine residues might have favored to lithium binding property for LBP (1-3). The peptide molecule displayed on the cell surface contain functional groups conferring negative charges favors the possibility of adsorbing metal cations[43]. However, the charges of amino acids disappear after integration into peptide structure[44]. The amino acid aspartic acid has a side chain, which allows the maintenance of negative charge even after the introduction into the peptide structure[44]. This might be the reason behind increased lithium recovery by the peptide GPGDP (LBP2).

The decline in lithium recovery ability by tetrameric peptide construct was determined by performing topological studies (fig. 2.8). Based on the study LBP repeats found the monomeric, dimeric and trimeric construct was available in the periplasmic region. However, with the tetrameric construct, two repeats of LBP fell into transmembrane and only two repeats were available in the extracellular region. The differences in location of peptide repeats might be the cause for the reduced lithium recovery by the tetrameric LBP. Further three dimensional structures of OmpC-(LBP) x (1-4) were constructed (Fig. 2.9). The color cyan depicts the OmpC, colors pink and green denotes LBP repeats localized in the periplasm and the transmembrane region.

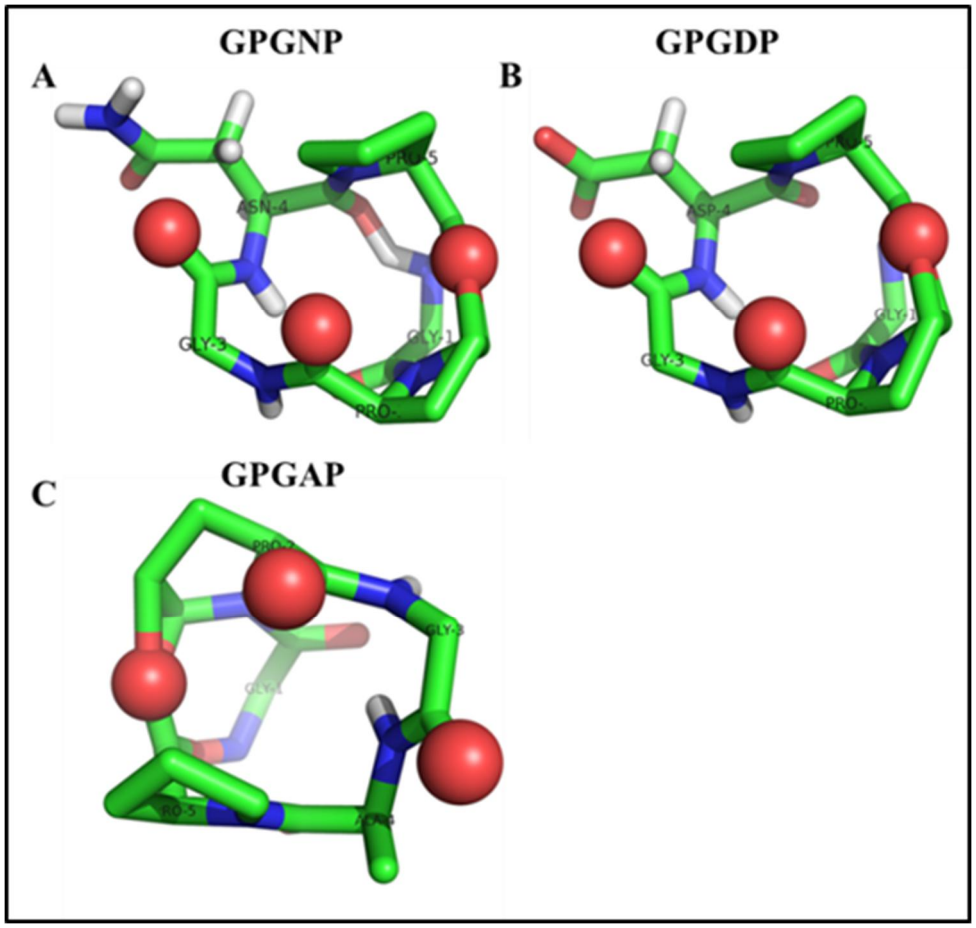

Fig. 2.7 Molecular model of the peptide OmpC-LBP(1-3); the red sphere structure represents the possible sites lithium binding. (A) OmpC-LBP1, (B) OmpC-LBP2, (C) OmpC-LBP3

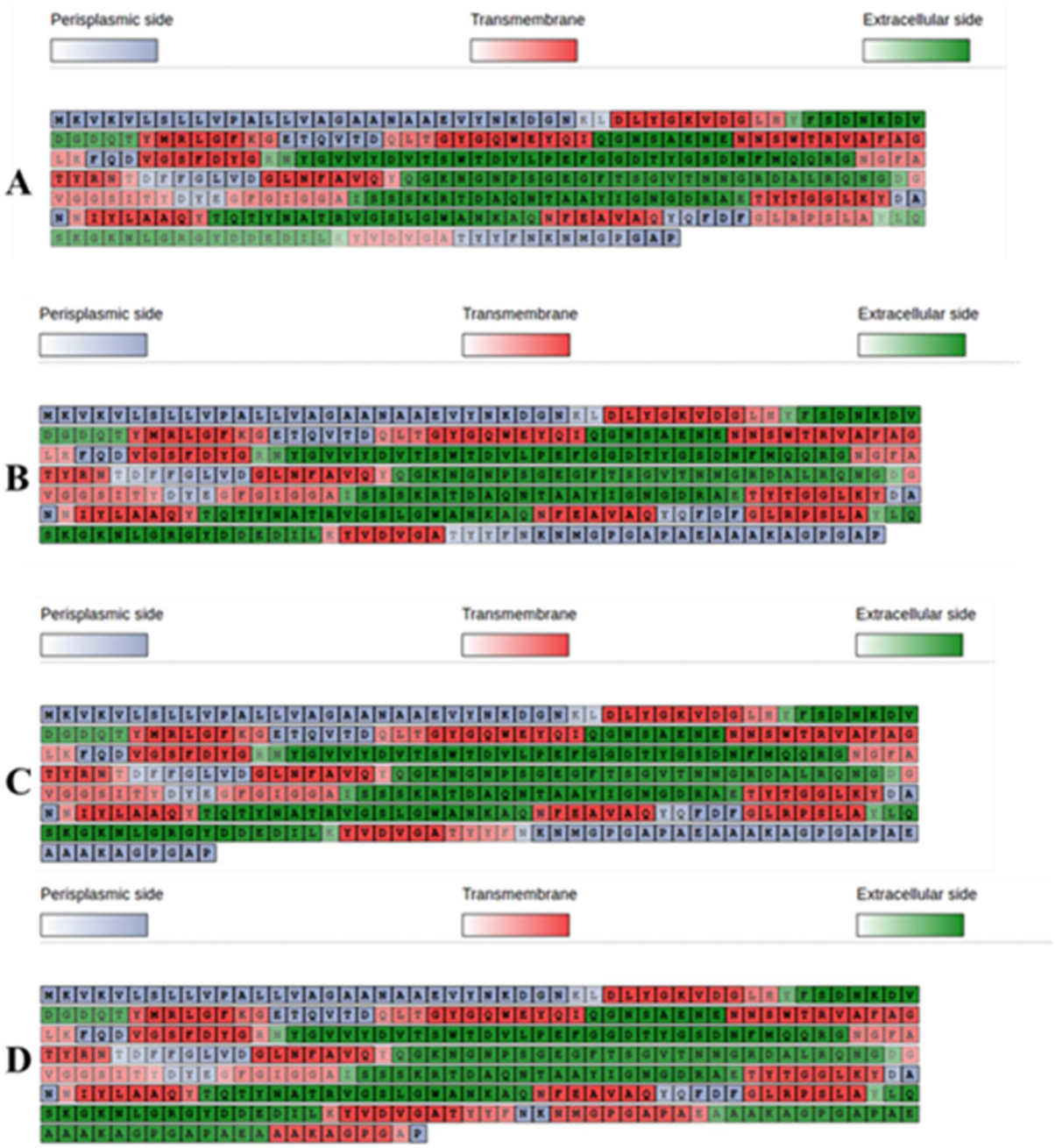

Fig. 2.8 Topological characterization of cell surface displayed LBP. (A) Monomer, (B) Dimer, (C) Trimer, and (D) Tetramer respectively. The colors grey, red and green represents periplasm, transmembrane and extracellular regions of *E. coli* membrane respectively.

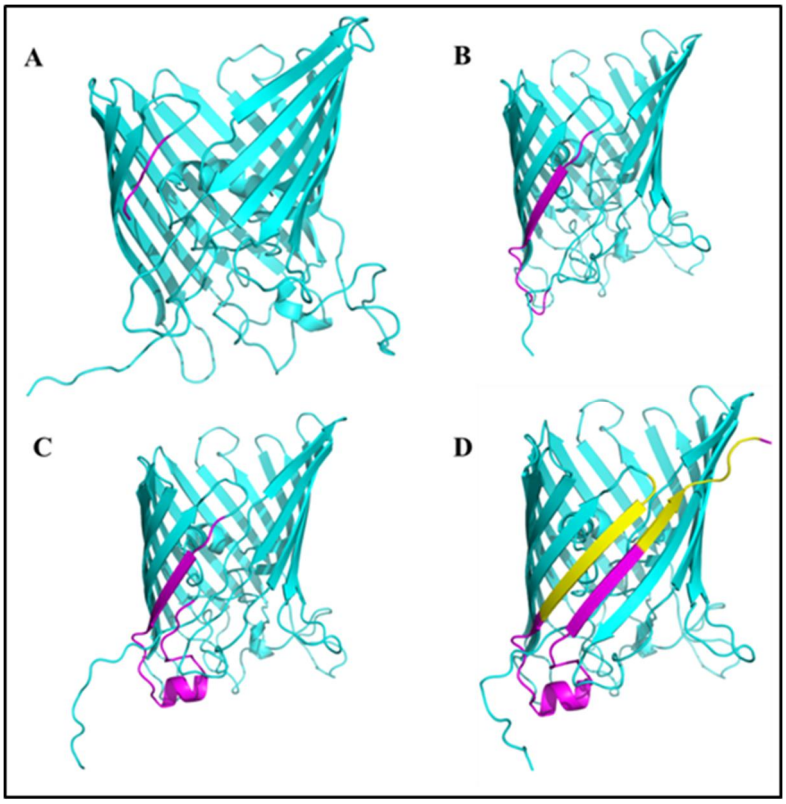

Fig. 2.9 Three-dimensional structure of OmpC-LBP$_{*(1-4)}$ (A-D). The color cyan and pink represents OmpC and LBP.

2.4.6 FE-SEM and TEM analysis

It is remarkable that nanoparticles were found on the surface of recombinant *E. coli* (OmpC-LBP) after lithium recovery with a 20 mM lithium solution. The size of the nanoparticles was about 25 -100 nm and mostly attached to the cell wall as revealed by FE-SEM and TEM (Figs. 2.10 B and 2.10 D). However, wild-type *E. coli* (BL21) which has no lithium binding site did not induce the formation of nanoparticles although the cell was similarly incubated with lithium solution (Figs. 2.10 A and 2.10 C). It is believed that the dark nanoparticles in TEM images of the recombinant *E. coli* are inorganic nanoparticles of lithium salt. As explained in the lithium recovery study, lithium ions are adsorbed onto the wall of recombinant *E. coli* from the solution because the cell surface has numerous binding

sites for lithium ions. After the cell was washed with PBS and dried, the nanoparticles of lithium salt could be formed near the cell wall where lithium ions were locally accumulated. It is intriguing that most of the nanoparticles were attached to the cell wall. This implies that nanoparticles were formed at the cell wall by epicellular mineralization[45]. Previous studies reported by various groups have demonstrated the biosynthesis of inorganic particles such as gold, platinum, silver, cobalt, palladium and calcium carbonate by metal binding peptides[36, 46-49]·[50]. The mineralization involves the precipitation of inorganic materials by reaction of ions on the cell wall. The cell wall provides binding sites that produce localized regions of high density of metal ions. These sites can accumulate ions locally and increase a high supersaturation to induce the association of ion clusters and furthermore to form solid nanoparticles at the cell wall.

The surface morphology of recombinant *E.coli* was analyzed by FE-SEM and TEM after performing lithium recovery with lithium solutions (1-100 mM) (Fig. 2.11). While any noticeable amount of nanoparticles was not produced at 0.1 mM, nanoparticles remarkably appeared at the cell surfaces after treatment with solutions of concentration larger than 1 mM. It should be noted that the number of the nanoparticles adsorbed onto the cell wall was increased by increasing lithium concentration. The amount of lithium adsorbed onto the cell surface is closely related to the concentration of the lithium solution. The more the solution contains lithium ions, the more the recombinant cell binds the ions. Therefore, the formation of nanoparticles could be enhanced by the increased number of adsorbed lithium ions. It is also notable that the cells were disintegrated when treated with 100 mM solution. This may be caused by toxicity exhibited to *E. coli* at high concentration lithium [51].

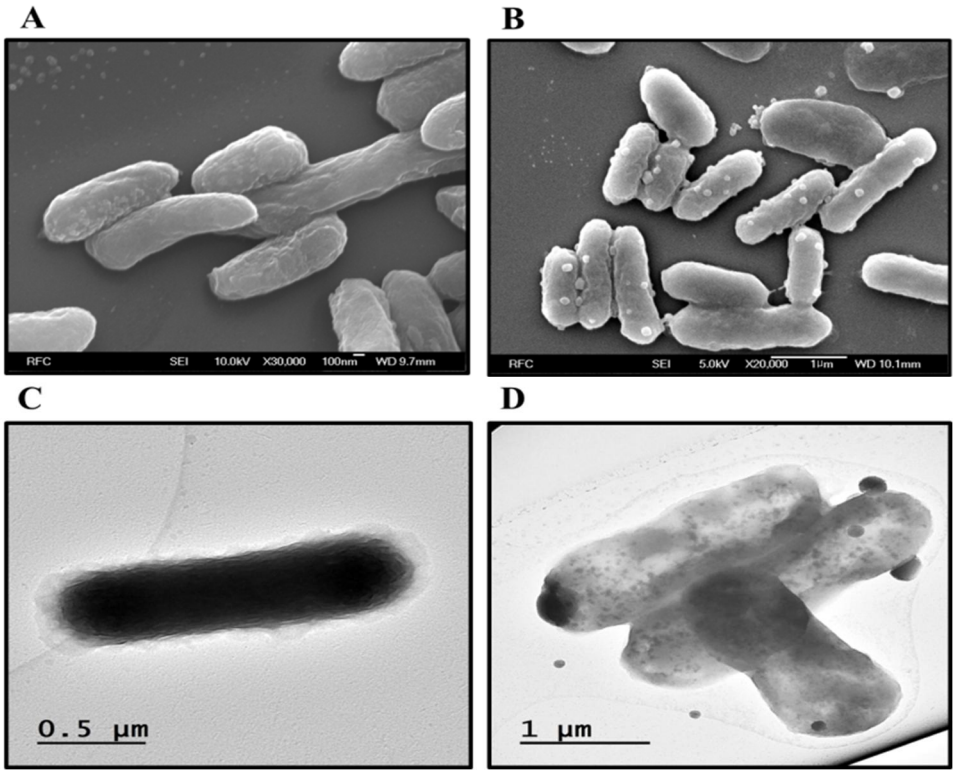

Fig. 2.10 FE-SEM and TEM image of recombinant strains containing OmpC-LBP. (A) (B) SEM images of *E. coli* and recombinant *E. coli* after lithium recovery respectively. (C) & (D) TEM images of *E. coli* and recombinant *E. coli* after lithium recovery respectively.

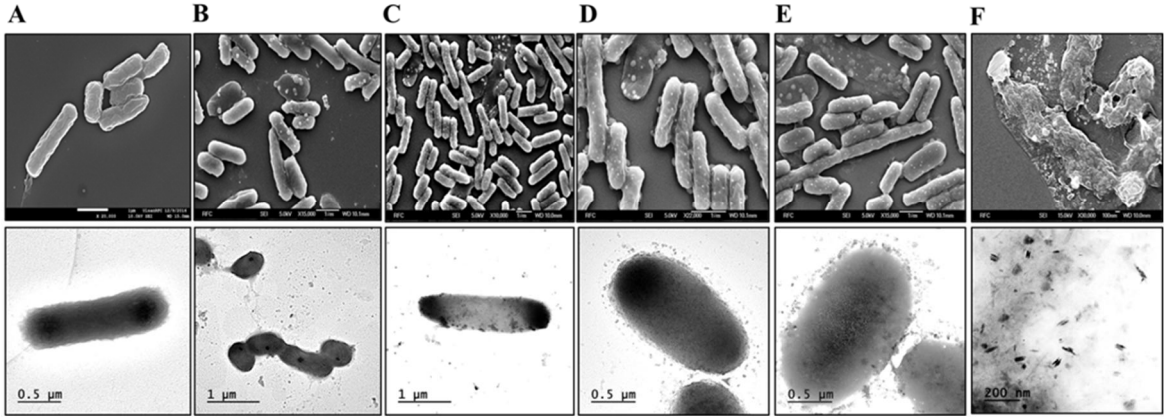

Fig. 2.11 Change in surface morphology of recombinant *E.coli* with varying concentration of lithium (A) 0 mM, (B) 0.1 mM, (C) 1mM, (D) 10mM, (E) 20mM, and (F) 100 mM respectively.

2.4.7 The application of OmpC-LBP system for real wastewater

The effect of LBWW on the growth of plants was analyzed (Fig. 2.13). Three pots were planted with mustard seeds and labeled as A, B, and C. The pots were watered regularly with normal water, LBWW and LBWW after lithium recovery. The growth of the plants was monitored at regular intervals. The growth of the plant in pot B was significantly reduced when compared to pot A and B. Irrigation of plants with lithium polluted water might have contributed the stunted plant growth [52]. Lithium considered to be a micro-nutrient and could be tolerated by most plants up to 5 ppm. However, a higher concentration of lithium in soil alters the gravitropic growth of root [53]. Also, there was a major morphological change found in the leaf, root, and stem of the plants from pot B. The damage can be observed at root tips, additionally, necrotic spots can be observed on the leaf surface [54]. The quality of leaves from all three pots was analyzed. When compared to pot A and C, a leaf from pot B was very tiny and distorted. Fewer and poorly developed stomata were observed in leaves from pot B (Fig. 2.14). This finding shows that lithium present in the LBWW affected the

growth of the plants. The pots were watered continuously, however, after 15 days the plants in the pot B were wilted. Higher concentration of lithium might have inhibited plant growth [55]. This finding supports the ability of the developed lithium recovery system towards bioremediation.

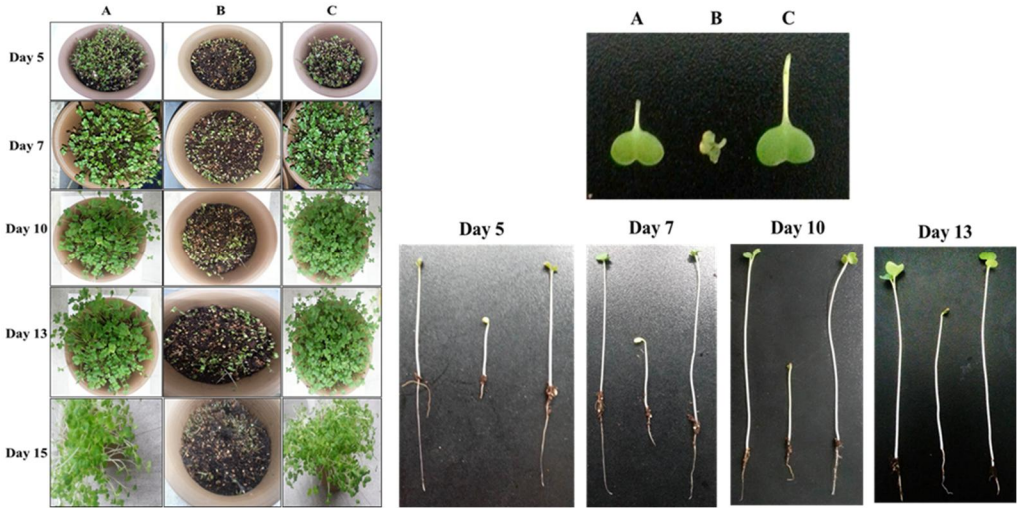

Fig. 2.13 The effect of lithium battery polluted water on the plant growth. Three pots were planted with mustard seeds and watered regularly with (A) normal water (B) LBWW and (C) LBWW after lithium recovery with CSD LBP respectively.

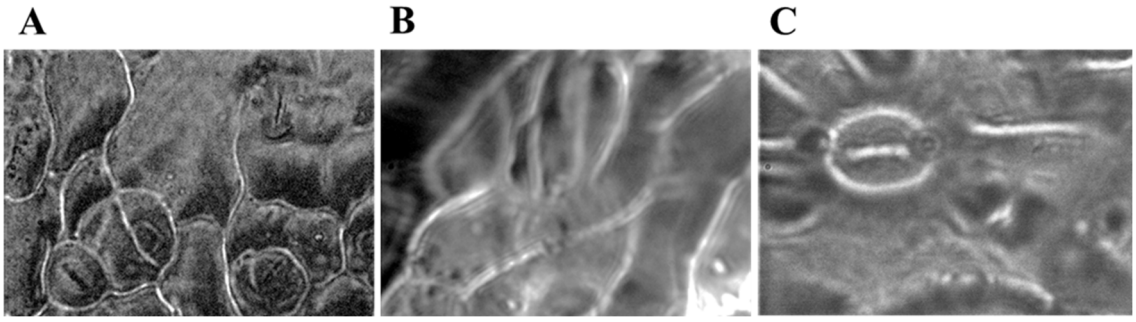

Fig. 2.14 Physiological characterization of leaves from pot (A) normal water (B) LBWW and (C) LBWW after lithium recovery with surface displayed LBP respectively.

2.4.8 FT-IR spectroscopy

FT-IR was performed to characterize the changes in functional groups of recombinant *E. coli* after lithium recovery. It is an effective characterization to obtain metal microbe bonds[56]. The difference in Ft-IR spectrum of *E. coli* displayed with LBP and without LBP was recorded after lithium adsorption (Fig. 2.15 A). LiCl salt was also included in the experiment as a control. The IR spectrum of both LBP displayed *E. coli* after lithium recovery and LiCl had a similar pattern, this further confirms the presence of lithium on the cell surface. However, wild-type cells did not show much correspondence with LiCl, this validated that the lithium recovery was due to the surface display of LBP. Regarding the functional groups, the peak at 1038 cm^{-1} is due to the interaction of *E. coli* with a metal solution. Complexation of phosphate or carboxyl groups by coordination with metal ions causes the shift[57, 58]. The peaks at corresponds to 2853 cm^{-1} CH_3 asymmetric stretching vibrations, 2925 cm^{-1} CH_2 asymmetric stretching, 2957 cm^{-1} CH_3 asymmetric stretching, 1534 cm^{-1} C-N stretching in amide II group, 1398 cm^{-1} COO- stretching of carboxyl groups, 1236 cm^{-1} P=O asymmetric stretching of phosphate groups, 969 cm^{-1} N-containing bio-ligands respectively[43].

2.4.8 UV-Vis spectroscopy

The effect of pH on properties of bio adsorbed lithium was studied by UV-Vis spectroscopy. The recombinant cells displayed with LBP was exposed to LiCl at various pH and UV spectrum was recorded (Fig. 2.15 B). In the spectrum, a small hump was observed around 310nm. According to Mie theory reported by Ramirez et al., this band was assigned to the surface plasmon in lithium colloidal nanoparticles [59]. At pH 3 a minor shift in the peak location was found. The surface plasmon in nanoparticles or agglomerates with a size higher than 10 nm might have contributed the shift[60, 61].

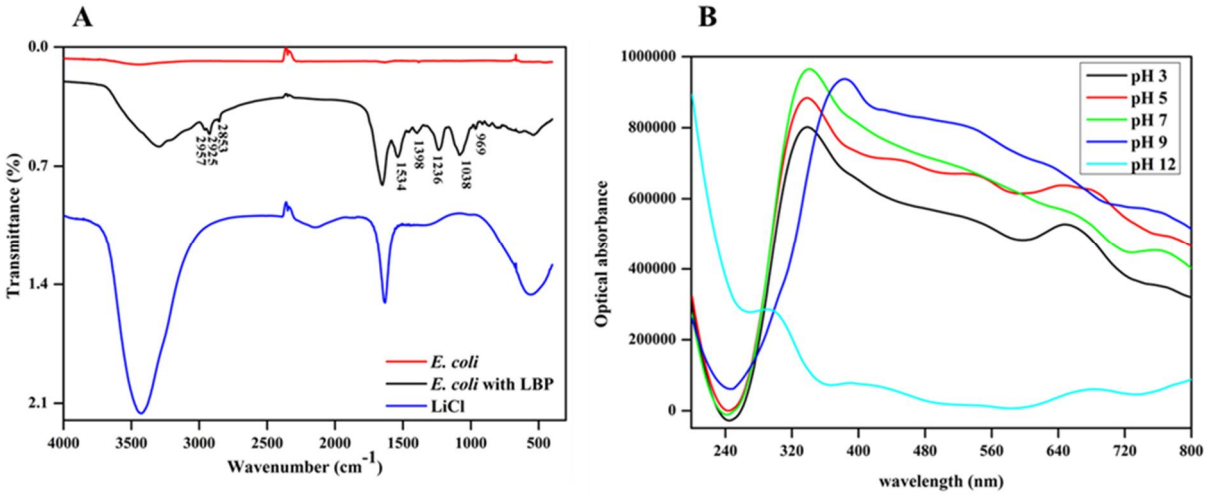

Fig. 2.15 Physiochemical characterization of lithium recovered by recombinant *E. coli*; (A) FT-IR, and (B) UV-Vis

2.4.9 Raman spectroscopy

Based on the UV-Vis results Raman spectroscopy was performed to further study the optical properties of the adsorbed lithium (Fig. 2.16). This technique is sensitive towards the morphological and structural changes of the nanoparticle. The lyophilized samples of recombinant *E. coli* after lithium recovery were used for this study. A band was observed around 280 Cm^{-1}. It is attributed to vibrational modes present in the smaller sized lithium

particles. This again confirms the presence of lithium particles on the surface of recombinant *E. coli* [60]. The wild-type strain does not show any peak. Lithium nanoparticles are grouped as highly flammable and corrosive. A study explained the green synthesis of lithium nanoparticle using *Opuntia ficus-indica* (*Ofi*) plant extract [62]. Employing plant extracts for nanoparticle biosynthesis is highly unspecific**[59, 63, 64]**. The present study aids in the green synthesis of lithium nanoparticles.

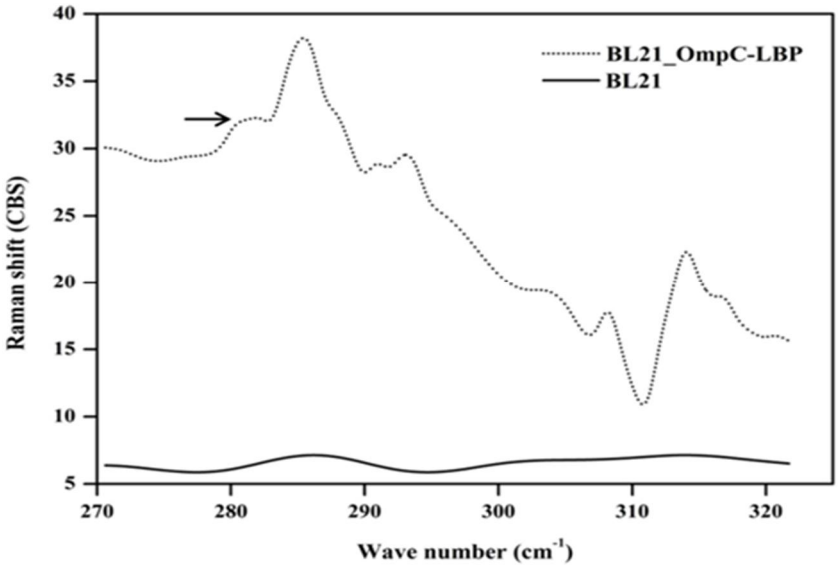

Fig. 2.16 Raman spectroscopy of BL21 displayed with LBP by employing OmpC as an anchoring motif. Wild-type BL21 was included as a control.

2.5 Conclusions

The growth in consumption of electronic goods is directly proportional to the increase in electronic waste and the immediate management techniques, recovery and reuse are considered to be a mandatory measure. Additionally, the increase in the use of LIBs and poor disposable systems, demands the need for the immediate development of lithium recovery systems. Therefore, the treatment of e-waste should be approached not only for cleaning but also for mining.

The sorbents for lithium could be prepared by designing, expression and implementation of the peptides having the five amino acids in their sequence. These peptides showed the high specificity toward lithium and can extract the metals from the solutions containing various metals under the mild condition without any chemicals and energy input. The ability of the peptides for lithium recovery can be strengthened by cell surface display on the recombinant bacteria. Through CSD of the multimeric construct of the peptides, cutting down the production cost, increasing the adsorption capacity and value-adding the product are all possible. Lithium nanoparticles were obtained after lithium adsorption and the whole-cell biosorbents could be functioned as a template for a nanoparticle. Designing peptides allow the synthesis of nanoparticles having excellent properties even if they are not necessarily applied for wastewater. Further studies are required for the characterization of nanoparticles synthesized on the cell surface in order to design novel peptide sequences. The current study is also focused on recycling and reuse of LBWW for plant irrigation and the ability of the developed system towards bioremediation are confirmed.

2.6 References

1. Y. Luo, N. Marets and T. Kato, *Chemical Science*, 2018, **9**, 608-616.
2. J. Nan, D. Han and X. Zuo, *Journal of Power Sources*, 2005, **152**, 278-284.
3. J. W. Fergus, *Journal of Power Sources*, 2010, **195**, 939-954.
4. C.-X. Zu and H. Li, *Energy & Environmental Science*, 2011, **4**, 2614-2624.
5. T. Bell.
6. H. Sanderson, *The Financial Times Limited*, 2017.
7. A. K. Shukla and T. P. Kumar, *The Journal of Physical Chemistry Letters*, 2013, **4**, 551-555.
8. V. Ari, *E-Waste in Transition - From Pollution to Resource*, 2016.
9. C. Hanisch, J. Diekmann, A. Stieger, W. Haselrieder and A. Kwade, in *Handbook of Clean Energy Systems*, John Wiley & Sons, Ltd, 2015.
10. J. Li, X. He and X. Zeng, *Environmental Technology*, 2017, **38**, 652-660.
11. H. Zou, E. Gratz, D. Apelian and Y. Wang, *Green Chemistry*, 2013, **15**, 1183-1191.
12. H. Kanoh, K. Ooi, Y. Miyai and S. Katoh, *Separation Science and Technology*, 1993, **28**, 643-651.
13. R. Chitrakar, H. Kanoh, Y. Miyai and K. Ooi, *Industrial & Engineering Chemistry Research*, 2001, **40**, 2054-2058.

14. K. Pollmann, S. Kutschke, S. Matys, J. Raff, G. Hlawacek and F. L. Lederer, *Biotechnology Advances*, 2018, **36**, 1048-1062.

15. M. k. Maruthamuthu, S. P. Nadarajan, I. Ganesh, S. Ravikumar, H. Yun, I.-k. Yoo and S. H. Hong, *Bioprocess and Biosystems Engineering*, 2015, **38**, 2077-2084.

16. S. Y. Lee, J. H. Choi and Z. Xu, *Trends in Biotechnology*, 2003, **21**, 45-52.

17. S. Wendel, E. C. Fischer, V. Martínez, S. Seppälä and M. H. H. Nørholm, *Microbial Cell Factories*, 2016, **15**, 71.

18. W. Bae, A. Mulchandani and W. Chen, *Journal of Inorganic Biochemistry*, 2002, **88**, 223-227.

19. C. Sousa, Kotrba, P., Ruml, T., Cebolla, A., De Lorenzo, V., *Journal of Bacteriology*, 1998, **180**, 2280-2284.

20. Z. Xu, Lee, S.Y., *Applied and Environmental Microbiology*, 1999, **65**, 5142-5147.

21. M. kannan Maruthamuthu, J. Hong, K. Arulsamy, S. Somasundaram, S. Hong, W.-S. Choe and I.-K. Yoo, *Bioprocess and biosystems engineering*, 1-9.

22. M. kannan Maruthamuthu, S. P. Nadarajan, I. Ganesh, S. Ravikumar, H. Yun, I.-k. Yoo and S. H. Hong, *Bioprocess and biosystems engineering*, 2015, **38**, 2077-2084.

23. M. kannan Maruthamuthu, V. Selvamani, S. P. Nadarajan, H. Yun, Y.-K. Oh, G. T. Eom and S. H. Hong, *Journal of industrial microbiology & biotechnology*, 1-11.

24. N. F. S. O. Lesmana, F. E. Soetaredjo, J. Sunarso, and S. Ismadji, , *Biochemical Engineering Journal*, 2009, **44**, 19–41.

25. T. S. J. J.-G. Na, M. S. Kim, S. G. Jeon, S. H. Hong and S. H. Chung, *Korea Pat. 10-2016-0154400, 2016.*

26. I. L. Karle, *Journal of the American Chemical Society*, 1978, **100**, 1286-1289.

27. N. Cruz, S. Le Borgne, G. Hernández-Chávez, G. Gosset, F. Valle and F. Bolivar, *Biotechnology Letters*, 2000, **22**, 623-629.

28. A. J. Link and D. A. Tirrell, *Journal of the American Chemical Society*, 2003, **125**, 11164-11165.

29. T. T. L. Nguyen, H. R. Lee, S. H. Hong, J.-R. Jang, W.-S. Choe and I.-K. Yoo, *Applied Biochemistry and Biotechnology*, 2013, **169**, 1188-1196.

30. D.-Y. Tsai, Y.-J. Tsai, C.-H. Yen, C.-Y. Ouyang and Y.-C. Yeh, *RSC Advances*, 2015, **5**, 87998-88001.

31. T. Tsuruta, *Journal of Bioscience and Bioengineering*, 2005, **100**, 562-566.

32. L. Talens Peiró, G. Villalba Méndez and R. U. Ayres, *JOM*, 2013, **65**, 986-996.

33. I. L. Karle, *Journal of the American Chemical Society*, 1978, **100**, 1286-1289.

34. T. E. LYNN and J. N. KUSHICK, *International journal of peptide and protein research*, 1984, **23**, 601-609.

35. U. N. Andersen and G. Bojesen, *Journal of the Chemical Society, Perkin Transactions 2*, 1997, 323-328.

36. F. E. Antonio Jesús Muñoz, Manuel Moya, and Encarnación Ruiz, 2015, **2015**, 12.

37. E. Foulquier, *IMGT®, the international ImMunoGeneTics information system®*.

38. S. Johansson, M. Ruscalleda and J. Colprim, *Chemical Engineering Journal*, 2017, **327**, 881-888.

39. R. Hall Sedlak, M. Hnilova, C. Grosh, H. Fong, F. Baneyx, D. Schwartz, M. Sarikaya, C. Tamerler and B. Traxler, *Applied and Environmental Microbiology*, 2012, **78**, 2289-2296.

40. C.-Y. Chiu, Y. Li and Y. Huang, *Nanoscale*, 2010, **2**, 927-930.

41. D. B. Pacardo, M. Sethi, S. E. Jones, R. R. Naik and M. R. Knecht, *ACS Nano*, 2009, **3**, 1288-1296.

42. R. R. Naik, S. J. Stringer, G. Agarwal, S. E. Jones and M. O. Stone, *Nature materials*, 2002, **1**, 169-172.

43. B. Lian, Q. Hu, J. Chen, J. Ji and H. H. Teng, *Geochimica et Cosmochimica Acta*, 2006, **70**, 5522-5535.

44. K. Inaba, T. Kuroda, T. Shimamoto, T. Kayahara, M. Tsuda and T. Tsuchiya, *Biological and Pharmaceutical Bulletin*, 1994, **17**, 395-398.

45. K. A. K. Aftab, A. Jabbar, I. H. Bukhari, and R. Noreen,, *Water Research*, 2013, **47**, 4238–4246.

46. B. M. R. Aravindhan, J. R. Rao, and B. U. Nair, , *Journal of Chemical Technology and Biotechnology* 2004, **79**, 1251–1258.

47. M. A. M. ı.-L. G. Bl´azquez, G. Tenorio, and M. Calero,, *Chemical Engineering Journal*, 2011, **168**, 170–177.

48. L. P. RAMÍREZ-RODRÍGUEZ, M. CORTEZ-VALADEZ, J.-G. BOCARANDO-CHACON, H. ARIZPE-CHÁVEZ, M. FLORES-ACOSTA, S. VELUMANI and R. RAMÍREZ-BON, *Nano*, 2014, **09**, 1450070.

49. R. A. B. Álvarez, M. Cortez-Valadez, R. Britto-Hurtado, L. O. N. Bueno, N. S. Flores-Lopez, A. R. Hernández-Martínez, R. Gámez-Corrales, R. Vargas-Ortiz, J. G. Bocarando-Chacon, H. Arizpe-Chavez and M. Flores-Acosta, *Vibrational Spectroscopy*, 2015, **77**, 5-9.

50. J. A. Creighton and D. G. Eadon, *Journal of the Chemical Society, Faraday Transactions*, 1991, **87**, 3881-3891.

51. R. A. B. Álvarez, M. Cortez-Valadez, R. Britto-Hurtado, L. O. N. Bueno, N. S. Flores-Lopez, A. R. Hernández-Martínez, R. Gámez-Corrales, R. Vargas-Ortiz, J. G. Bocarando-Chacon, H. Arizpe-Chavez and M. Flores-Acosta, *Vibrational Spectroscopy*, 2015, **77**, 5-9.

52. M. Cortez-Valadez, J. G. Bocarando-Chacon, A. R. Hernández-Martínez, R. B. Hurtado, R. A. B. Alvarez, J. F. Roman-Zamorano, J. Flores-Valenzuela, R. Gámez-Corrales, H. Arizpe-Chávez and M. Flores-Acosta, *Nanoscience and Nanotechnology Letters*, 2014, **6**, 580-583.

53. J. G. Bocarando-Chacon, M. Cortez-Valadez, D. Vargas-Vazquez, F. Rodríguez Melgarejo, M. Flores-Acosta, P. G. Mani-Gonzalez, E. Leon-Sarabia, A. Navarro-Badilla and R. Ramírez-Bon, *Physica E: Low-dimensional Systems and Nanostructures*, 2014, **59**, 15-18.

54. G. R. Bradford, *Soil Science*, 1963, **96**, 77-81.

55. T. J. Mulkey, *Gravitational and space biology bulletin: publication of the American Society for Gravitational and Space Biology*, 2005, **18**, 119-120.

56. A. B. M. A. Kabata-Pendias, in *Trace Elements from Soil to Human*, Springer Berlin Heidelberg, Berlin, Heidelberg, 2007, pp. 87-104.

57. B. Shahzad, M. Tanveer, W. Hassan, A. N. Shah, S. A. Anjum, S. A. Cheema and I. Ali, *Plant Physiology and Biochemistry*, 2016, **107**, 104-115.

58. U. Laemmli, *Nature*, 1970, 680-685.

59. D.-Y. Tsai, Tsai, Yi-Jung, Yen, Chia-Ho, Ouyang, Chun-Yu, Yeh, Yi-Chun, *RSC Advances*, 2015, **5**, 87998-88001.

60. M. k. Maruthamuthu, I. Ganesh, S. Ravikumar and S. H. Hong, *Biotechnology Letters*, 2015, **37**, 659-664.

61. W. B. Eswar N, Marti-Renom MA, Madhusudhan MS, Eramian D, Shen M-Y, Pieper U, Sali A *In: Coligan JE (ed) Current protocols in protein science. Wiley*, 2001.

62. N. Eswar, B. Webb, M. A. Marti-Renom, M. S. Madhusudhan, D. Eramian, M.-y. Shen, U. Pieper and A. Sali, in *Current Protocols in Protein Science*, John Wiley & Sons, Inc., 2001.

63. S. F. Altschul, T. L. Madden, A. A. Schaffer, J. Zhang, Z. Zheng, W. Miller and D. J. Lipman, *Nucleic Acids Res*, 1997, **25**.

Chapter 3

Cell surface display of cobalt binding peptide as whole-cell biocatalyst for photocatalytic reduction of methylene blue

Chapter-3

3.1 Abstract

A recombinant *E. coli* was developed by cell surface engineering of cobalt binding peptide (CP1&CP2). The peptides were displayed with the aid of YiaT as an anchoring motif. The structure of the recombinant peptide (YiaTCP2 &YiaTCP3) was modelled. The difference in binding potential towards cobalt was evaluated. Further the ability of CP2 & CP3 to adsorb and recover cobalt was evaluated in three different environments including Luria-Bertani(LB), artificially polluted wastewater (AWW) and battery polluted wastewater (BWW). CP3 was observed to recover higher percentage of cobalt (1907.766 µmol/g drycell weight) when compared to CP2. Further the physio-chemical properties of recombinant cells after cobalt adsorption was characterized by fourier transform infrared spectroscopy (FT-IR), UV-Vis spectroscopy. The recombinant cells were exposed to cobalt at various pH (3, 5, 7, 9 and 11). The bound cobalt was observed to be a nano sized particles and visualized by scanning emission microscopy (SEM) and transmission emission microscopy (TEM). The presence of cobalt on the cell surface was mapped by energy-dispersive X-ray spectroscopy (EDX). Further the recombinant strains bound with cobalt is used for photocatalytic reduction of methylene blue. The percentage of reduction was found to be 59.52%.

3.2 Introduction

Metals are solid substances with versatile applications. It is used in electronic, medicine, building construction, jewelry, farming, cooking, furniture, security systems, machinery and automobiles. Thus metals are considered to be inevitable in everyday life. However many years of experience in using metals have led to exhaustion of natural resources. Metals are not consumed during manufacture and hence it can be usually recycled.

It is essential to recover metals from the scrap, it can also be considered as secondary raw material.. Cobalt is one such metal with versatile application. It is essential for animal metabolism as it is an important component of vitamin B_{12}. It is naturally found in the earth's crust combined form. Since ancient times cobalt is used in jewelry and paints for its distinct blue colour. In recent times it is effectively incorporated in making alloys, batteries, and electroplating.

A study reported by approximately 25% of global demand for cobalt is for rechargeable batteries[1]. Metals often used in lithium ion batteries (LIB's) includes; cobalt (5-20 wt%), lithium (15 wt%), nickel (5-10 wt%), organics and plastics (7 wt%)[2, 3]. Electronic industry is the major user of LIB's. The advent growth in electronic industry has resulted in constant replacement of old devices. This has contributed in tremendous generation of electronic waste (EW). It contains valuable metals like cobalt and lithium. The use of cobalt in LIB's has increased from 700 to 1200 tpa during the year 1995-2005. The increasing price of cobalt makes it essential to recover from the spent EW[4]. The elevated demand of portable electronic devices like mobile phones, notebook, computer, and cameras [2, 5, 6].

The metals from the scrap EW seeps into to soil and groundwater when it comes in contact with industrial waste sewage. Especially cobalt once enters the environment it cannot be destroyed. It may react with other particles or adsorb on soil particles or water sediments. Recycling of metals can improve the use of natural resources and can help in reduce the production cost of batteries[7]. Additionally it will help in reducing the environmental

problems associated with it. Though cobalt is considered to be essential for human health at higher concentration it may cause low blood pressure, paralysis, diarrhea and bone defects[8]. Also, cobalt is distinguished to be a harmful radioactive material with longer half-life of 5.27[8]. Hence it is essential to clean up the cobalt that is present in the environment. Several studies have been reported towards recycle and recover cobalt from the spent LIB's by chemical precipitation, ion exchange, coagulation, flocculation, pyro metallurgy, and hydrometallurgy or bio-hydrometallurgy processes [9, 10]. However, it is essential to consider the cost effective and eco-friendly approach towards cobalt recovery. Also, the above methods failed at removing cobalt particularly at lower concentration[11, 12]. In recent years application of micro-organism towards metal recovery is gaining greater attention. Microbes are employed used in two ways bioleaching and bio sorption[13].

The former deals with extraction or solubilization of minerals however, the later deals with surface adsorption of metals by microbes[8]. Hence bio-sorption can be considered as an alternative approach to recover valuable metals from environment. The effectiveness of the bio sorption can be further enhanced by combining Cell surface display (CSD) of short metal binding peptides [14]. It will aid in selective recovery of specific metals. CSD is approaches were protein; peptide and enzyme is displayed on microbial surface with anchoring proteins available on the outer membrane. In the current study CSD of cobalt binding peptides (CP2, CP3) was performed on the surface of *E. coli*. The display was realized by employing YiaT as an anchoring protein. Further the effectiveness of the system towards cobalt recovery was analyzed in three different environment including luria bertani (LB), artificially polluted waste water (AWW), battery polluted waste water (BWW). The

peptide showing higher affinity towards cobalt was chosen for further study. The presence of cobalt on the cell surface of recombinant *E. coli* was visualized and mapped by scanning emission microscopy (SEM), transmission emission microscopy (TEM) and energy-dispersive X-ray spectroscopy (EDX) respectively. The cell surface bound cobalt was employed towards photocatalytic reduction of methylene blue. Various studies have demonstrated the photocatalytic properties of nanoparticles synthesized by green techniques [15, 16]. Since dye polluted waste water considered one of the major pollutants, there is a need for conventional process towards remediation of pollutants.

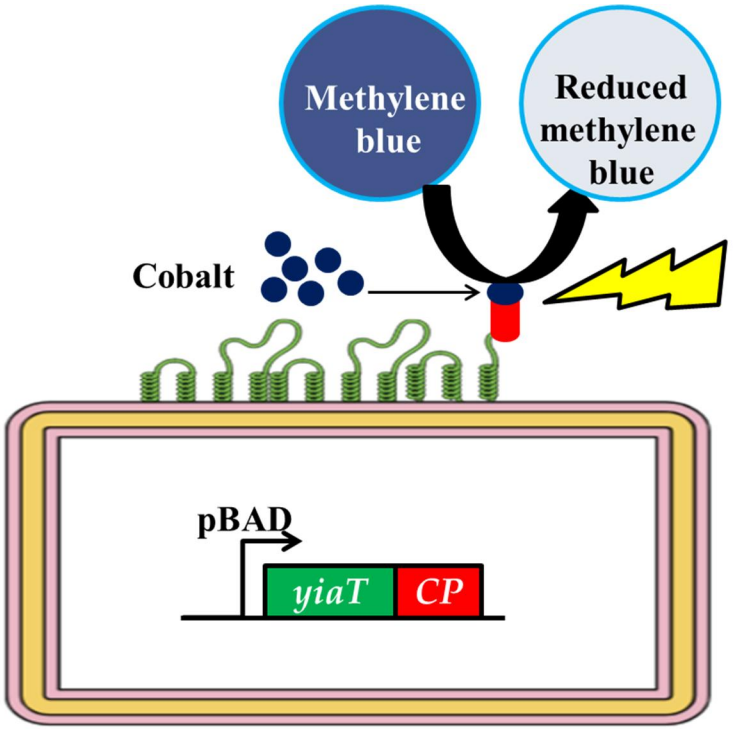

Fig. 3.1 Cell surface display of cobalt binding peptide as whole-cell biocatalyst towards reduction of methylene blue

3.3 Materials and methods

3.3.1 Bacterial strains and growth conditions

The bacterial strains used in this study are listed in Table 3.1. The strains were grown in LB medium (10 g/L bacto-tryptone, 5 g/L bacto-yeast extract and 5 g/L NaCl) with 100 mg/L ampicillin at 37 ºC with vigorous shaking at 250 rpm.

Table 3.1. Bacterial strains and plasmids used in the study

Strain/Plasmid	Relevant genotype/ property	Source
***E. coli* strains**		
XB	*recA1 endA1 gyrA96 thi-1 hsdR17 supE44 relA1 lac [F´ proAB lacIq ZΔM15 Tn10 (Tetr)].*	Novagen
TOP10	*F- mcrA Δ(mrr-hsdRMS-mcrBC) φ80lacZΔM15 ΔlacX74 nupG recA1 araD139 Δ(ara-leu)7697 galE15 galK16 rpsL(Str^R) endA1 λ$^-$*	Stratagene
Plasmids		
pBAD30	Amp^R	NEB[a]
pBADCp$_2$	pBAD30 containing YiaT- CBP2	This work
pBADCp$_3$	pBAD30 containing YiaT- CBP3	This work

3.3.2 Recombinant plasmid construction

The gene for cobalt binding peptide was integrated with the C-terminus of the truncated *yiaT* at loop5 (696 bp) and amplified by polymerase chain reaction (PCR) performed with an MJ Mini Personal Thermal Cycler (Bio-Rad Laboratories, Hercules, CA, USA) using the Expand High Fidelity PCR system (Roche Molecular Biochemicals, Mannheim, Germany). The nucleotide sequence of the CP2&3 is GGCATGGTGCCGAGCGGCGCGAGCACCGGCGAACATGAAGCGGTGGAACTGCG C & CATTATCCGACCCTGCCGCTGGGCAGCAGCACCACC respectively. These sequences were designed considering the codon usage. The primers used in the work are mentioned in Table 3.2. The PCR products were cloned into the pBAD30 plasmid using *SacI* and *KpnI* restriction enzymes to construct pBAD30CP2 and pBAD30CP3. Expression of YiaT-CBP2, 3 was induced by the addition of arabinose. These plasmids were transformed into *E. coli* Top10 strains for further studies.

Table 3.2 Primers used in this work

Name	Sequence (5' to 3')
C_F	**GAGCTC**ATGTTAATTAATCGCAATATTGTGGCGTTATTTG
CP_2_Ol_R	CGCCGGTGCTCGCGCCGCTCGGCACCATGCCACGATCAATC ATCGGGCTGTCGGTAATACGATCAATCATCGGGCTGTCGGT
CP_2_R	**GGTACC**GCGCAGTTCCACCGCTTCATGTTCGCCGGTGCTCG CGCCGCTCGGC ACCATG
CP_3_R	**GGTACC**GGTGGTGCTGCTGCCCAGCGGCAGGGTCGGATAAT GACGATCAATCATCGGGCTGTCGGTAAT

3.3.3 SDS page analysis

The recombinant *E. coli* displaying the CBP2 & CBP3 was cultured overnight in LB medium at 37°C, and the cultures were then diluted 100-fold in the same. After reaching an optical density at 600nm (OD600) reached 0.5, arabinose was added to the culture broth at different concentrations of 0 to 1 % and further incubated at 30°C for 5 h. The recombinant strains were harvested by centrifuging at 13,000rpm for 10 minutes and incubated with B-7M urea buffer at room temperature for 30 minutes with agitation. The cells were centrifuged at 8000rpm to remove cell debris. The outer membrane fractions from the cell pellet were separated by adding 10 mM Tris-HCl (pH 7.5) and the suspended cells were kept in 4°C overnight. The lifted the membrane fractions were analyzed by 12% (w/v) sodium dodecyl sulfate polyacrylamide gel electrophoresis (SDS-PAGE) [17] and stained with Coomassie brilliant blue R-250 (Bio-Rad Laboratories, Hercules, CA, USA).

3.3.4 Molecular modeling studies

The binding of cobalt with CBP displayed by YiaT was determined by performing a computational study. A homology model of the peptide YiaT-CP2 and YiaT-CP3 was constructed with help of I-TASSER server. Further the binding potential of peptides towards cobalt was predicted.

3.3.5 Cobalt recovery analysis

The recombinant *E. coli* strains were grown overnight in LB medium supplemented with 100 mg/L ampicillin at 37°C. The overnight cultures were diluted 100-fold in fresh LB medium and incubated until OD600 reached 0.5. The cells were induced with arabinose, and the strains were further incubated at 30 °C for 5 h. The strains were washed twice with 0.85% (w/v) of NaCl, and the cells were incubated in a solution containing a varying

concentration of lithium chloride (0-1mM). To realize the specificity of LBP_3 artificially polluted waste water (AWW) was used in bio-adsorption studies. AWW was created by mixing 1000ppm of the following salts like lithium chloride (LiCl), copper chloride ($CuCl_2$), and cobalt chloride ($CoCl_2$). Also, the real world application of Cp2 and Cp3 was evaluated by performing the adsorption experiments using battery polluted waste water samples. The battery polluted waste water was prepared by incubating the 10g of lithium ion batteries in water for overnight. After the performing adsorption for the recombinant strains were washed twice with 0.85% (w/v) NaCl to remove any physically adsorbed lithium. Further cobalt adsorbed by the peptides was eluted by incubating with 1mM EDTA for 30minutes in ice. The adsorbed lithium was quantitatively measured by ICP-OES (Agilent technologies 5110) (CHOI 2005).

3.3.6 Physiochemical characterization of bio-adsorbed cobalt

The properties of the lithium after performing bio-adsorption was analyzed using Fourier transform infrared spectroscopy (FT-IR), UV-Vis spectroscopy, Raman spectroscopy, Scanning emission microscopy (SEM), and Transmission emission microscopy (TEM)

3.3.6.1 FT-IR analysis

FT-IR (Thermo scientific Nicolet iS5) analysis was carried out to determine which functional groups contributed to the cobalt adsorption. After adsorption, the dried bacteria biomass was mixed and ground with 150 mg of KBr (Spectranal) in a mortar. Translucent disks were prepared by pressing with a pressure bench press. The cell pellets were immediately analyzed with a spectrophotometer in the range of 4000-400 cm^{-1} with the resolution of 4 cm^{-1}. The influence of atmospheric water and CO_2 were subtracted from

every measurement.

3.3.6.2 UV-Vis spectroscopy

Based on the Raman results, to confirm whether the adsorbed cobalt is in the form of nanoparticle UV-Vis spectroscopy (Specord 210 plus and WinAspect plus software) was performed. To perform the experiment bio-adsorption was performed at varying pH (2.5, 5, 7, 10, and 12.5).

3.3.7 FE-SEM, TEM and EDS analysis

The lithium adsorbed strains were visualized using FE-SEM (JEOL JSM-6500F). The recombinant *E. coli* cells after adsorption were washed with 0.85% NaCl (pH 5.8) to remove the unbound cobalt on the cell surface. After washing the cells were fixed and incubated at 4 ^{o}C for 14h using 2.5% glutaraldehyde. The fixed cells were washed with PBS and then the cells were mounted on ultra-flat silicon wafers and dried to visualize it on a FE-SEM. To visualize through TEM the cobalt adsorbed recombinant *E. coli* was fixed with the above procedure and coated on copper grids. Further the metal elements present on the cell surface were mapped by EDS analysis.

3.3.8 Photocatalytic properties of cobalt nanoparticle

The photocatalytic ability of cobalt nanoparticle was determined by degrading methylene blue dye. To realize this cell displayed with CBP were mixed with 100ml of 10ppm methylene blue solution. The suspension was kept in dark for 30 min to attain adsorption-desorption equilibrium and irradiated to solar light generated by 150W Xe lamp having cutoff filter. Samples were drawn at regular time interval (0, 10, 30, 60 and 90 min). The samples were filtered by Millipore filter and analyzed by UV-vis spectrophotometer at 664 nm. To evaluate the real photo catalysis a control experiment was performed under

similar conditions. The dye degradation experiment was carried out in triplicates under ambient conditions. The percentage of dye degradation was estimated by executing relation shown in Eq. (1).

$$\text{Degradation percentage } = \left[\frac{(C_i - C_f)}{C_i}\right] 100 \qquad \text{(Eq. (1))}$$

Where C_i, initial concentration of methylene is blue and C_f is concentration of dye after degradation.

3.4 Results and discussion

Recombinant *E. coli* was developed for cobalt recovery by displaying the cobalt binding peptide (CBP2 and CBP3) on the surface of the cell membrane using YiaT as an anchoring motif. To realize this strategy CBP was integrated with the truncated *yiaT* at 696 bp. The constructed plasmid is pBADCP2 and pBADCP3 regulated by the arabinose promoter (Fig. 3.2). Generally, expression of heterologous protein in *E. coli* results in metabolic liability, this leads to reduced protein expression, cell growth and stability in the recombinant plasmid [18]. Hence it is necessary to optimize the growth and expression conditions.

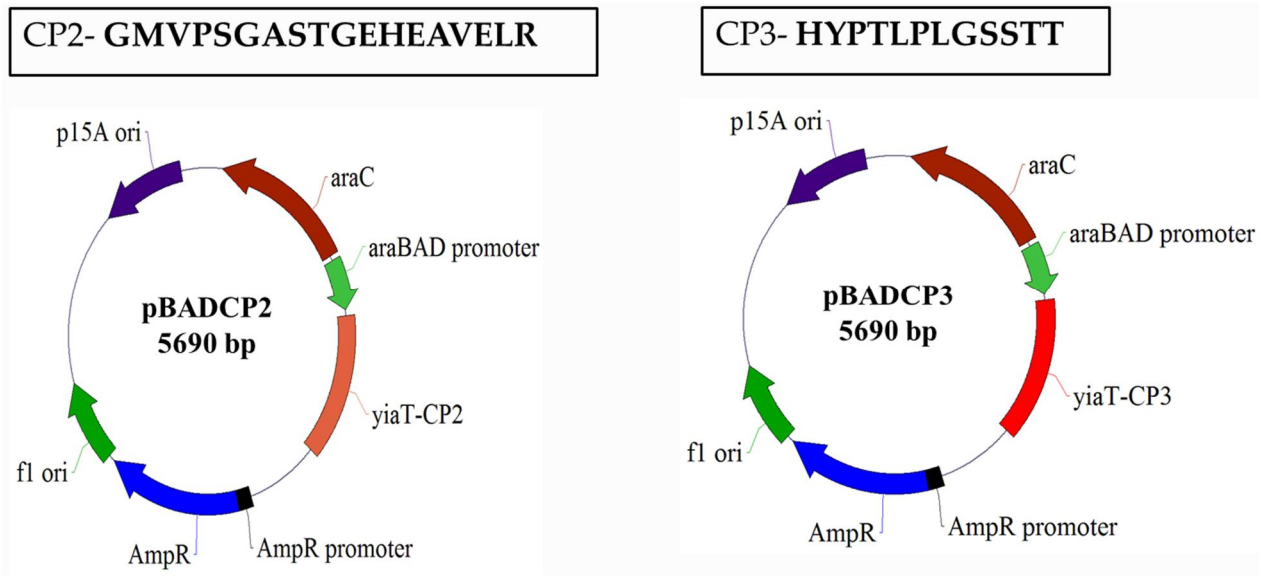

Fig. 3.2 Construction of recombinant plasmids CSD of cobalt binding peptide. (A) YiaT-CP2 and (B) YiaT-CP3 was cloned in pBAD30 vector regulated by araBAD promoter.

3.4.1 Optimization of expression conditions

The recombinants plasmids contain are induced by the addition of arabinose. The concentration of arabinose (0.0 – 1.0%) was varied to optimize the expression of the OmpC-LBP3 peptide. The expression of the recombinant peptide (CBP2 &CBP3) was analyzed by SDS PAGE (Fig. 3.3). Maximum expression of both peptides were observed at 0.05% of arabinose and declined with further increase in arabinose. Further the effect of arabinose concentrations towards cobalt adsorption was evaluated. Maximum adsorption was observed at 0.05% of arabinose, which further corroborates with the SDS-PAGE results.

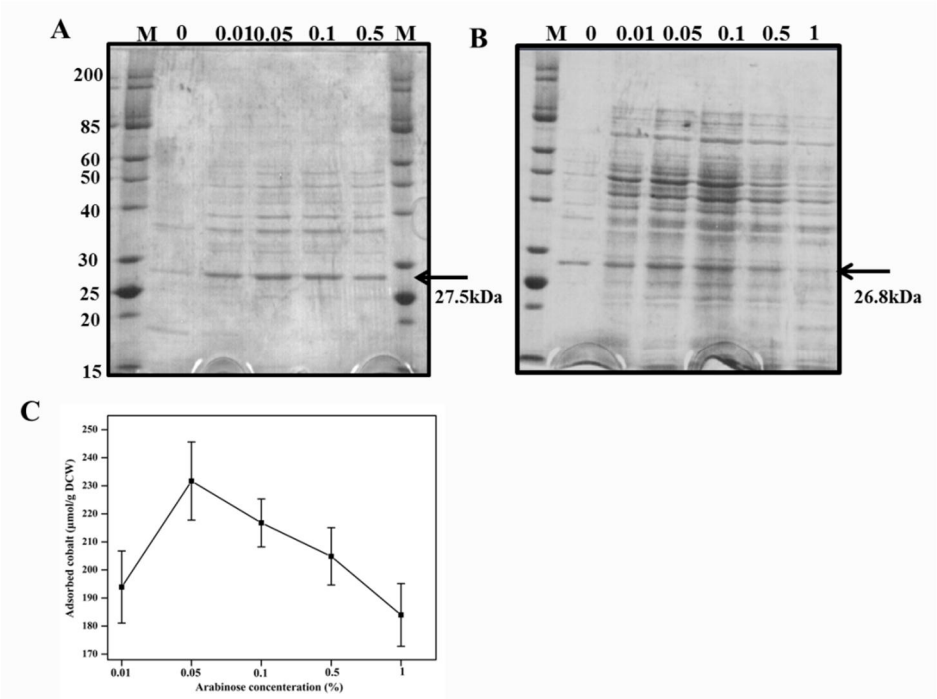

Fig. 3.3 Optimization of expression conditions. SDS-PAGE analysis of recombinant protein (A)YiaT-CP2 (27.5kDa) (B) YiaT-CP3 (26.8kDa) containing *E. coli*. M. Molecular weight marker in KDa. (C) Effect of arabinose concentration towards cobalt recovery.

3.4.2 Cobalt bio-adsorption studies

Adsorption of cobalt by the peptide YiaT-CBP2 and YiaT-CBP3 was evaluated by culturing the recombinant *E. coli* in LB medium supplemented with ampicillin. The peptides were overexpressed by the addition of arabinose at 30 ^{o}C for 5 hours. The plasmid containing YiaT without CBP3 was used as a control. After overexpression of the peptides the recombinant *E. coli* was exposed to various concentration of cobalt (0-1 mM) (Fig. 3.4 A). The peptides CBP2 and CBP3 showed maximum adsorption of 1521 and 1907.766 µmol/g DCW at 1mM concentration of cobalt chloride respectively. The recovery exhibited

by CBP3 displayed cells are 82.90% higher than the control strains. Thus bio-sorption of adsorption of cobalt was due to surface display of CBP.

The Specificity of CBP2 and CBP3 towards cobalt were evaluated by exposing the recombinant *E. coli* (AWW) containing 1000ppm of each metal like Li, Cu, Co in distilled water (Fig. 3.4 B). The recombinant *E. coli* containing overexpressed CBP2 and CBP3 was exposed to AWW. Both the peptides showed superior specificity towards cobalt. The specificity of the peptides were in the order of Co > Cu > Li (CP2-175.4866 > 7.495894 >19.07025 and CP3-181.1905 > 8.478065 > 17.44903 μmol/g DCW) respectively. These observed results prove that the CSD system developed in the present study is highly specific for cobalt.

The ability of the CP2&CP3 towards cobalt adsorption from BWW was evaluated (Fig. 3.4 C). It was performed by exposing recombinant *E. coli* containing CP2 & CP3 peptide to BWW. CP3 was observed to show maximum cobalt (193.6849 μmol/g DCW). These results confirm that the CP displayed recombinant *E. coli* cells can be efficiently employed to recover cobalt from various sources.

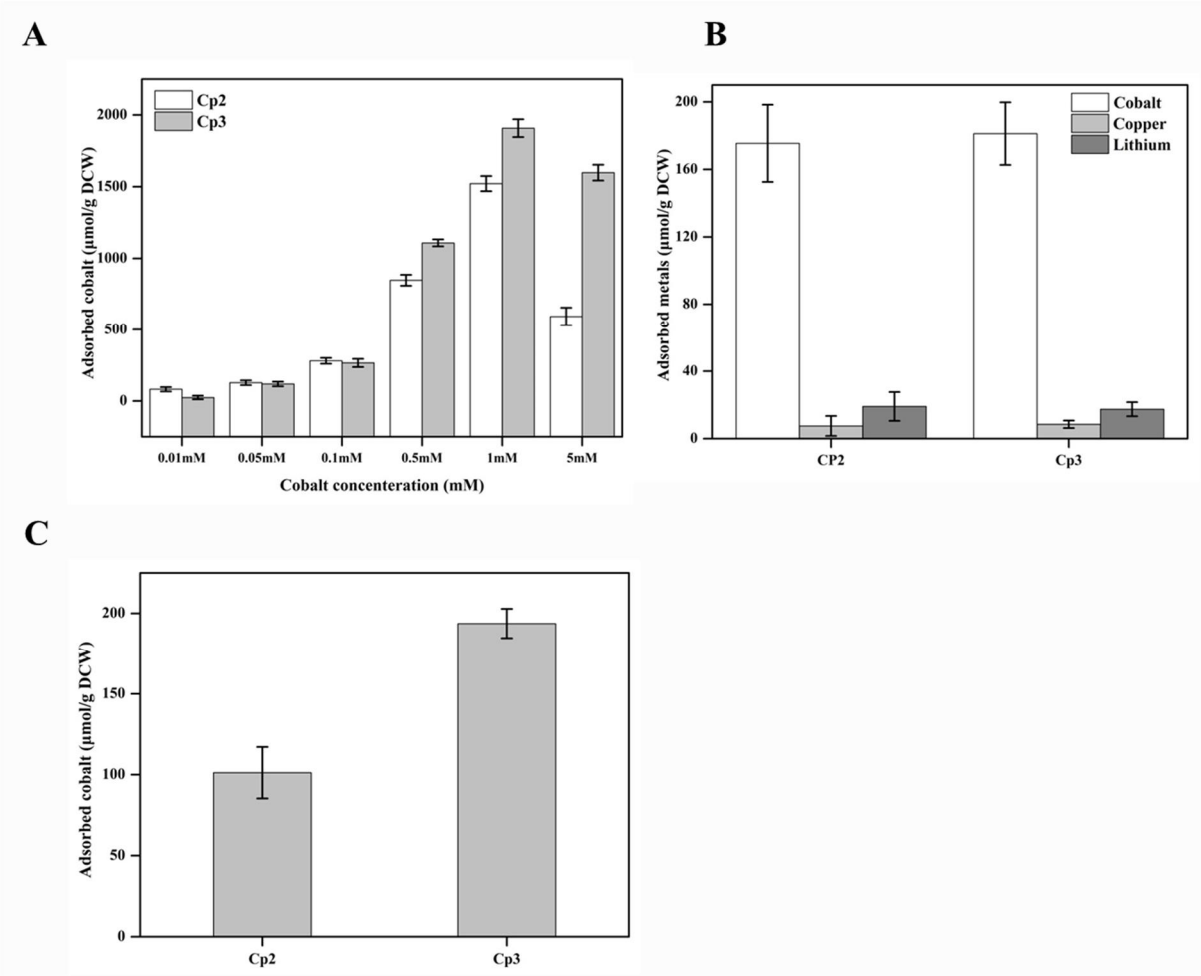

Fig. 3.4 Cobalt bio-adsorption studies with *E. coli* strains harboring pBADCP2&3, in A, LB medium, B, AWW and C, LBWW. All the experiments were independently performed in triplicates and standard deviation was determined.

3.4.3 Molecular modelling and docking

The molecular structure of the recombinant peptides YiaT-CP2 & YiaT-CP3 was modelled by I-TASSER server. The peptides were observed to form beta-barrel structure confirming the property of outer membrane protein. The binding potential of peptide was determined by MIB: metal ion-binding site prediction and docking server (Fig. 3.5). The cobalt molecule was docked with the recombinant peptides. Among two peptides YiaT-CP3

was found to have higher binding potential. These results validate the increased cobalt recovery by YiaT-CP3 peptide. The presence of charged amino acids arginine and histidine form the cobalt binding co-ordinates of CP2&3. The recombinant peptide YiaT-CP3 was found to be more hydrophilic when compared to YiaT-CP2. This might have contributed for increased cobalt binding by CP3.

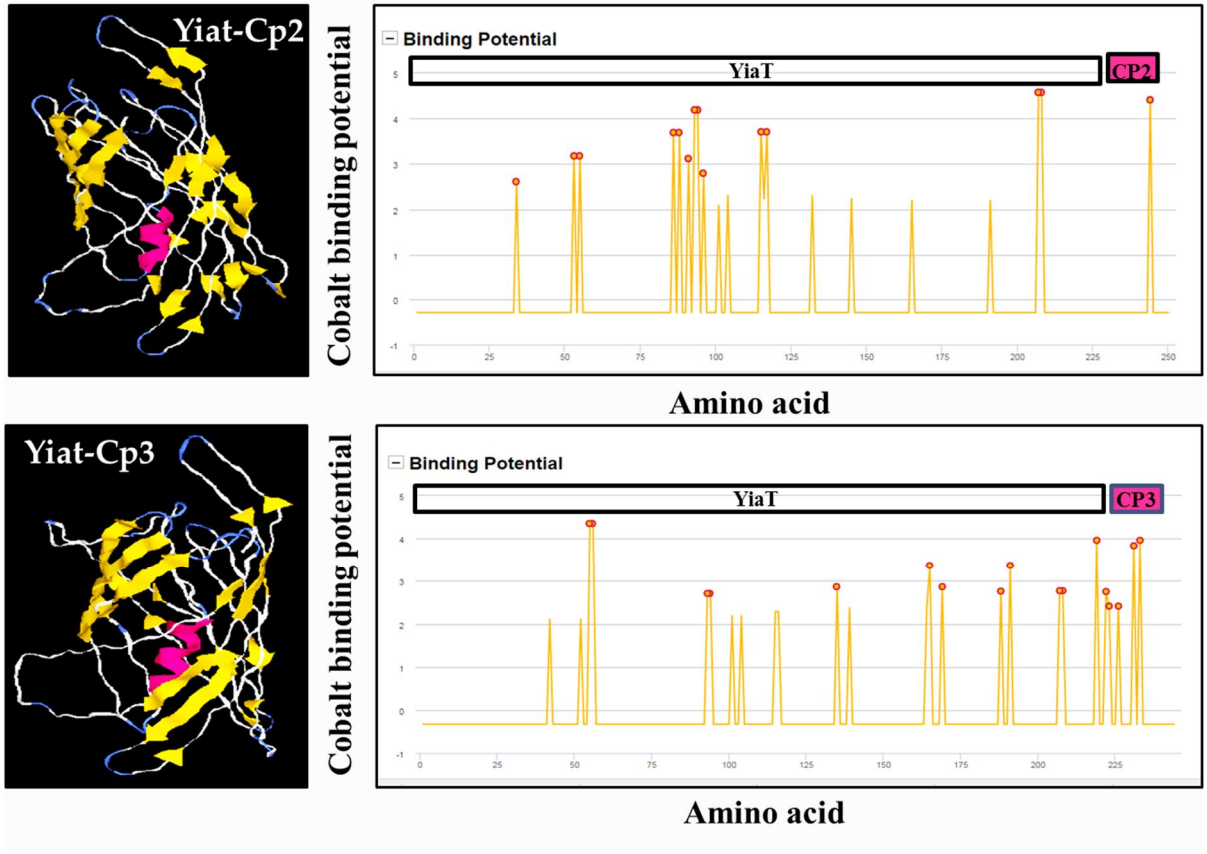

Fig. 3.5 Molecular modelling and binding potential of YiaT-CP2 and YiaT-CP3

3.4.4 Physiochemical characterization of bio-adsorbed cobalt

3.4.4.1 FT-IR spectroscopy

The recombinant strains displayed with CP2&CP3 after cobalt adsorption were analyzed by FT-IR analysis (Fig. 3.6). Cobalt chloride salt was included as control. The peaks observed in cobalt chloride matches with the spectrum of CP2&CP3. Additionally absorption band around 3432 cm^{-1} in the CP3 spectra can be attributed to a characteristic stretching vibration of hydroxyl functional group (O-H) on the nanoparticle surface[19]. The peak at 1632 and 1400.73 cm^{-1} correspond to stretching vibration of C=C and C-O respectively. A small band at 438 cm^{-1} is might be due to tetrahedral cluster of the particles[20].

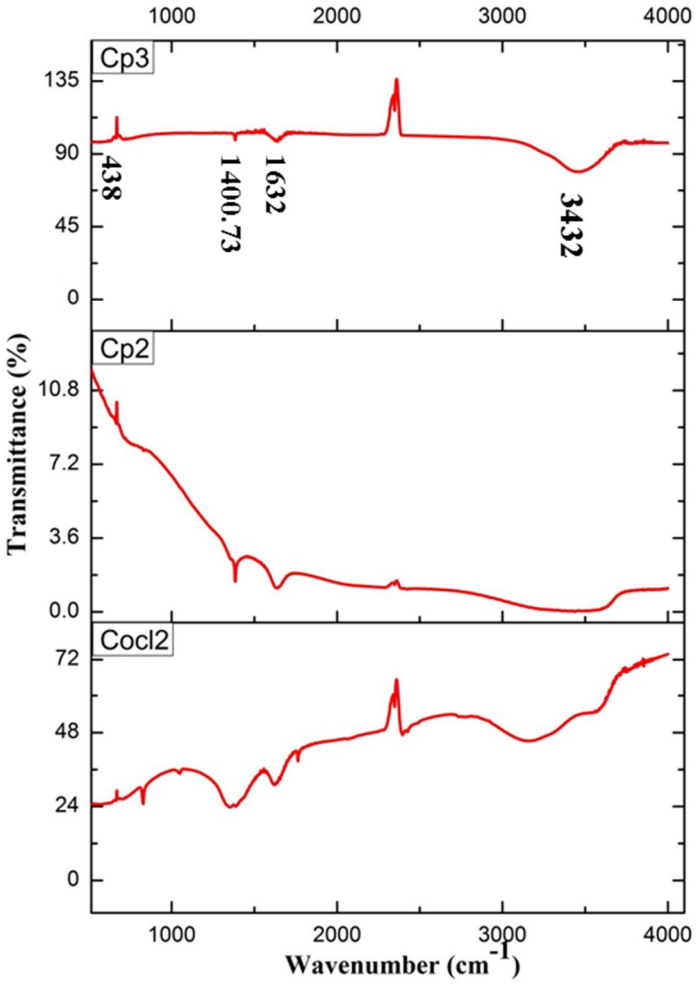

Fig. 3.6 FT-IR spectrum of recombinant strains displayed with CP2 and CP3 after cobalt adsorption. $CoCl_2$ was included as a control.

3.4.4.2 UV-Vis spectroscopy

As nano sized cobalt particles were observed in the FT-IR spectrum of CP3, the properties were further analyzed by UV-vis (Fig. 3.7A). The UV-spectrum of cobalt chloride is similar with the CP3 spectrum, further confirming the presence of cobalt on the recombinant *E. coli*. Surface plasmon resonance (SPR) is an important feature of metal nanoparticles observed in UV-vis region when interacted with exciting light [21]. The characteristic cobalt is a sharp SPR at 350-550 nm regions. Also the effect of pH (3, 5, 7, 9 and 11) towards changes in SPR of CP3 was analyzed (Fig. 3.7B). It is clear from the figure

3.7B that the absorbance increased with change in pH, but the wavelength of absorbance was not changed. The SPR absorption may change with the shape of the nanoparticle[22]. The single peak denotes that particle is more likely to nano spheres [21].

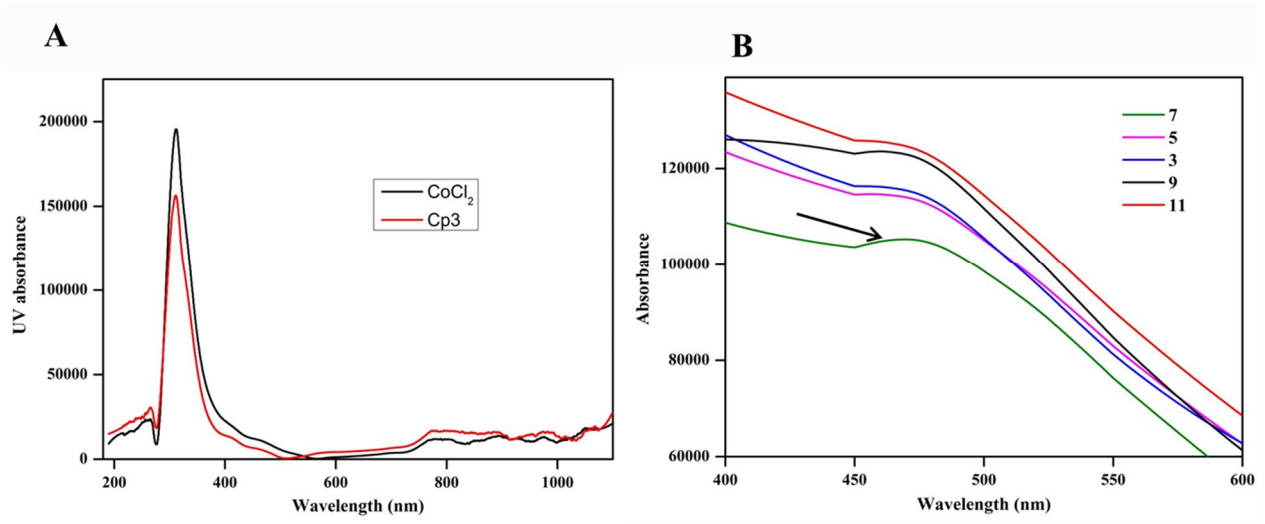

Fig. 3.7 The UV-Vis spectrum of *E. coli* containing pBADCP3 was analyzed. (A) UV-Vis spectrum of CP3 displayed *E. coli* after cobalt adsorption, $CoCl_2$ was included as control. (B) UV-Vis spectrum of CP2 displayed cells after performing cobalt adsorption at various pHs (3, 5, 7, 9 and 12).

3.4.6 SEM, TEM and EDS analysis

The morphological changes of recombinant *E. coli* after cobalt adsorption was observed by SEM Wild type *E. coli* was included as a control (Fig. 3.8 A & B), the cells displayed with CP3 peptide had particles bound on the cell surface. Further the details of the adsorbed particles were analysed by TEM (Fig. 3.8 C & D). The particles bound on the cell surface were spherical in shape and the size was measured to be 5-8 nm. Further the elements present on the recombinant *E. coli* displayed with CP2 and CP3 was mapped by EDX (Fig. 3.8 E & E). The spectrum shows the presence of cobalt on the cell surface.

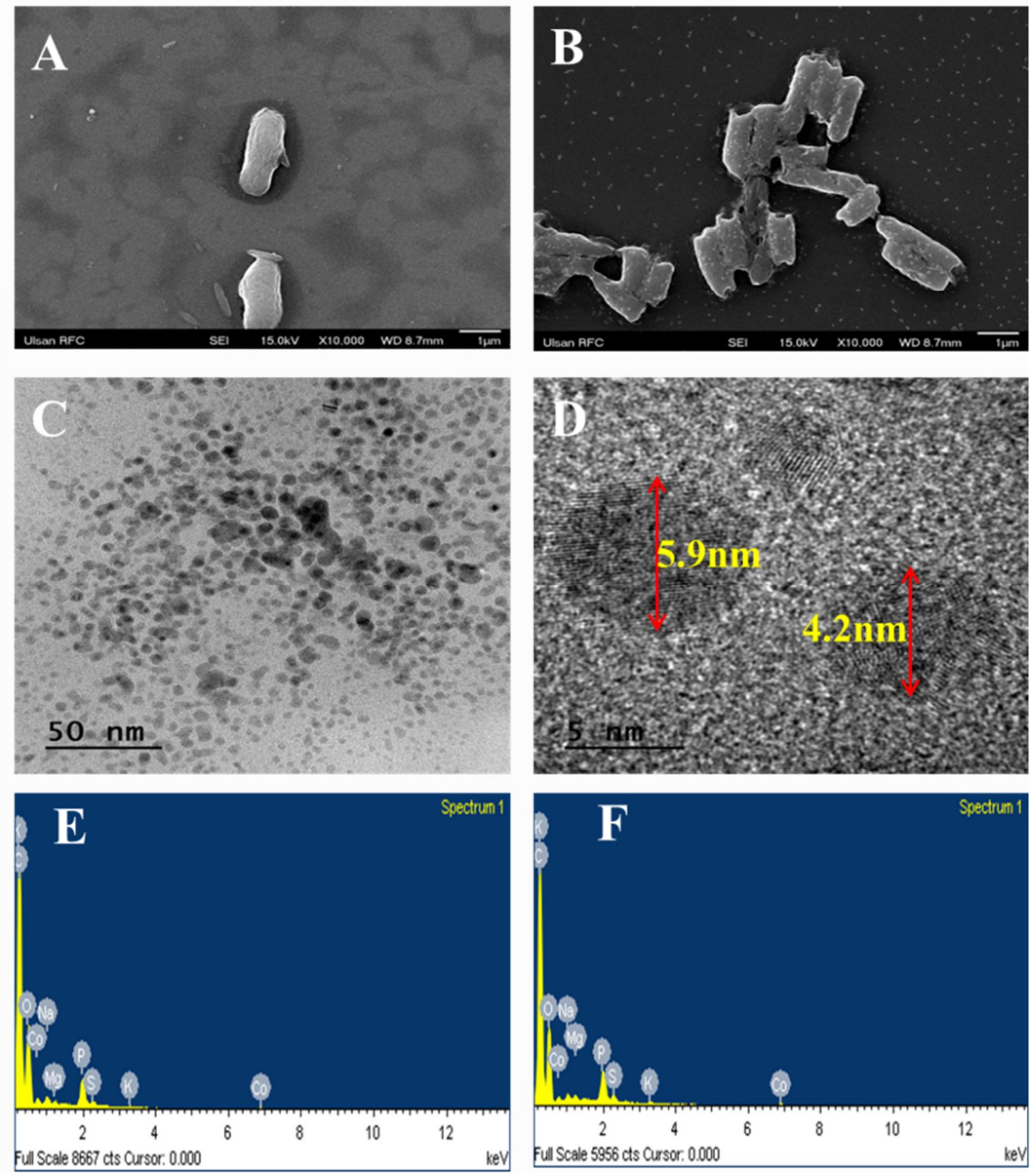

Fig. 3.8 Morphological characterization of recombinant *E. coli* after cobalt adsorption. (A) & (B) FE-SEM images of wild type *E. coli* & CP3 displayed recombinant *E. coli* respectively. (C) & (D) TEM images of nano sized cobalt particles adsorbed by CP3 displayed recombinant *E. coli*. (E) & (F) EDS spectrum of recombinant *E. coli* containing CP2 and CP3.

3.4.7 Photo-catalytic activity

Photo-catalytic degradation of methylene blue (MB) dye was studied using recombinant E. coli displayed with CP3 after cobalt adsorption (Fig. 3.9).In UV-Vis spectrum MB shows maximum at 664 nm. The MB solution was mixed with cell surface bound cobalt particles and exposed to solar light. The sample was retrieved at regular time intervals and analysed UV-Vis spectroscopy after filteration. It could be observed that the peak at 664 nm were reduced with increase in time. This further confirms the photocatalytic degradation of MB by cobalt nanoparticles. The percentage of photocatalytic activity was observed to be 59.52%. The semicoducting material abosrbs light of energy grater or equal to its band gap that leads to excitations of valence electrons is defined as photocatalysis. The activation of nanoparticles by light ($h\upsilon$) produce electron-hole pairs, these are considered to be powerful oxidizing and reducing agents. The hydroxyl radical derived from the oxidation of adsorbed water is the primary oxidant [15, 16, 23]. These radicals are very efficient oxidizers for degradation of pollutants[24, 25]. In presence of oxygen the recombination of hole-electron pairs were prevented. This may result in carbon dioxide and water as final products [26, 27]. These results prove that cobalt nanoparticles could be possibly employed for the treatment of dye polluted waste water.

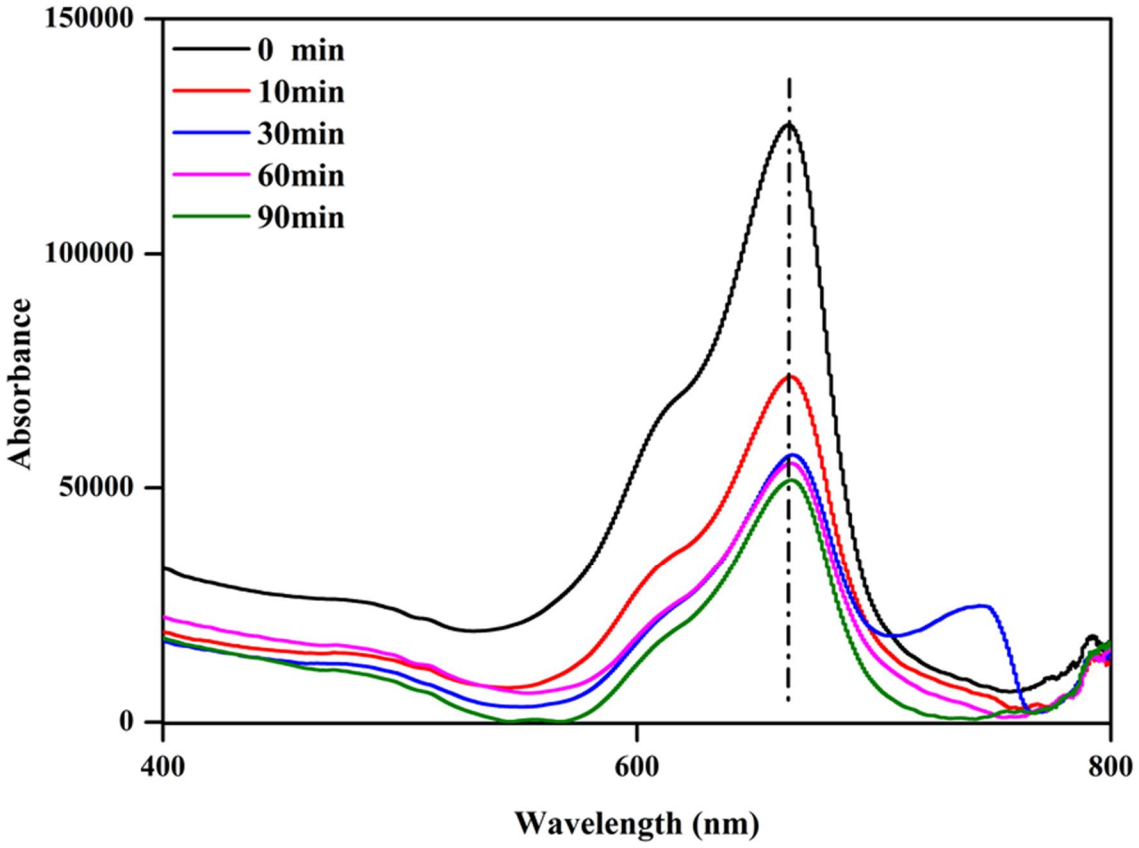

Fig. 3.9 UV absorption spectra of methylene blue photocatalytic reduced using cobalt nanoparticles biosynthesized by surface displayed CP3.

3.5 Conclusions

Cobalt is considered one of the major metal pollutants present in electrical waste (EW). However it could be considered as a secondary raw material, the precious metals present in the EW can be recovered and recycled. In this study a highly cobalt recovery system was developed by CSD of synthetic cobalt binding peptide. Two peptides CP2 and CP3 were displayed on the cell surface with YiaT as anchoring motif. The cells were found to recover 1521 and 1907.766 µmol/g DCW at 1mM concentration of cobalt chloride respectively. Further the morphological characterization of cobalt bound recombinant cells were observed by SEM and TEM. The presence of cobalt was mapped by EDX analysis. The

cobalt particles on the cell surface were found to be nano sized spheres. Further recombinant cells were used as a whole-cell biocatalyst for photocatalytic reduction of methylene blue was observed to be 59.52%.

3.6 References

1. Dewulf, J., et al., *Recycling rechargeable lithium ion batteries: Critical analysis of natural resource savings.* Resources, Conservation and Recycling, 2010. **54**(4): p. 229-234.
2. Bertuol, D.A., et al., *Application of spouted bed elutriation in the recycling of lithium ion batteries.* Journal of Power Sources, 2015. **275**: p. 627-632.
3. Kang, J., et al., *Recovery of cobalt sulfate from spent lithium ion batteries by reductive leaching and solvent extraction with Cyanex 272.* Hydrometallurgy, 2010. **100**(3): p. 168-171.
4. Li, L., et al., *Recovery of metals from spent lithium-ion batteries with organic acids as leaching reagents and environmental assessment.* Journal of Power Sources, 2013. **233**: p. 180-189.
5. Agency., U.S.E.P., *Introduction to Hazardous Waste Identification (40 CFR Parts 261)*. EPA530-K-05-012; US EPA: Washington, DC, , September 2005. **available online: http://www.epa.gov/osw/inforesources/pubs/training/hwid05.pdf.**
6. Ogunseitan, O.A., et al., *The Electronics Revolution: From E-Wonderland to E-Wasteland.* Science, 2009. **326**(5953): p. 670-671.
7. Bertuol, D.A., et al., *Recovery of cobalt from spent lithium-ion batteries using supercritical carbon dioxide extraction.* Waste Management, 2016. **51**: p. 245-251.
8. Krebs, W., et al., *Microbial recovery of metals from solids.* FEMS Microbiology reviews, 1997. **20**(3-4): p. 605-617.
9. Freitas, M.B.J.G., V.G. Celante, and M.K. Pietre, *Electrochemical recovery of cobalt and copper from spent Li-ion batteries as multilayer deposits.* Journal of Power

Sources, 2010. **195**(10): p. 3309-3315.

10. Schippers, A., et al., *Biomining: metal recovery from ores with microorganisms*, in *Geobiotechnology I*. 2013, Springer. p. 1-47.
11. Dotto, G.L., et al., *Surface modification of chitin using ultrasound-assisted and supercritical CO2 technologies for cobalt adsorption.* Journal of hazardous materials, 2015. **295**: p. 29-36.
12. kannan Maruthamuthu, M., et al., *Construction of a high efficiency copper adsorption bacterial system via peptide display and its application on copper dye polluted wastewater.* Bioprocess and Biosystems Engineering, 2015. **38**(11): p. 2077-2084.
13. Pollmann, K., et al., *Novel Biotechnological Approaches for the Recovery of Metals from Primary and Secondary Resources.* Minerals, 2016. **6**(2): p. 54.
14. Maruthamuthu, M.k., et al., *Manganese and cobalt recovery by surface display of metal binding peptide on various loops of OmpC in Escherichia coli.* Journal of Industrial Microbiology & Biotechnology, 2018. **45**(1): p. 31-41.
15. Ahmmad, B., et al., *Green synthesis of mesoporous hematite (α-Fe2O3) nanoparticles and their photocatalytic activity.* Advanced Powder Technology, 2013. **24**(1): p. 160-167.
16. Joy Prabu, H. and I. Johnson, *Plant-mediated biosynthesis and characterization of silver nanoparticles by leaf extracts of Tragia involucrata, Cymbopogon citronella, Solanum verbascifolium and Tylophora ovata.* Karbala International Journal of Modern Science, 2015. **1**(4): p. 237-246.
17. Laemmli, U.K., *Cleavage of structural proteins during the assembly of the head of bacteriophage T4.* nature, 1970. **227**: p. 680-685.

18. Nguyen, T.T.L., et al., *Selective Lead Adsorption by Recombinant Escherichia coli Displaying a Lead-Binding Peptide.* Applied Biochemistry and Biotechnology, 2013. **169**(4): p. 1188-1196.

19. S. Sathiya, K.P., M. Anbarasu and K. Balamurugan *FT-IR, XRD, and SEM Study of CoFe2O4 Nanoparticles by Chemical Co-Precipitation Method* An International Research Journal of Nano Science & Technology, April-June 2015. **Vol.5(4-6),**: p. 133-138.

20. R. Nongjai, S.K., K. Asokan, H. Ahmed, I. Khan, , J. Appl. Phys. , 2012. **112, 084321**.

21. NAVED AZUM, S.B.K., MALIK ABDUL RUB, ABDULLAH M. ASIRI1, and KHALID A. ALAMRY, *Kinetic Behavior of Cobalt Nanoparticles Facilitated byCationic Surfactant.* hemical Engineering Communications, 2016. **203**: p. 446-451.

22. Jain, P.K., Lee, K. S., El-Sayed, I. H., and El-Sayed, M. A.).,.,, , *Calculated absorption and scattering properties of gold nanoparti-cles of different size, shape, and composition: applications in bio-logical imaging and biomedicine.* J. Phys. Chem. B, 2006. **110**: p. 7238–7248.

23. Nayereh Soltani , E.S., Mohd Zobir Hussein , Maryam Erfani , Alam Abedini ,Ghazaleh Bahmanrokh , Manizheh Navasery and Parisa Vaziri, *Visible Light-Induced Degradation of Methylene Blue in the presence of Photocatalytic ZnS and CdS Nanoparticles.* Int. J. Mol. Sci. , 2012. **13**(12242-12258).

24. Torres-Martínez, C.L.K., R.; Mian, O.I.; Mehra, R.K.. J. , *Efficient photocatalytic degradation of environmental pollutants with mass-produced ZnS nanocrystals.* Colloid Interface Sci.

, 2001. **240,** (525–532).

25. Pouretedal, H.R.N., A.; Keshavarz, M.H.; Semnani, . *A. Nanoparticles of zinc sulfide doped with manganese, nickel and copper as nanophotocatalyst in the degradation of organic dyes.* J. Hazard. Mater. , 2009. **162**(674–681).

26. Zhao, J.Y., X., *Photocatalytic oxidation for indoor air purification: A literature review.* . Build. Environ. , 2003. **38**: p. 645–654.

27. Das, D.P.B., N.; Martha, S.; Parida, K.M. , *Solar-light induced photodegradation of organic pollutants over CdS-pillared zirconium–titanium phosphate (ZTP).* J. Mol. Catal. A, 2011. **349** (36–41).

Chapter 4

Cell surface display of indium binding peptide with novel anchoring protein (yaiO)

4.1 Abstract

In Cell surface display the anchoring protein is vital for the efficient display of peptide on the microbial surface. In this study, a novel anchoring motif was developed with an outer membrane protein YaiO. Its topological study revealed the presence of 7 loops for the display. The loop 7 was truncated at 237th amino acid residue to expose the peptides in the extracellular region. The efficiency of YaiO as an anchoring protein was evaluated by displaying indium binding peptides (IBP 1 & 2) SLAPDSTWFALF, TNSSSQEWAIP respectively. The ability of the displayed peptide to recover indium was analyzed. In addition, the recombinant *E. coli* were elongated by cisplatin treatment to increase the indium bio-adsorption. The cells with adsorbed indium were visualized by SEM and TEM techniques. The indium particles present on the bacterial surface was mapped by EDS analysis. Further Raman spectroscopy reveals that the indium is found as cubic In_2O_3.

4.2 Introduction

Indium is an important metal; it is used widely in electronics, photovoltaic and LED industries (White and Hemond 2012; White, Keach et al. 2015). It is exposed to environment primarily from industries and minor quantities are contributed from electronics and semiconductors. Industrial emissions of indium are already larger than natural emissions. However, the increased use of electronics may change this scenario (White 2012). All indium compounds should be regarded as highly toxic. Indium compounds damage the heart, Kidney, and liver and may be teratogenic. The technological advancement and increasingly short production cycles of the electronic device, LCD with flat screen's TV have become a major component of e-waste destined for landfill. According to European Union indium was

categorized under critical raw material (European Commission, 2010)(Laura Rocchetti and Beolchini 2015). The global indium market value is anticipated to grow by 70% by 2025 relative to the year 2015(Licht, Peiró et al. 2015). On its own indium ore is not available in earth's crust, it is extracted as a by-product of zinc smelting and refining. At present 15000 tonnes of indium reserves are available out of which two-thirds are found in China. The LCD scraps are one of the alternative resources for indium. Cell surface display (CSD) approach could be successfully employed for metal recovery; further, the adsorbed metals can be recycled for various applications.

CSD is a strategy that enables protein or peptide expression on the cell surface of the microorganisms. It is one of the highly exploited strategies in biotechnological and industrial applications for biocatalysts, bioremediation, biosensors and so on (Lee, Choi et al. 2003; Jose 2006; van Bloois 2011). The target protein or peptide is displayed as a fusion protein with anchoring protein. Several outer membrane proteins were employed as anchoring proteins OmpC(Maruthamuthu, Nadarajan et al. 2015), OmpA(Verhoeven, Alexeeva et al. 2009), OmpX(Rice and Daugherty 2008), LamB, FhuA (Samuelson 2002), Ice-nucleation protein INP(Jung, Lebeault et al. 1998), lipoproteins, autotransporters (Jose 2006), surface appendages and S-layer proteins for surface display. It is essential to use a compatible anchoring motif to realize stable protein display(Han and Lee 2015). Target proteins of various capacities from antibodies to small peptides are displayed using the existing anchoring proteins. Hence, it is essential to develop new anchoring motifs that are compatible with the target peptides (Lee, Choi et al. 2003; Nhan, de Valdivia et al. 2011; Han and Lee 2015). In this study, we developed a novel anchoring protein YaiO for surface display of indium binding peptide (IBP). Two peptides (IBP1 and IBP2) were displayed on the cell

surface of *E. coli*. Further, the ability of the peptides to recover indium was analyzed (Fig. 4.1). The recombinant *E. coli* elongated by cisplatin treatment was employed to increase the indium bio-adsorption. The recombinant bacteria with bio-adsorbed indium were visualized by FE-SEM and TEM. Further, the properties of the adsorbed indium were studied by Raman spectroscopy.

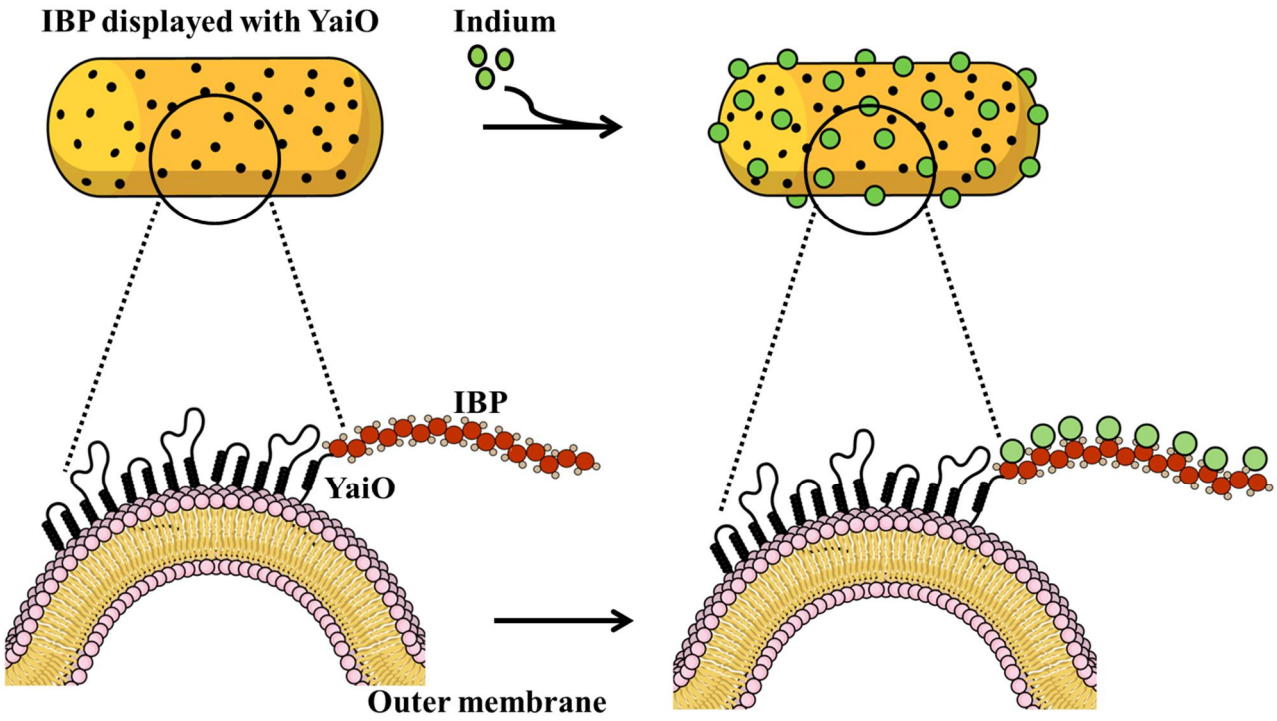

Fig. 4.1 Cell surface display of indium binding peptide (IBP) with YaiO as an anchoring motif.

4.3 Materials and methods

4.3.1 Bacterial strains and growth conditions

The bacterial strains and plasmid used are listed in Table 4.1. The recombinant plasmids harboring bacterial strains were cultured and expressed in LB (Luria-Bertani) medium (10 g/L bacto-tryptone, 5 g/L bacto-yeast extract, and 5 g/L NaCl). The cells were

cultured with 100mg/L of ampicillin at 37 ºC with shaking (250rpm). After reaching an optical density of 0.5 at 600 nm (OD600), IPTG was added to the culture broth further incubated at 30ºC for 5 h.

4.3.2 Recombinant plasmids construction

The recombinant plasmids were constructed by cloning the fusion protein YaiO-IBP into the pET21a plasmids using *BamHI* and *HindIII* restriction enzymes. Based on the structural analysis of YaiO, the peptide IBP (1&2) were fused at the 7th loop (726 bp). The genes for the fusion peptide were amplified by polymerase chain reaction (PCR) with an MJ Mini Personal Thermal Cycler (Bio-Rad Laboratories, Hercules, CA, USA) using the Expand High Fidelity PCR system (Roche Molecular Biochemicals, Mannheim, Germany). The nucleotide sequence of peptides IBP (1&2) and the primers used in this study are listed in Table 4.2. The expression of the recombinant peptide was induced by the addition of IPTG and regulated by the T7 promoter.

Table 4.1 Bacterial strains and plasmids used
\

Strain/Plasmid	Relevant genotype/ property	Source
***E. coli* strains**		
XB	*recA1 endA1 gyrA96 thi-1 hsdR17 supE44 relA1 lac [F′ proAB lacIq ZΔM15 Tn10 (Tetr)].*	Novagen
TOP10	*F- mcrA Δ(mrr-hsdRMS-mcrBC) φ80lacZΔM15 ΔlacX74 nupG recA1 araD139 Δ(ara-leu)7697 galE15 galK16 rpsL(Str^R) endA1 λ$^-$*	Stratagene
Plasmids		
pET21a	Amp^R	NEB[a]
pETIP1	pET21a containing YaiO-IBP2	This work
pETIP2	pET21a containing YaiO-IBP2	This work

[a]New England Biolabs, Beverly, MA, U.S.A.

Table 4.2 Primers used in this work

Name	Sequence (5' to 3')
YaiO_F	**GGATCC**ATGATTAAACGCACCCTGCTGGCGGCGGCGA
YaiO_R	AAATTTCCAGGTCAGGCGCGCCGCCAGCTGCAGGCCGTTAA AATCATCGGTC
IP1_R	**AAGCTT**CGGAATCGCCACCACAAACTGGCTGCTGCTGTTGG TAAATTTCCAGGTCAGGCGCGCCGCCAGCTG
IP2_R	**AAGCTT**AAACAGCGCAAACCAGGTGCTATCCGGCGCATGGC TAAATTTCCAGGTCAGGCGCGCCGCCAGCTG

4.3.3 YaiO-IBP (1&2) expression analysis

It is essential to optimize and analyze the expression of the recombinant peptide. Varying concentrations of IPTG (0-1 mM) was into the culture broth containing recombinant *E. coli*. Further, the cells were incubated at 30ºC for 5 h. The recombinant strains were harvested by centrifuging at 13,000 rpm for 10 minutes. The cells were washed to remove remnants of LB. The harvested cells were incubated with B-7M urea buffer (7M urea, 0.1M NaH_2PO_4, 0.01M Tris.cl) pH 8.0 at room temperature for 30 minutes with agitation. The cells were centrifuged at 8,000 rpm to remove cell debris. The outer membrane fractions from the cell pellet were separated by adding 10 mM Tris-HCl (pH 7.5) and the suspended cells were kept in 4 ºC overnight. The lifted the membrane fractions were analyzed by 12% (w/v) sodium dodecyl sulfate-polyacrylamide gel electrophoresis (SDS-PAGE) (Laemmli 1970) and stained with Coomassie brilliant blue R-250 (Bio-Rad Laboratories, Hercules, CA, USA).

4.3.4 Indium recovery studies

The recombinant protein (IBP1&2) expressed cells were harvested by centrifugation and washed twice with 0.85% (w/v) of NaCl. The cells were incubated with varying concentration indium chloride solution (0.01- 5 mM). The specificity of the displayed peptide

towards indium was also evaluated. To realize this AWW containing lithium chloride ($InCl_2$), copper chloride ($CuCl_2$), cobalt chloride ($LiCl_2$) 1000ppm each was prepared. The adsorption experiment was performed at 25 oC for 30 minutes with agitation. After performing adsorption the cells were centrifuged and washed twice with 0.85% (w/v) of NaCl to remove the unbound lithium. Indium adsorbed was eluted by incubating the cells with 1 mM EDTA for 30 minutes in ice. It is quantitatively measured using inductively coupled plasma optical emission spectroscopy (ICP-OES).

4.3.5 Raman spectroscopy

The properties of Indium adsorbed by recombinant *E. coli* displayed with IBP were evaluated by Raman spectroscopy (Thermo- scientific, DXR Raman microscope 532nm full range). After adsorption, the cells were washed and lyophilized using EYELA FDU-2200 freeze dryer. Wild-type *E. coli* was included in the study as a control.

4.3.6 FE-SEM, EDX and TEM analysis

The presence of indium on the cell surface was confirmed by field emission scanning emission microscopy (FE-SEM), energy dispersive X-ray spectroscopy (EDS) and transmission emission spectroscopy (TEM). To perform this recombinant *E. coli* displayed with IBP 1&2 after lithium recovery were employed. The cells were washed and fixed with 2.5% glutaraldehyde at 4ºC for 14 h. The fixed cells were washed with PBS and mounted on ultra-flat silicon wafers. The cells were dried and visualized by FE-SEM (JEOL JSM-6500F) equipped with EDS. In order to visualize the cells by TEM; the bacterial samples were prepared using the drop-casting method. Sterile copper grids were coated with 20 µl of lithium adsorbed recombinant *E. coli* dissolved in PBS. After 3 minutes the majority of the liquid on the grid was removed by touching the edges using filter paper. Further, the grids

were washed and air dried. The samples were visualized by TEM.

4.4 Results and discussion

CSD is employed to display proteins or peptides on the cell surface. It is very important to choose the ideal anchoring protein to enable efficient display of the carrier protein. Hence it is essential to identify new anchoring motifs. A study performed by Marani et al. predicted the outer membrane localization of five uncharacterized outer membrane proteins (YtfM, YaiO, YfaZ, CsgF, and YliI)(Marani, Wagner et al. 2006). Among the five proteins, YaiO and YliI were observed in the outer membrane fractions. The topology of both the proteins was predicted by PRED-TMBB (http://bioinformatics.biol.uoa.gr/PRED-TMBB/) (Bagos, Liakopoulos et al. 2004). According to this algorithm if the sequence scores lower than the threshold value of 2.965 it is more likely to be an outer membrane protein. The sequence score of YaiO and YliI are 2.886 and 3.027 respectively. Thus the possibility of YliI to form a beta-barrel structure on the cell membrane is low. Hence we chose to precede our system with YaiO as an anchoring motif. It is an outer membrane protein, made of 257 amino acids. It is reported that the YaiO has a signal sequence composed of 19 amino acids, which is essential for anchoring proteins as it aids transportation through the membrane(Lee, Choi et al. 2003). This protein is predicted to have 14 transmembrane strands and exhibits no significant similarity to any other real or hypothetical proteins of *E. coli*. This aids in the formation of a beta-barrel structure with 7 external loops. The topological analysis of YaiO (Fig. 4.2), revealed that 7 loops, it is well known that these loops are less conservative and can be employed for insertion or deletion(Xu and Lee 1999). In our study 7^{th} loop was employed for the CSD of IBP.

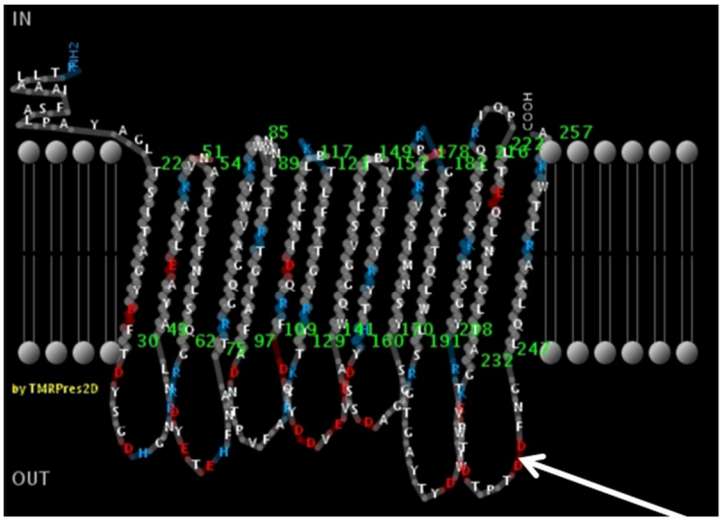

Fig.4.2 Topological study of YaiO loop structure. The loop employed for the display is indicated by the arrow.

4.4.1 Construction of recombinant plasmid

The recombinant plasmids (pETIP1 & pETIP2) were constructed by cloning the fusion protein YaiO-IBP into pET21A vector (Fig. 4.3 A&B). It is essential to optimize the expression. The expression of a recombinant protein may cause metabolic burden, which may indirectly affect the protein expression, cell growth, and stability of recombinant plasmid. The expression of the recombinant protein was induced by the addition of β-D-1-thiogalactopyranoside (IPTG) regulated by the T7 promoter. The concentration of IPTG was varied and the difference in protein expression was analyzed SDS PAGE (Fig. 4.3C&D). The expression IBP1 and IBP2 were optimum at 0.3 and 0.7 mM of IPTG respectively.

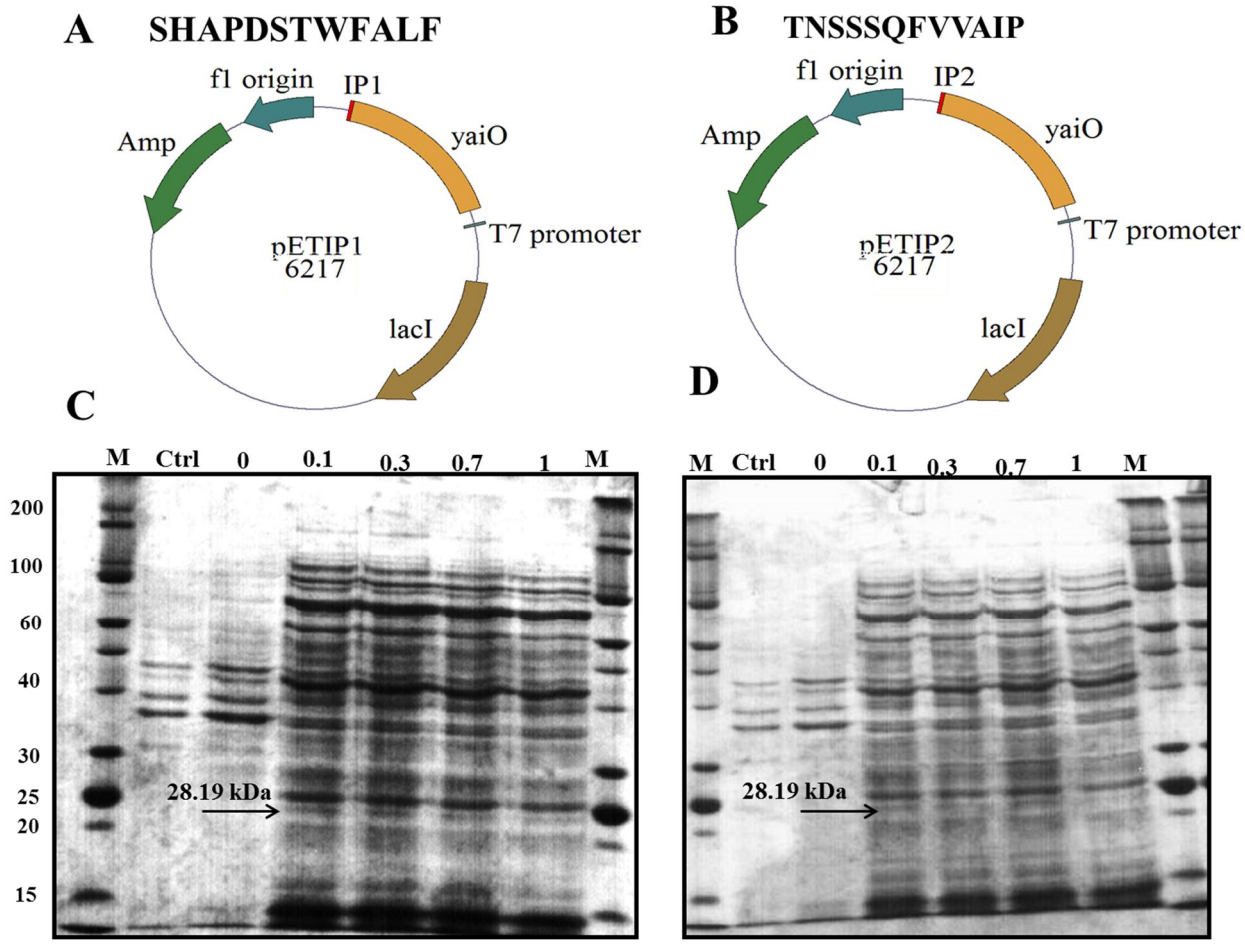

Fig. 4.3 Construction of recombinant plasmid and protein expression analysis; A &B plasmids containing YaiO-IBP1 & YaiO-IBP2 respectively; SDS-PAGE analysis of peptides C, IBP1 & D, IBP2 (28.19 kDa). M. Molecular weight marker in kDa.

4.4.2 Indium bio-adsorption studies

After the expression of the recombinant peptide YaiO-IBP (1&2), the cells were harvested by centrifugation. The metal recovery conditions such as temperature, time of exposure were optimized (Fig. 4.4 C &D). The ideal conditions for indium recovery were observed to be 25 ^{o}C and 30 minutes of metal exposure. The ability of the cells to recover indium was analyzed by exposing to varying concentrations of Indium chloride solution (Fig. 4.4A). Among the peptides, IBP 1&2 showed higher indium recovery was found with IBP2 at

5mM of Indium chloride which is 1763.73 µmol/g DCW. Also, the specificity of the IBP 1&2 was evaluated by exposing the cells to AWW containing $InCl_2$, $CuCl_2$, and $CoCl_2$ (Fig. 4.4B). Among other exposed metals, the recombinant *E. coli* showed increased specificity towards indium. As indium is one of the highest used metals in electrons. The current system could be employed to recover indium selectively. It is reported the morphology of the cells play important role in bio-sorption. Hence in our study, we employed a strategy to increase the cell size, which will eventually increase the peptide display count on the cell surface. To realize cisplatin (15, 25, and 50 µmol) platinum-based salt was added into growth medium containing recombinant *E. coli*. This favored the fila mental bacterial growth(Rosenberg, Van Camp et al. 1965; Rosenberg, Renshaw et al. 1967). A further effect of cisplatin treatment of indium recovery was analyzed (Fig. 4.5). When compared to recombinant *E. coli* grown in LB devoid of cisplatin a minor increase in indium recovery was achieved with 15 µmol concentration of cisplatin-treated cells was observed.

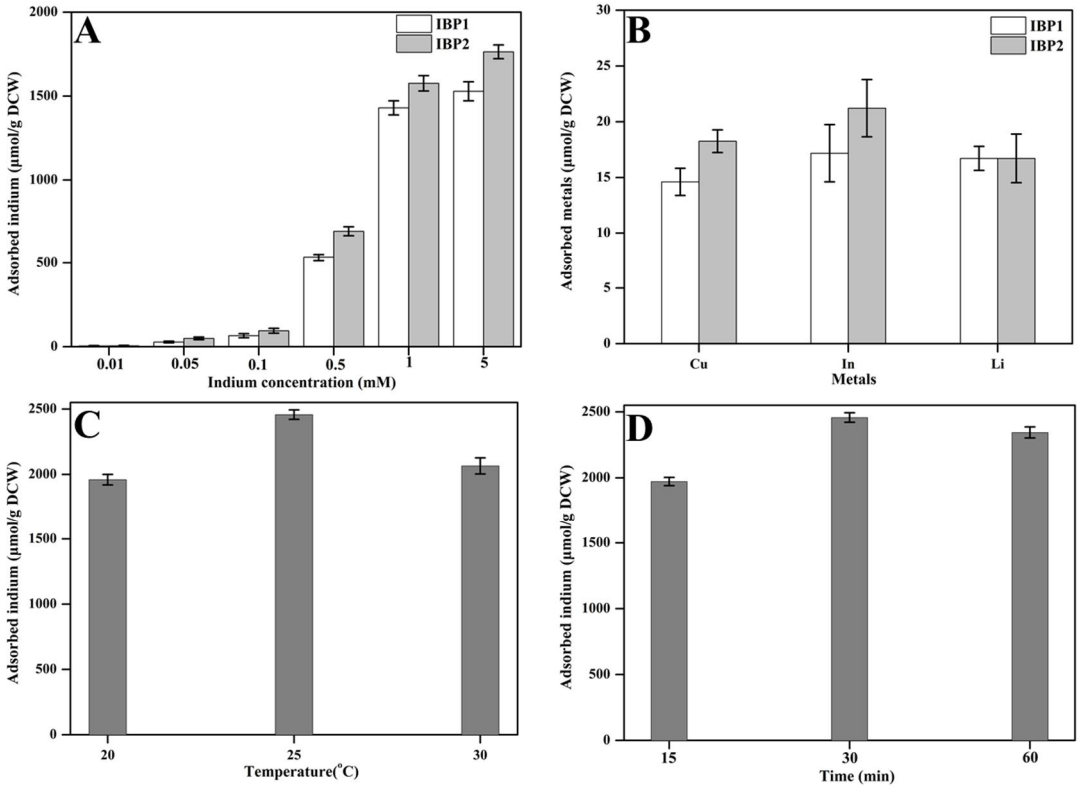

Fig. 4.4 Indium bio-adsorption studies with cells displayed with indium binding peptide. A, LB, B, AWW. (C) Effect of temperature on indium recovery, and (D) Effect of time on indium recovery

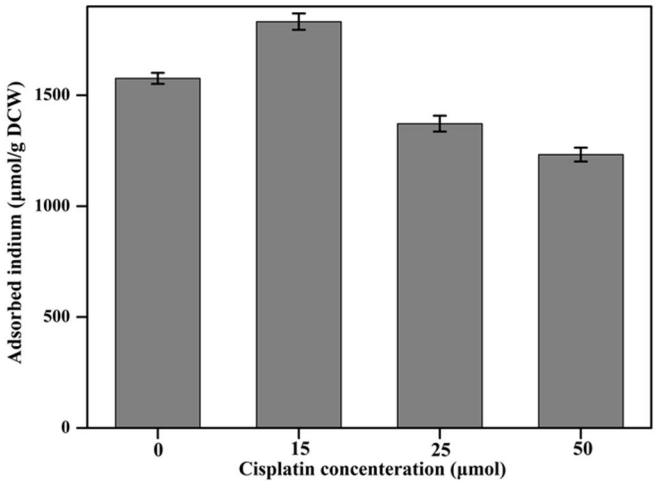

Fig. 4.5 Effect of cisplatin towards indium recovery by recombinant *E. coli* displayed with IBP2

4.5.3 Raman spectroscopy

The properties of the bio-adsorbed indium by the recombinant *E. coli* was studied by Raman spectroscopy. Based on the Raman spectrum shown in Fig. 4.6, the peak at 109 cm^{-1} and 133 cm^{-1} is a sign for the presence of cubic In_2O_3 structure(Sobotta, Neumann et al. 1990; Wang, Dai et al. 2008). The Raman shift peaks at 231 and 304 cm^{-1} can be attributed to characteristic E_g mode of cubic In_2O_3 (Wang, Chen et al. 2005). The results further confirm the presence of indium on the cell surface of recombinant *E. coli*.

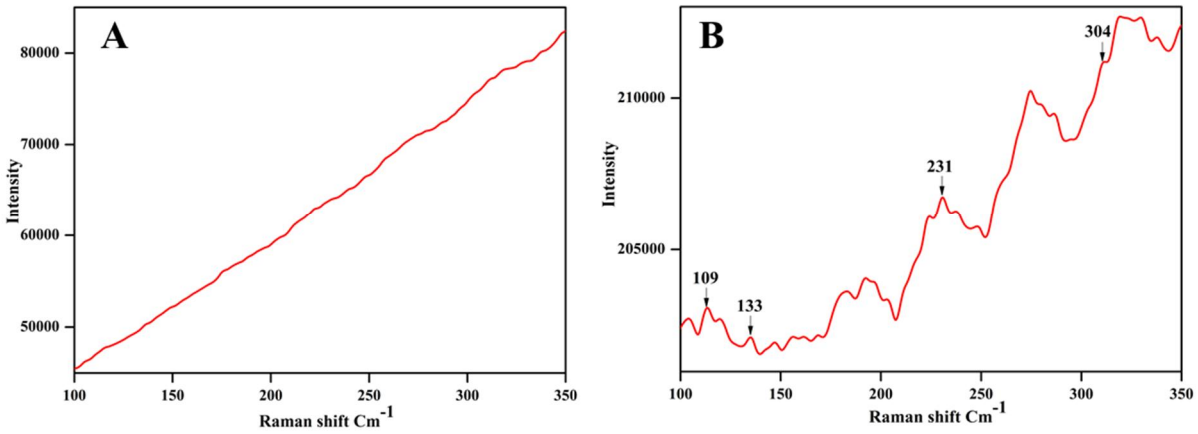

Fig. 4.6 Raman spectroscopy. (A) Recombinant *E. coli* displayed with IP by employing YaiO as an anchoring motif. (B) Wild-type BL21 was included as a control.

4.5.4 FE-SEM, TEM, and EDS analysis

The indium adsorbed by the IBP (1&2) displayed recombinant *E. coli* was visualized by SEM and TEM. From the Raman spectroscopy results it was known that the adsorbed indium is in the form of cubic In_2O_3 particles it is further confirmed with SEM images (Fig. 4.7 A, B &C). The recombinant exposed with Indium showed cubic particles on the cell surface. Further TEM was performed similar results were observed (Fig. 4.7 C, D &E). The wild-type *E. coli* BL21 was included as control no particles were found the cell surface this further confirms metal adsorption was due to cell surface display of IBP by YaiO anchoring protein. The

particles present on the cell surface were confirmed to be indium by EDS analysis (Fig. 4.8 A&B). The morphological changes of the cells observed after cisplatin treatment was visualized by the SEM (Fig 4.9A-D).

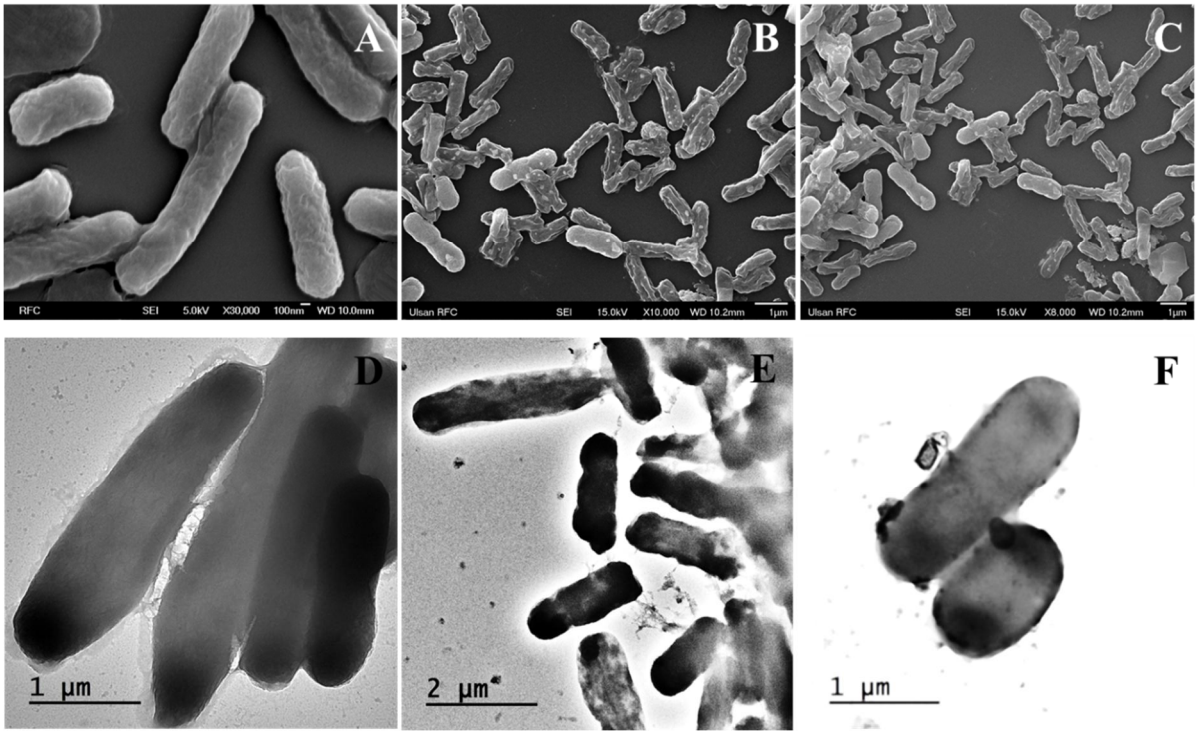

Fig. 4.7 FE-SEM and TEM image of recombinant strains containing YaiO-IBP. A & D SEM and TEM images of BL21, B, C & E, F SEM and TEM images of recombinant *E. coli* after indium recovery respectively.

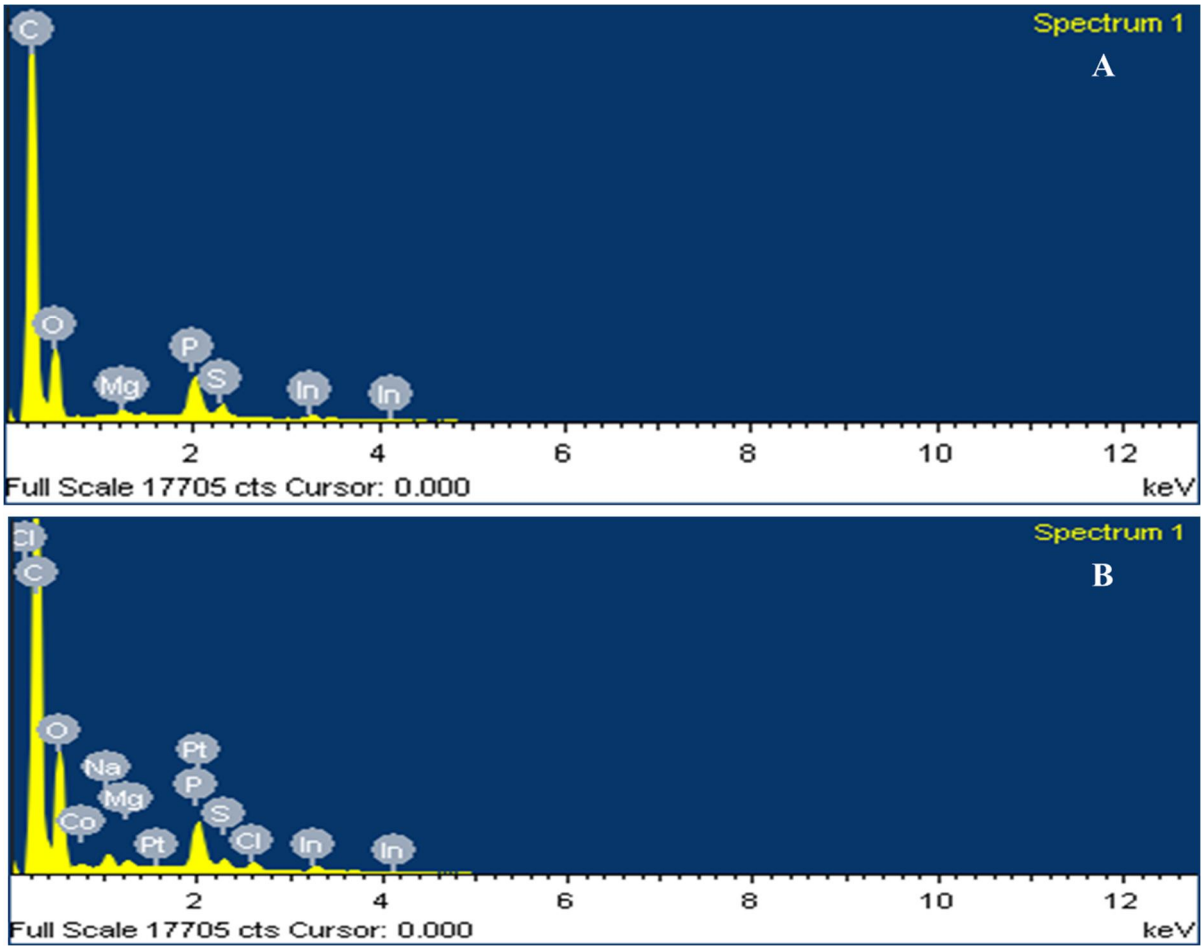

Fig. 4.8 EDS spectrum of recombinant *E. coli* displayed with indium binding peptide after bio-adsorption. A YaiO-IBP1 & B, YaiO-IBP2.

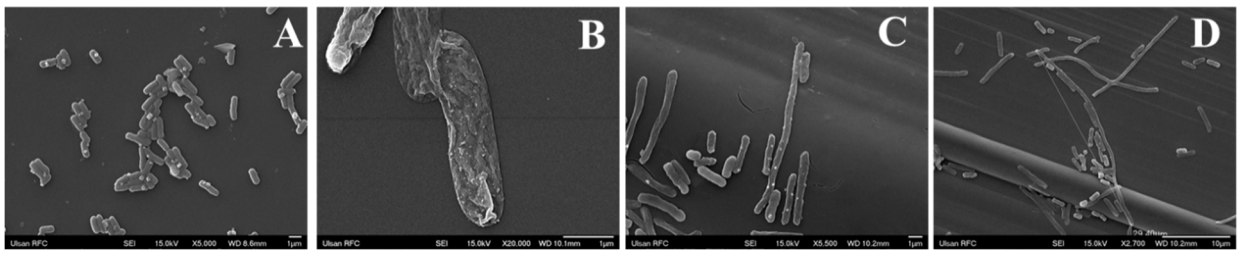

Fig.4.9 SEM images of cisplatin-treated recombinant *E. coli* after indium bio-adsorption. (A-D) 0, 15, 25, 50 µmol of cisplatin respectively.

4.5 Conclusions

The growth in consumption of electronic goods is directly proportional to the

increase in electronic waste. Thus demands immediate management techniques, recovery and reuse are considered to be a mandatory measure. CSD of peptides and proteins were employed in decontamination and recovery of inorganic pollutants present in the environment. However, the anchoring proteins play a pivotal role in the efficient display of proteins. Thus urges the need to develop novel anchoring proteins. In this study, the topology of YaiO an outer membrane protein was studied. This revealed the presence of 7 external loops, for the display of heterologous peptides. At 237th amino acids, YaiO truncated and fused with IBP 1&2. The recombinant *E. coli* was employed for indium bio-adsorption. Further, the recovery was increased by elongating the recombinant *E. coli* with cisplatin treatment. The indium particles found on the bacterial surface was visualized by SEM and TEM analysis. The particles were mapped to be indium by EDS analysis. The observed indium particles were available as cubic In_2O_3 was confirmed by Raman spectroscopy. Thus the anchoring motif YaiO developed in this study enabled the efficient display of IBP of the bacterial surface.

4.6 References

Bagos, P. G., T. D. Liakopoulos, et al. (2004). "PRED-TMBB: a web server for predicting the topology of β-barrel outer membrane proteins." Nucleic acids research **32**(suppl_2): W400-W404.

Han, M.-J. and S. H. Lee (2015). "An efficient bacterial surface display system based on a novel outer membrane anchoring element from the Escherichia coli protein YiaT." FEMS Microbiology Letters **362**(1): 1-7.

Jose, J. (2006). "Autodisplay: efficient bacterial surface display of recombinant proteins." Appl Microbiol Biotechnol **69**.

Jung, H.-C., J.-M. Lebeault, et al. (1998). "Surface display of Zymomonas mobilis levansucrase by using the ice-nucleation protein of Pseudomonas syringae." Nature Biotechnology **16**: 576.

Laemmli, U. (1970). "Cleavage of structural proteins during the assembly of the head of bacteriophage T4." Nature(227): 680-685.

Laura Rocchetti, A. A., Viviana Fonti, Francesco Vegliò, Francesc and Beolchini (2015). "Innovative Method to Extract Indium from LCD Panels." CHEMICAL ENGINEERING TRANSACTIONS **43**: 1987-1992

Lee, S. Y., J. H. Choi, et al. (2003). "Microbial cell-surface display." Trends in Biotechnology **21**(1): 45-52.

Licht, C., L. T. Peiró, et al. (2015). "Global substance flow analysis of gallium, germanium, and indium: Quantification of extraction, uses, and dissipative losses within their anthropogenic cycles." Journal of Industrial Ecology **19**(5): 890-903.

Marani, P., S. Wagner, et al. (2006). "New Escherichia coli outer membrane proteins

identified through prediction and experimental verification." Protein science **15**(4): 884-889.

Maruthamuthu, M. k., S. P. Nadarajan, et al. (2015). "Construction of a high efficiency copper adsorption bacterial system via peptide display and its application on copper dye polluted wastewater." Bioprocess and Biosystems Engineering **38**(11): 2077-2084.

Nhan, N. T., E. G. de Valdivia, et al. (2011). "Surface display of Salmonella epitopes in Escherichia coli and Staphylococcus carnosus." Microbial Cell Factories **10**(1): 22.

Rice, J. J. and P. S. Daugherty (2008). "Directed evolution of a biterminal bacterial display scaffold enhances the display of diverse peptides." Protein Engineering, Design and Selection **21**(7): 435-442.

Rosenberg, B., E. Renshaw, et al. (1967). "Platinum-induced filamentous growth in Escherichia coli." Journal of bacteriology **93**(2): 716-721.

Rosenberg, B., L. Van Camp, et al. (1965). "Inhibition of cell division in Escherichia coli by electrolysis products from a platinum electrode." Nature **205**(4972): 698-699.

Samuelson, P., Gunneriusson, E., Nygren, P.-Å., Ståhl, S. (2002). "Display of proteins on bacteria." Journal of Biotechnology **96**(2): 129-154.

Sobotta, H., H. Neumann, et al. (1990). "Infrared lattice vibrations of In2O3." Crystal Research and Technology **25**(1): 61-64.

van Bloois, E., Winter, Remko T., Kolmar, Harald, Fraaije, Marco W. (2011). "Decorating microbes: surface display of proteins on Escherichia coli." Trends in Biotechnology **29**(2): 79-86.

Verhoeven, G. S., S. Alexeeva, et al. (2009). "Differential Bacterial Surface Display of Peptides by the Transmembrane Domain of OmpA." PLOS ONE **4**(8): e6739.

Wang, C. Y., Y. Dai, et al. (2008). "Phase stabilization and phonon properties of single crystalline rhombohedral indium oxide." Crystal growth and Design **8**(4): 1257-1260.

Wang, J., H. Chen, et al. (2005). "Synthesis and characterization of In2O3/SnO2 hetero-junction beaded nanowires." Journal of crystal growth **284**(1-2): 73-79.

White, S. J. O. and H. F. Hemond (2012). "The Anthrobiogeochemical Cycle of Indium: A Review of the Natural and Anthropogenic Cycling of Indium in the Environment." Critical Reviews in Environmental Science and Technology **42**(2): 155-186.

White, S. J. O., C. Keach, et al. (2015). "Atmospheric Deposition of Indium in the Northeastern United States: Flux and Historical Trends." Environmental Science & Technology **49**(21): 12705-12713.

White, S. J. O. C. (2012). "The natural and industrial cycling of indium in the environment." Massachusetts Institute of Technology.

Xu, Z. and S. Y. Lee (1999). "Display of Polyhistidine Peptides on theEscherichia coli Cell Surface by Using Outer Membrane Protein C as an Anchoring Motif." Applied and Environmental Microbiology **65**(11): 5142-5147.

Chapter – 5

Conclusions and Future Perspectives

Chapter-5

6.1 Conclusions and Future Perspectives

The growth in consumption of electronic goods is directly proportional to the increase in electronic waste and the immediate management techniques, recovery and reuse are considered to be a mandatory measure. Additionally, the increase in the use of LIBs and poor disposable systems, demands the need for the immediate development of lithium recovery systems. Therefore, the treatment of e-waste should be approached not only for cleaning but also for mining.

The sorbents for lithium could be prepared by designing, expression and implementation of the peptides having the five amino acids in their sequence. These peptides showed the high specificity toward lithium and can extract the metals from the solutions containing various metals under the mild condition without any chemicals and energy input. The ability of the peptides for lithium recovery can be strengthened by cell surface display on the recombinant bacteria. Through CSD of the multimeric construct of the peptides, cutting down the production cost, increasing the adsorption capacity and value-adding the product are all possible. Lithium nanoparticles were obtained after lithium adsorption and the whole-cell biosorbents could be functioned as a template for a nanoparticle. Designing peptides allow the synthesis of nanoparticles having excellent properties even if they are not necessarily applied for wastewater. Further studies are required for the characterization of nanoparticles synthesized on the cell surface in order to design novel peptide sequences. The current study is also focused on recycling and reuse of LBWW for

plant irrigation and the ability of the developed system towards bioremediation are confirmed.

Cobalt is considered one of the major metal pollutants present in electrical waste (EW). However it could be considered as a secondary raw material, the precious metals present in the EW can be recovered and recycled. In this study a highly cobalt recovery system was developed by CSD of synthetic cobalt binding peptide. Two peptides CP2 and CP3 were displayed on the cell surface with YiaT as anchoring motif. The cells were found to recover 1521 and 1907.766 µmol/g DCW at 1mM concentration of cobalt chloride respectively. Further the morphological characterization of cobalt bound recombinant cells were observed by SEM and TEM. The presence of cobalt was mapped by EDX analysis. The cobalt particles on the cell surface were found to be nano sized spheres. Further recombinant cells were used as a whole-cell biocatalyst for photocatalytic reduction of methylene blue was observed to be 59.52%.

The growth in consumption of electronic goods is directly proportional to the increase in electronic waste. Thus demands immediate management techniques, recovery and reuse are considered to be a mandatory measure. CSD of peptides and proteins were employed in decontamination and recovery of inorganic pollutants present in the environment. However, the anchoring proteins play a pivotal role in the efficient display of proteins. Thus urges the need to develop novel anchoring proteins. In this study, the topology of YaiO an outer membrane protein was studied. This revealed the presence of 7 external loops, for the display of heterologous peptides. At 237th amino acids, YaiO truncated and fused with IBP 1&2. The recombinant *E. coli* was employed for indium bio-adsorption. Further, the recovery was increased by elongating the recombinant *E. coli* with

cisplatin treatment. The indium particles found on the bacterial surface was visualized by SEM and TEM analysis. The particles were mapped to be indium by EDS analysis. The observed indium particles were available as cubic In_2O_3 was confirmed by Raman spectroscopy. Thus the anchoring motif YaiO developed in this study enabled the efficient display of IBP of the bacterial surface. Thus cell surface display strategy could be employed to display various kinds of peptides to develop a whole-cell biosorbents without further contaminating the environment.